The wireless telegraph is not difficult to understand.
The ordinary telegraph is like a very long cat. You pull the tail in
New York, and it meows in Los Angeles. The wireless is the same, only without
the cat.

– Albert Einstein

University of Alberta

MULTIUSER DETECTION IN TH-UWB COMMUNICATION SYSTEMS

by

Iraj Hosseini

A thesis submitted to the Faculty of Graduate Studies and Research
in partial fulfillment of the requirements for the degree of

Master of Science
in
Communications

Department of Electrical and Computer Engineering

Examining Committee

Dr. Norman C. Beaulieu, Electrical and Computer Engineering

Dr. Byron Schmuland, Mathematical and Statistical Sciences

Dr. Chintha Tellambura, Electrical and Computer Engineering

To my lovely wife ...
for her support, patience, and true love
and to my dear parents ...
for their help, encouragement, and sacrifice.

Abstract

Multiple access interference (MAI) in time-hopping (TH) ultra-wideband (UWB) systems is known to be non-Gaussian. Several statistical models have been proposed for the MAI, and based on them various nonlinear single-user receivers have been designed. In this thesis, an accurate mathematical model for the probability density function (PDF) of the MAI in TH-UWB systems is introduced. This model explains important features of the PDF of the MAI, namely impulses, singularities and the behaviour of tails. Using this model, the optimal error rate performance is obtained and the performances of other receivers are benchmarked against it. The single-user conventional matched filter (CMF) receiver is widely used in TH-UWB systems. All the nonlinear single-user receivers apply transformations on the chip correlator outputs of the CMF receiver to detect the transmitted information bit. It is proved that the output of the matched filter in the conventional UWB receiver cannot provide a sufficient decision statistic for detecting the information bits transmitted by the desired user in MAI. Finally, using multiuser detection (MUD) algorithms, several novel multiuser TH-UWB receivers are proposed which outperform all the previous single-user TH-UWB receivers.

Acknowledgements

First of all, I would like to express my gratitude to my supervisor, Dr. Norman C. Beaulieu, for his many helpful suggestions, important advice and constant encouragement during the course of my graduate study.

I also wish to express my appreciation to Dr. Chintha Tellambura for serving as one of the examination committee members. Special thanks are due to Dr. Byron Schmuland from the Department of Mathematical and Statistical Sciences for being willing to read my thesis and be my external examiner.

My keen appreciation goes to Amirmasoud Rabiei for his unconditional support and the caring he provided. I would also like to thank Mahdi Ramezani for his warm friendship. He was particularly helpful with technical issues.

My special appreciation goes to my parents, my brother and my sister, who always supported me, loved me, and encouraged me to concentrate on my study.

Finally, I would like to express special thanks to my wife Shadi for her love, patience, support, and understanding. Without her help and encouragement, this study would not have been completed.

Table of Contents

List of Figures

List of Tables

List of Abbreviations

Abbrv.	Definition	First Use
UWB	ultra wideband	1
FCC	Federal Communications Commission	1
SNR	signal-to-noise ratio	3
LPI	low probability of interception	3
LPD	low probability of detection	3
RF	radio frequency	4
MAI	multiple access interference	4
ADC	analog to digital converter	4
WPAN	wireless personal area network	5
BER	bit error rate	5
TH	time-hopping	5
PDF	probability density function	6
MAP	maximum a posteriori	6
MUD	multiuser detection	6
IR	impulse radio	7
CDMA	code division multiple access	7
OFDM	orthogonal frequency division multiplexing	7

Chapter 1

Introduction

Ultra-wideband (UWB) wireless has emerged in the very recent history of communications. Although UWB was used for positioning, military communications, radar and sensing 20 years ago, it has been focused on consumer electronics and communications only very recently. The Federal Communications Commission (FCC) has allocated 7.5 GHz bandwidth for UWB transmission opening the spectrum for commercial deployment.

The aim in many wireless systems is to bring flexible data rates and several kinds of applications to the mobile users. However, limited bandwidth is the important constraint for this goal. But, UWB systems posses almost an unlimited bandwidth, so they are allowed to coexist with current radio systems. In fact, most of the wireless communication systems use separate narrowband frequencies in order to avoid interference to each other. However, in order for UWB systems to avoid interference with other services, they have to meet the spectral mask defined in the FCC's report [3] in February 2002 which means they emit in very low level power regimes.

UWB has some distinctive features making it different from other wireless communication systems. Two unique characteristics of UWB are its large bandwidth and low duty cycle. The huge bandwidth leads to short duration pulses (pico- to nano-seconds) to carry one information bit. In fact, UWB transmits low power signals across a very wide range of frequencies instead of broadcasting high power signals on separate frequencies. Therefore, UWB transmissions appear as background noise. Because of this, UWB is dedicated to indoor applications which need high data rates communications with hundreds of Mbps to several Gbps in a very short distance of 1 to 10 meters. The duty cycle is defined as the ratio of the time

that a pulse is present to the time interval in which one pulse is transmitted; it has a very small value in practical UWB systems, around 0.005 [4, 5].

1.1 Definition

Any wireless communication technology whose fractional bandwidth is more than 20 percent or its actual bandwidth is larger than 500 MHz is called UWB based on the FCC's report [3]. The definition of fractional bandwidth, B_f, is the ratio of bandwidth at the 10 dB points to the central frequency.

$$B_f = \frac{2(f_h - f_l)}{(f_h + f_l)} \times 100\% \qquad (1.1)$$

where f_h and f_l are the upper and lower cutoff frequencies, respectively. In the FCC's report [3], UWB operation has been categorized into three groups: 1) Communication and measurement systems, 2) Vehicular radar systems and 3) Imaging systems, including ground penetrating radar, through-wall imaging, surveillance systems, and medical imaging. Here, we are mostly concerned about the spectral mask of the first group shown in Fig. 1.1. As seen, the allocated frequency spectrum for UWB transmission is from 3.1 to 10.6 GHz and the maximum allowed power level for UWB emission is -41.3 dBm/MHz. This power level is under the noise power floor for other wireless communication systems.
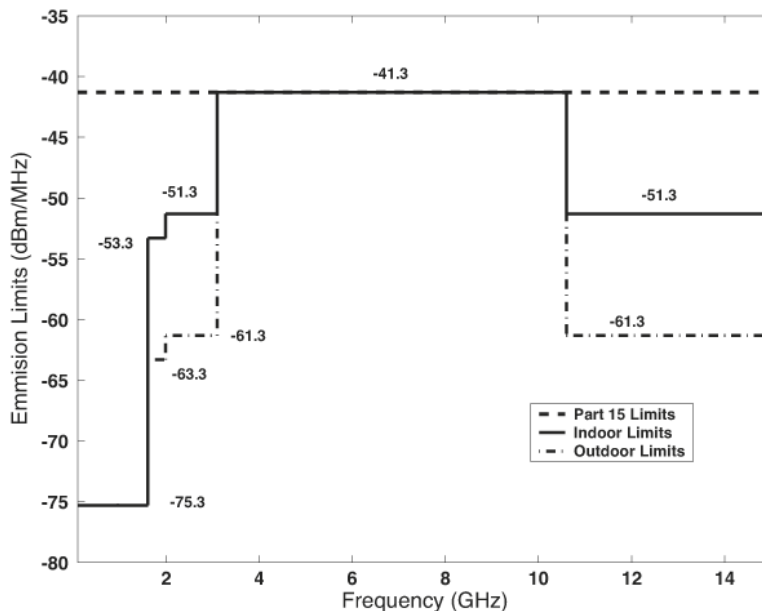
Figure 1.1: FCC allocated spectral mask.

1.2 Capacity of UWB Wireless Systems

Shannon's famous equation for capacity can give us some insights about the benefits of UWB wireless systems. According to Shannon's law, the potential capacity of a channel is written as

$$C = B \times \log_2(1 + \frac{S}{N}) \tag{1.2}$$

where S and N indicate the total signal power and noise power over the bandwidth, respectively, and B is the bandwidth of the channel. The low level transmission power of UWB systems can be seen as a drawback for the capacity of the channel; however, UWB systems have such a large bandwidth that can compensate the effect of low signal-to-noise ratio (SNR). Therefore, UWB systems are supposed to offer potentially high capacity wireless communications [5].

1.3 Benefits of UWB Systems

Although the unique feature of UWB systems is that they can take advantage of unlicensed usage of a large bandwidth in the frequency spectrum, there are numerous other advantages that make UWB systems different from conventional narrowband systems [1, 2, 5, 6]. In particular, UWB systems

✓ are able to share the frequency spectrum, so they can coexist with other services (Fig. 1.2). The FCC's power requirements require UWB systems to transmit noise-like signals, and as a result they will have a low probability of interception/detection (LPI/LPD).

✓ have the ability to trade off between the data rate and distance. Suppose that for conveying one information bit, N_s pulses are transmitted. For long link distances, in order to have a reliable transmission, N_s can be increased which results in a low data rate. On the other hand, N_s can be decreased for short distances which leads to higher data rates. Therefore, the more pulses per bit, the longer the achievable transmission distance and the lower the data rate.

✓ offer robust performances in severe multipath and jamming because of short duration pulses. This is because receivers can capture an excellent energy from the transmitted pulses due to many distinct multipath components which can be observed.

✓ have simple transmitters and receivers. UWB systems can get benefits of digital transceivers without need of radio frequency (RF) blocks such as oscillators, up-conversion and down-conversion modules. This is because of the baseband nature of UWB signals.
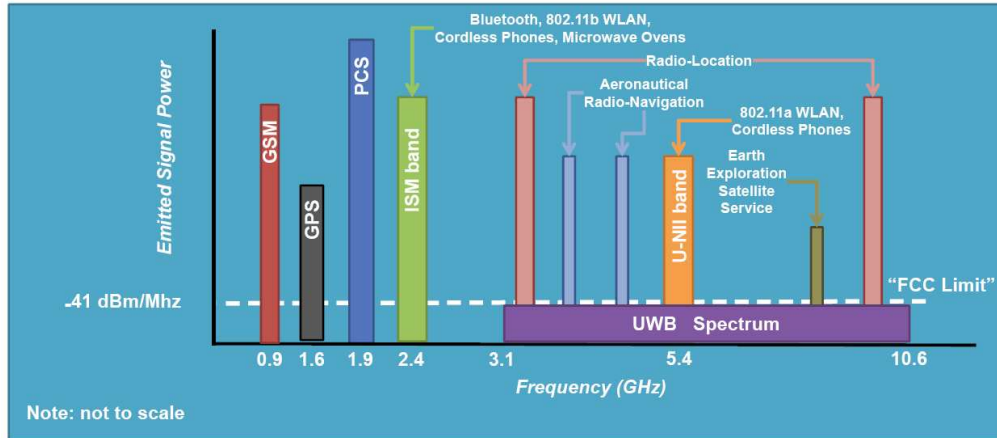
Figure 1.2: Coexistence of UWB systems with narrowband and wideband systems.

1.4 Challenges

There are many challenges emerging in use of UWB systems for wireless communications. Among them, some items are listed below [2, 4–7]:

✓ Multi-octave bandwidth antenna design

✓ Avoiding interference with other existing narrowband services

✓ Detection and cancelation of strong narrowband interferences

✓ High frequency synchronization to extremely narrow pulses

✓ Estimation of channel parameters such as multipath channel delays and coefficients

✓ Multiple accessing, multiple access code design, and multiple access interference (MAI) cancelation

✓ Adaptive, simple, low-cost and low-power transceiver design

✓ Practical limitations of analog to digital converters (ADCs)

4

1.5 Applications

Different applications from vehicular radars to wireless communications have been proposed for UWB technology. The UWB capability of material penetration allows it to be employed for medical imaging, ground penetration radars, surveillance systems and mining industries. Location finding is another important application of UWB technology. Last but not least is the wireless communication application.

Currently, there are two IEEE standards for UWB systems. IEEE 802.15.3a is associated with high data rate connectivity between a host and its peripherals in a short distance [8]. One example can be data transfer between a personal computer and devices such as mouse, printer and monitor. In summary, IEEE 802.15.3a functions as a "cable replacement" and is supposed to bring the wireless personal area network (WPAN) concept to consumers making home networking with data rates over 2 Gbps feasible. Another UWB application is for sensor networks requiring transfer rate of 50 Kbps to 1 Mbps with ranges of 100 meters as well as centimeter accuracy in positioning. Addressing this application, IEEE 802.15.4a introducing UWB applications for low data rates and moderate range wireless communications is a promising solution for such networks [9]. Hence, UWB supports a new range of applications including oil and petroleum industries, medical applications, family communications, and military uses.

1.6 Thesis Overview

There are three primary topics of interest discussed in this thesis, including bit error rate (BER) of time- hopping (TH) UWB receivers in multiuser interference, design of novel partial-multiuser TH-UWB receivers, and a low-complexity multisampling multiuser detector for TH-UWB systems.

Chapter 2 provides some basic background information on UWB systems. Two common schemes for UWB transmission are discussed. Next, various practical UWB pulses are introduced and several modulation techniques are explained. Later, multiple access algorithms such as TH and direct sequence methods are studied in impulse radio UWB systems. This chapter is concluded by introducing some basic UWB receiver designs.

Chapter 3 starts with studying the conventional matched filter receiver decision statistics. Then, the exact mathematical expressions for the probability density

function (PDF) of the MAI for some simple low-duty cycle pulses, rectangular and triangular, are obtained. It is impossible to employ these two pulses in practical UWB systems, because they cannot meet the FCC spectral emission constraints. However, the exact mathematical PDF of the MAI derived using these two pulses highlights expected features of the PDF of the MAI and explains why the Gaussian approximation fails. Then, the PDF of the MAI for a practical UWB pulse is obtained. Based on the model obtained for the PDF of the MAI and exploiting the maximum a posteriori (MAP) receiver design rule, the optimal attainable BER performance of binary TH-UWB receivers is numerically determined. The performances of some recently proposed UWB receivers are benchmarked against the optimal performance showing that some of them achieve the near-optimal performance.

It is claimed and proved in Chapter 4 that the output of the matched filter in the conventional UWB receiver cannot provide a sufficient decision statistic for detecting the information bits transmitted by the desired user. Using multiuser detection (MUD) algorithms, two novel partial-multiuser TH-UWB receivers are proposed for detecting the information bits. These partial-multiuser receivers are much less complex than corresponding MUD receivers. In terms of implementation, they employ only one matched filter instead of a bank of matched filters resulting in simple and low-cost TH-UWB receivers. Also, they outperform previous single-user TH-UWB receivers in ideal free-space propagation channels as well as multipath fading UWB channels.

Nonlinear single-user TH-UWB revivers are simple, however, all suffer from error floors, and hence limited user capacity. A thorough discussion on MUD is given in Chapter 5. We discuss the sparsity of TH-UWB signals due to the low duty cycle of TH-UWB systems and clarify the concept of effective interfering users. MUD is considered for offering high performances at the cost of complexity that grows exponentially with the number of users. Thought to be too complex for low-cost UWB receivers, MUD applied in TH-UWB systems benefits from the small number of effective interfering users. In this chapter, optimal MUD algorithms with frame-duration and pulse-duration observation times are studied, and their pros and cons are discussed. Further, a novel low-complexity multisampling multiuser detector inspired by the inferiority of single-user receivers and the small number of effective interfering users in TH-UWB systems is proposed.

Chapter 2

UWB System Model

This chapter provides an overview of UWB communication systems. Several transmission schemes for UWB systems are introduced. Then, we focus on the impulse radio (IR) UWB systems and study the practical UWB pulses, data mapping methods and spectrum spreading algorithms. Next, several basic IR-UWB receivers are described. Finally, various Rake receiver structures and some diversity combining techniques are presented.

2.1   UWB Transmission Schemes

Many different solutions may be introduced for UWB communication systems to satisfy the FCC requirements. However, there are two common schemes for UWB: multiband and IR.

The multiband approach partitions the frequency spectrum into some smaller non-overlapping bands with bandwidths greater than 500 MHz. "The idea is to utilize the UWB spectrum by transmitting multiple UWB signals at the same time which do not interfere with each other because they operate at different frequencies. To effectively fill the specified spectrum, multiple frequency bands of energy must be generated with different center frequencies and must be spaced across the spectrum" [5]. Therefore, the transmitter is able to prevent potential interference with other users, by avoiding transmission over certain bands such as IEEE 802.11a at 5 GHz. Several methods such as code division multiple access (CDMA), orthogonal frequency division multiplexing (OFDM), and direct sequence spread spectrum have been proposed for multiband modulation schemes. However, the OFDM method has been nominated for the physical layer of IEEE 802.15.3a standard. The most important criticism about OFDM-UWB scheme is its complexity due to employing fast

7

Fourier transform (FFT) blocks.

Another impressive scheme is IR-UWB. The basic idea for this method is the generation of a sequence of very short duration pulses for transferring information bits. One of the salient features of IR-UWB is the baseband intrinsic of this technique which simplifies the structure of transceivers. However, IR-UWB systems are criticized by multiband OFDM advocates because of their possible interference with other narrowband services. One of the common systems in the IR-UWB scheme is based on TH randomization techniques and binary phase shift keying (BPSK) modulation.

2.2   Multiband Scheme

Multiband modulation is one of the approaches for modulating data with UWB technology. The 7.5 GHz of the UWB spectrum is split into multiple bands with bandwidths greater than 500 MHz. In this approach, UWB pulses are not as narrow as in the IR-UWB technique. Therefore, synchronization requirements are more relaxed. There are several methods for the UWB multiband scheme. Here, we focus on the application of OFDM in the UWB systems. In fact, OFDM is a special case of multi carrier transmission where subcarriers are allowed to overlap in the frequency domain without interfering each other and hence spectral efficiency is increased. Also, OFDM is more robust against multipath interference. Moreover, OFDM offers improved performances for high data rate applications. "Unlike narrowband OFDM, the OFDM-UWB spectrum can have gaps between subcarriers" [4].

A block diagram for an OFDM system is shown in Fig. 2.1. The original serial bit stream is converted to N parallel substreams mapped by some modulation constellations to symbols $X_0, X_1, \ldots, X_{N-1}$. In fact, N symbols modulate N orthogonal
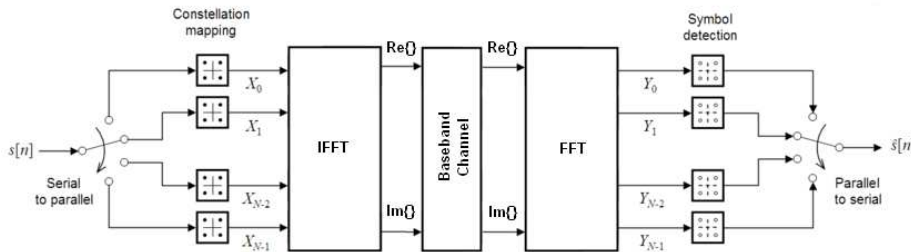
Figure 2.1: Block diagram of an OFDM transceiver.

carriers in the frequency domain. Fig. 2.2 shows the spectrum of OFDM-UWB systems. As seen, the spectrum is partitioned into some bands overlapping each other. An inverse FFT is applied to each set of symbols, providing a set of complex time domain samples. Here, we assume the baseband equivalent of the OFDM-UWB system. Therefore, the upconverter and downconverter are eliminated and the complex baseband channel is considered as the media between the transmitter and receiver. The receiver takes samples at the output of the channel and a forward FFT is used to convert the received data to the frequency domain symbols. Then, for each symbol the corresponding slicer (symbol detector) is used to convert it to information bits. A parallel to serial converter completes the receiver [1, 2, 4, 5, 7].
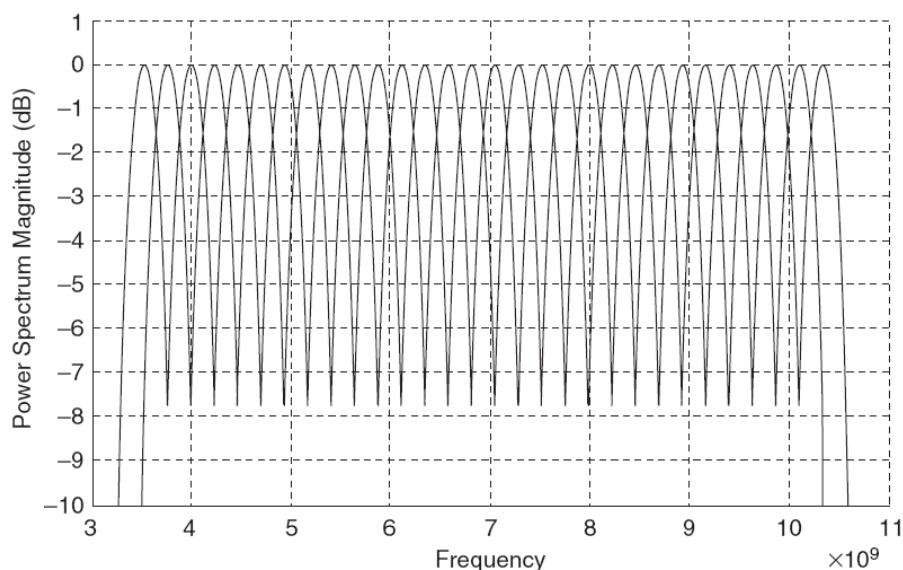
Figure 2.2: Spectrum of OFDM-UWB systems [1].

2.3   IR Pulses and Modulations

The basic model for the transmitted signal in the IR-UWB scheme can be represented as

$$s(t) = \sum_{k=-\infty}^{\infty} d_k p(t - kT_f) \tag{2.1}$$

where $p(\cdot)$ is the UWB pulse shape, d_k is the amplitude of the pulse, and T_f is the frame length. An IR-UWB pulse can be chosen from a variety of wideband pulses, such as Gaussian, Laplacian, chirp, Hermitian, wavelet, or Rayleigh. But, the most popular pulse shapes used for IR-UWB communication systems are the Gaussian

pulse and its derivatives. A Gaussian pulse is described mathematically as

$$p_{g_0} = \frac{1}{\sqrt{2\pi\sigma^2}} e^{-\frac{t^2}{2\sigma^2}} \tag{2.2}$$

where σ is the standard deviation of the Gaussian pulse in seconds. Note that the pulse duration is $2\pi\sigma$ for the Gaussian pulse. The Gaussian monocycle is the first derivative of the Gaussian pulse and is given by

$$p_{g_1} = \left(\frac{32\tau^6}{\pi} \right)^{1/4} t e^{-\tau t^2} \tag{2.3}$$

where τ is a constant determining the pulse duration. The 2nd-order Gaussian monocycle is the pulse introduced in [10]

$$p_{g_2}(t) = (1 - 4\pi(t - \tau)^2) e^{(-2\pi(t-\tau)^2)}. \tag{2.4}$$

In fact, if additional derivatives of the Gaussian pulse are taken, the relative bandwidth decreases, and the center frequency increases. Another UWB pulse shape is the Rayleigh monocycle [11], $p_r(t)$. The time domain representation of $p_r(t)$ is given by

$$p_r(t) = (t/\sigma^2) e^{-t^2/2\sigma^2}. \tag{2.5}$$

The modified Hermite pulses have been systematically applied to UWB communications in [12]. The nth order modified Hermite pulses can be expressed as

$$p_h(t) = (-\tau)^n e^{t^2/4\tau^2} \frac{d^n}{dt^n} (e^{-t^2/2\tau^2}). \tag{2.6}$$

New families of practical zero-DC time-limited UWB pulses are proposed in [13]. the even pulses of [13], $p_n^e(t)$, are expressed as

$$p_n^e(t) = \sum_{m=0}^{n} \frac{n(-1)^{(n-m)}[\frac{t}{\tau} - (\frac{n}{2} - m)]^{n-1}}{m!(n-m)!} \times u\left(\frac{t}{\tau} - \left(\frac{n}{2} - m \right) \right) \cos(2\pi f_c t) \tag{2.7}$$

where $u(\cdot)$ is the step function, f_c is the central frequency and τf_c has to be an integer value in order to generate a pulse with zero DC component. Also, pulse waveform parameters have to be selected carefully in order to have the smallest possible time duration, and to comply with the FCC spectral mask. Fig. 2.3 shows some of the practical UWB pulses as well as their autocorrelation functions (ACFs).

In order to transmit information in IR-UWB communication systems, it is necessary to modulate the sequence of pulses. Several modulation schemes may be found within IR-UWB systems including pulse position modulation (PPM), pulse amplitude modulation (PAM), on-off keying (OOK), orthogonal pulse modulation (OPM), and transmitted-reference modulation (TRM). Each data mapping scheme is briefly introduced in the following.
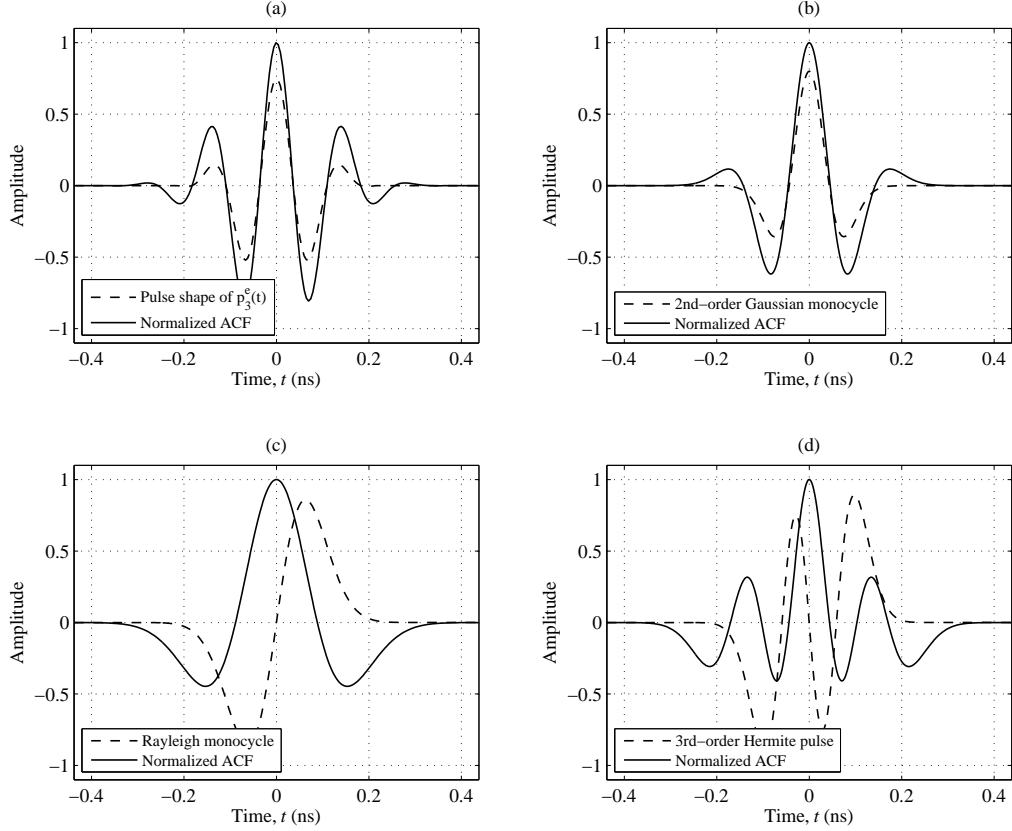
Figure 2.3: The pulse shape and the ACF of (a) $p_3^e(t)$, (b) the 2nd-order Gaussian monocycle, (c) the Rayleigh monocycle and (d) the 3rd-order Hermite pulse.

2.3.1 PPM

In PPM, the position of each pulse is varied in relation to the position of a reference time according to the bit which is transmitted. It means that for the binary PPM, one specific pulse waveform represents both bit 0 and 1, but with a shift in time domain compared to a reference point. Many positions can be used to increase the number of transmitted bits and hence we can have an M-ary PPM. The binary PPM signal can be represented as

$$s(t) = \sum_{k=-\infty}^{\infty} p(t - kT_f - \delta d_k) \tag{2.8}$$

where δ is the time shift and d_k takes values 0 and 1. In order to have orthogonal pulses in the time domain and as a result a better BER performance, δ_{opt} is chosen such that $\int_{-\infty}^{\infty} p(t)p(t - \delta_{\mathrm{opt}})dt = 0$.

2.3.2 PAM & OOK

In PAM, the information bits are carried on the amplitude of a train of pulses. Binary pulse amplitude modulation (BPAM) or, biphase modulation is the most famous form of PAM in UWB, where the positive and negative pulses are transmitted for bits 0 and 1, respectively. On the other hand, in OOK or unipolar signaling, a pulse is transmitted for the bit 1, and no pulse is transmitted for the bit 0. Although OOK is a simple pulse modulation technique, it has some drawbacks. Because of the absence of pulse for the transmission of the bit 0, time synchronization can be lost easily. Also, for a given power, the BER performance of OOK is worse than that of BPAM. The transmitted signal for OOK and BPAM is

$$s(t) = \sum_{k=-\infty}^{\infty} d_k p(t - kT_f) \qquad (2.9)$$

where d_k takes values $\{0, 1\}$ and $\{-1, 1\}$, respectively [1, 4, 5].

2.3.3 OPM

OPM which is a special case of pulse shape modulation (PSM) simply uses a set of orthogonal waveforms to transmit symbols. The advantage of OPM is that it makes an infrastructure for multiple access methods. However, it is worthy to note that OPM pulses suffer from timing jitters which cause them not to be orthogonal. The transmitted signal for the binary OPM can be written as

$$s(t) = \sum_{k=-\infty}^{\infty} (1 - d_k) p_0(t - kT_f) + (d_k) p_1(t - kT_f) \qquad (2.10)$$

where $p_0(\cdot)$ and $p_1(\cdot)$ represent two orthogonal pulse shapes and d_k takes values $\{0, 1\}$ [1,5,7]. Signals modulated by different techniques such as PPM, BPAM, OOK, and OPM are shown in Fig. 2.4. Here, the sequence of the transmitted information bits is $\{1, 0, 0, 1, 0\}$. Also, an unmodulated signal is shown for comparison.

2.3.4 TRM

TRM has recently been introduced in the field of UWB communications. This scheme does not require a very tough synchronization and is robust in multipath channels. TRM is defined as the transmission of a pair of pulses separated in time. The first and second pulses in the pair are the reference and data pulses, respectively. The reference pulse is unmodulated, so it does not carry any information. The data
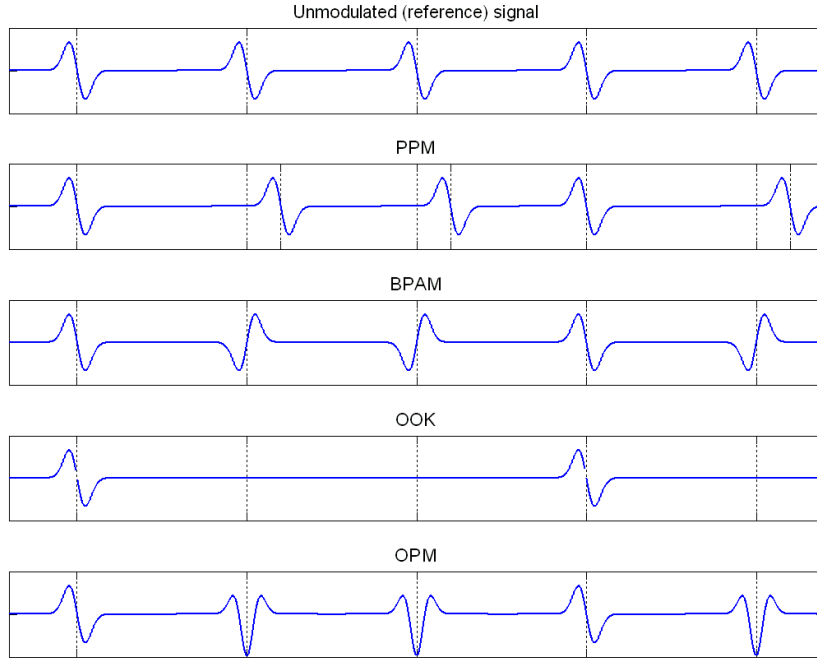
Figure 2.4: Comparison of signals modulated by different techniques with an unmodulated signal.

pulse modulated by BPAM follows the reference pulse after a certain time interval δ_{TRM}. The signal model for a TR modulated signal is written as

$$s(t) = \sum_{k=-\infty}^{\infty} p(t - kT_f) + d_k p(t - \delta_{\text{TRM}} - kT_f). \qquad (2.11)$$

We will discuss more about the benefits of TRM later, when the transmitted-reference (TR) receiver is introduced $[2, 4, 6, 7]$.

2.4 Confusion Between UWB and Spread Spectrum Systems

Many misconceptions are associated with the name of UWB. Some people do not differentiate between spread spectrum (SS) techniques and UWB. Although both approaches firstly had military applications, fundamental differences exist between them. Therefore, we briefly introduce two SS technologies to clarify their differences with the UWB technology.

2.4.1　Direct Sequence Spread Spectrum

In direct sequence spread spectrum (DSSS) systems, the pulses being transmitted
are multiplied by a "noise" signal. This noise signal is a pseudo random code of
0 and 1 values which is used to spread each pulse with a large number of chips
to a larger bandwidth required to transmit the original signal. Note that the chip
interval is much smaller than the pulse interval.

Fig. 2.5 shows a DSSS system. Here, the chip interval is a quarter of the pulse
interval. The sequence multiplied by the bit 0 is 0110 while the sequence multiplied
by the bit 1 is 1001. Multiplying the pulses with the shorter duration chips in the
time domain results in a spread of power in the frequency domain. If the DSSS
system is designed appropriately, the level of spread power can be the same as
narrowband receivers' noise floor which is hard to detect and is suitable for military
applications. In order to transmit data, each of the chips in the transmitted signal
is modulated with conventional narrowband techniques [1, 2, 5].
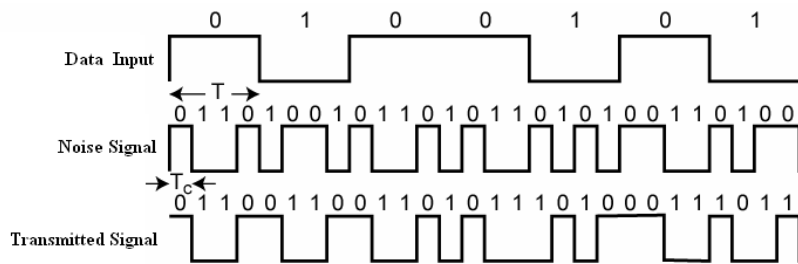
Figure 2.5: An example of a transmitted signal using the DSSS technique.

2.4.2　Frequency Hopping Spread Spectrum

Frequency hopping spread spectrum (FHSS) systems exactly like DSSS systems
try to spread the signal power in the frequency domain. For each transmission,
FHSS chooses a carrier frequency among available bandwidth according to a pseudo
random code known to both transmitter and receiver. Fig. 2.6 shows the signal
hops from one frequency to another one. Due to the rapid change in the carrier
frequency, detection becomes very difficult for those who do not have the pseudo
random code [2].
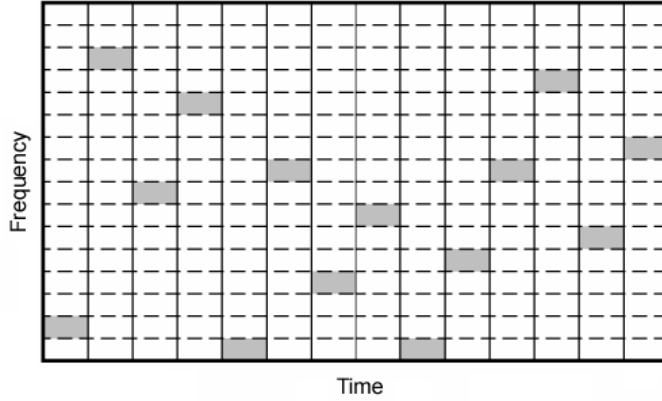
Figure 2.6: Frequency hopping in the FHSS technique.

2.4.3 Major Distinctions Between UWB and SS Technologies

Both UWB and SS technologies offer a spread in frequency domain giving several advantages over usual narrowband communications. But, the main difference is how to achieve the large bandwidth. In SS technologies, eventually the signals are modulated with a carrier frequency. But, the short duration UWB pulses have a wide bandwidth and often do not need to be modulated with a carrier frequency. Here, two questions arise: how large is the bandwidth in the UWB and SS technologies? And how much power do they use for transmission? UWB pulses usually present several gigahertz of bandwidth which is 10 times greater than what SS techniques can offer. On the other hand, SS technologies use more transmission power in comparison with UWB technology. Therefore, SS systems are more suitable for a long distance transmission [2, 4].

2.5 Spectrum Spreading Methods in UWB Systems

Generation of short duration pulses causes strong lines in the power spectral density (PSD) of the transmitted signal which can interfere with other communication systems. Therefore, some randomization techniques such as TH and direct sequence (DS) are applied to IR-UWB systems in order to reduce the power of those spectral spikes. Furthermore, TH-UWB and DS-UWB methods give multiple access capability to UWB systems. Randomization is typically realized in IR-UWB systems by pseudo random sequences. The spectrum of an UWB pulse train with and without randomizing techniques is depicted in Fig. 2.7. It is seen that the envelope of the spectrum is that of a single pulse [2, 4–7].

15
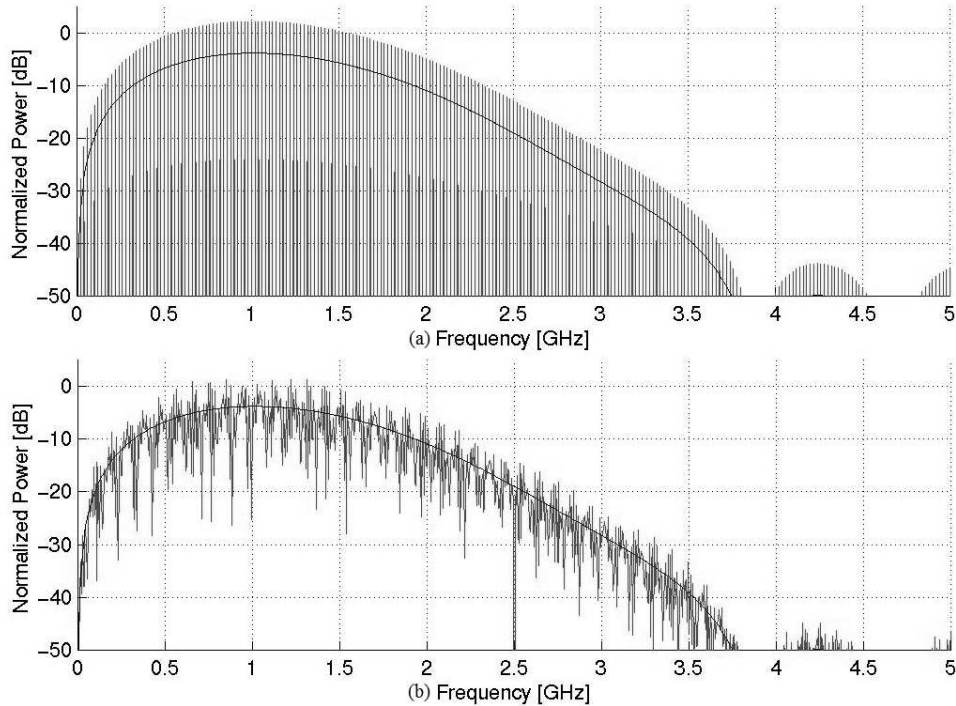
Figure 2.7: Comparison of the spectrum of an UWB pulse train (a) with and (b) without randomizing techniques.

2.5.1 DS-UWB

DS-UWB uses short duration UWB pulses combined with well-known DSSS technique to transmit and receive information. In the case of UWB systems, the pulse waveform acts like the chip in the DSSS technique. The DS-UWB approach can be used for PAM, OOK and PSM modulation schemes. PPM modulation is basically a TH technique since the position of the pulse in a transmission slot determines which data bit was transmitted. DS-UWB combined with PPM modulation forms a hybrid DS/TH structure for the signal and exploits benefits of both TH and DS techniques [1, 6, 7].

2.5.2 TH-UWB

In TH-UWB, a pseudo random code defines the pulse transmission instant. One data bit can be carried by N_s pulses. Therefore, by changing the number of pulses employed to carry a single information bit, the data rate of the transmission can be selected. Almost all the modulations discussed earlier can be used in the TH-UWB approach except OOK. This is because synchronization would be more problematic

in case of using TH-UWB. In the next section, we will introduce a TH-BPSK UWB system model and in the rest of this thesis this model will be used.

2.6 TH-BPSK UWB System Model

The asynchronous TH-BPSK UWB systems are considered in previous studies [10, 14, 15]. Using the same notation, the signal transmitted from the generic user in a TH-UWB system with BPSK modulation can be expressed as

$$s^{(n)}(t) = \sqrt{\frac{E_b}{N_s}} \sum_{k=-\infty}^{\infty} d_{\lfloor \frac{k}{N_s} \rfloor}^{(n)} p(t - kT_f - c_k^{(n)} T_c) \tag{2.12}$$

where the model parameters are described as follows:

✓ Symbol $d_{\lfloor \frac{k}{N_s} \rfloor}^{(n)}$ is the $\lfloor \frac{k}{N_s} \rfloor$th binary data symbol transmitted by the nth user, selected from the set $\{-1, +1\}$ with equal probabilities.

✓ The function $p(t)$ is the transmitted UWB pulse shape with duration T_p, and energy $\int_{-\infty}^{-\infty} p^2(t)dt = 1$. For the sake of simplicity and without loss of generality, it is assumed that $p(t)$ is non-zero in the range $[-T_p/2, T_p/2]$ and takes value zero outside of this range. The ACF of $p(t)$ is defined as

$$R_p(x) = \int_{-\infty}^{-\infty} p(t)p(t - x)dt. \tag{2.13}$$

✓ N_s is the number of pulses required for transmitting one information bit and E_b is the total energy of all N_s pulses.

✓ The chip duration and the frame duration are denoted by T_c and T_f, respectively. It is assumed that the chip duration, T_c, is at least twice larger than pulse duration, T_p. The bit duration, T_b, is defined as $N_s T_f$ which is the time that takes to transmit one information bit.

✓ $c_k^{(n)}$ is a TH pseudo-random code for the kth frame of the nth user. Each element of the hopping code takes an integer value in the range $0 \leq c_k^{(n)} < N_h$ and N_h satisfies the condition $N_h T_c \leq T_f$.

In practical TH-UWB systems, the duty cycle, D, which is defined as the fraction of time in the frame that a pulse is present, i.e.,

$$D = \frac{T_p}{T_f} \tag{2.14}$$

is usually less than 0.5 percent [2].

Here, an example is given to make the system model more clear. Suppose there are 3 users transmitting 2 pulses per one information bit, i.e., $N_s = 2$, and the number of chips per frame is 5, i.e., $N_h = 5$. For clarification, different time periods such as T_p, T_c, T_f, and T_b are shown in Fig. 2.8. Also, the data bits and pseudo-random sequences of each user are presented in Table 2.1.
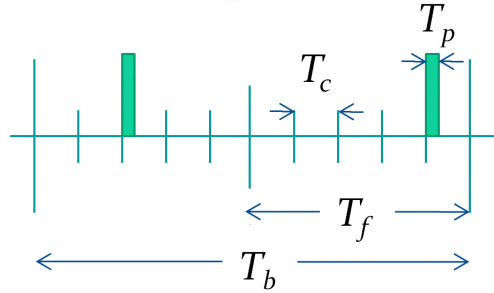
Figure 2.8: An example of different time durations in TH-UWB systems.

Table 2.1: Data bits and pseudo-random sequences of 3 users.

	Data bits	Pseudo-random TH codes
User 1	(0, 1, 1)	(0, 1, 3, 0, 2, 4)
User 2	(1, 0, 1)	(1, 3, 0, 4, 3, 2)
User 3	(1, 1, 0)	(4, 2, 3, 2, 3, 3)

The transmitted signals for different users in the time domain are drawn in Fig. 2.9. The red, green and blue rectangles represent pulses transmitted by user 1, 2 and 3, respectively to carry 3 information bits.
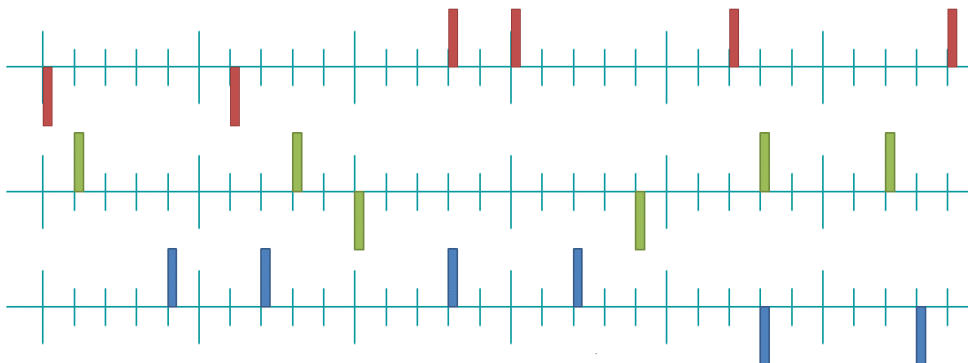
Figure 2.9: Transmitted signals by 3 different users in a TH-UWB system.

When N_u users transmit asynchronously on an additive white Gaussian noise (AWGN) channel in the same coverage area, the received signal can be written as

$$r(t) = \sum_{n=0}^{N_u-1} A^{(n)} s^{(n)}(t - \tau^{(n)}) + n(t) \qquad (2.15)$$

where $\{A^{(n)}\}_{n=0}^{N_u-1}$ and $\{\tau^{(n)}\}_{n=0}^{N_u-1}$ represent the channel attenuation and asynchronous delay of the nth user, respectively. The random variables $\{\tau^{(n)}\}_{n=0}^{N_u-1}$ are assumed to be uniformly distributed on a bit duration $[0, T_b]$ [16]. The random process $n(t)$ is a zero-mean AWGN process with two-sided PSD $\sigma^2 = N_0/2$.

2.7 Basic IR-UWB Receiver Structures

This section provides a review of some basic IR-UWB receiver structures designed for several modulation schemes. The choice of modulation method at the transmitter has direct influence on design parameters in UWB systems such as data rate, resistance to interference and noise, PSD of the transmitted signal, and transceiver complexity. In designing receivers, we always attempt to come up with an optimal solution in the sense of minimizing the probability of bit error. But, feasibility, cost, size, complexity, and power consumption of receivers are also important design concerns. In this section, first we introduce energy detectors which are simple receivers mostly used for detecting OOK modulated signals. Then, classical matched filter receivers are discussed. Finally, TR receivers are examined to reveal advantages of the TRM.

2.7.1 Energy Detectors

Energy detectors also known as threshold/leading edge detectors are simple suboptimal noncoherent IR-UWB receivers, which demodulate OOK modulated signals. In fact, the receiver decides which data bit was transmitted based on the amplitude level of the received energy and a threshold. The intersection of PDFs corresponding to energies for data bit 0 and 1 can be the optimum threshold. However, sometimes, noise spikes can be detected as a data pulse. Therefore, if the receiver monitors the input noise signal, it can adaptively set the threshold to mitigate the problem of false detection. As shown in Fig. 2.10, the received signal enters a squaring module. Then, the output of this module is integrated over the interval of the pulse duration. After sampling the output of the integrator, a decision threshold comparator decides if the signal is present or not.
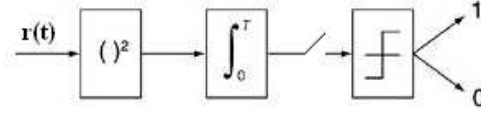
Figure 2.10: Block diagram of an energy detector [2].

Generally, energy detectors have very poor performances; however, they have simple implementations and require only coarse synchronization making them robust against the clock jitter [2, 4, 6, 7].

2.7.2 Classical Matched Filter Receivers

The conventional matched filter receiver is an optimal method for detecting a signal in random noise based on the correlation process. A block diagram of a matched filter receiver is shown in Fig. 2.11. The received signal is multiplied by a template waveform matched to the transmitted signal and integrated over the interval of pulse duration. This process maximizes the SNR of the incoming signal. Large samples of the integrator's output represent strong resemblance between the received and template waveforms, while small values close to zero represent low similarity between the two. Although these receivers are optimal in the presence of AWGN, they are suboptimal when the signal is distorted by MAI or narrowband interference, that do not have AWGN features [2, 4, 6, 7].
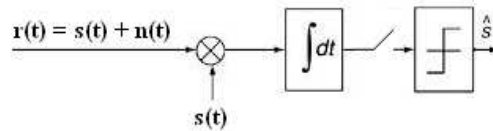
Figure 2.11: Block diagram of a matched filter receiver [2].

2.7.3 TR Receivers

A TR receiver uses the correlation method similar to the classical matched filter receivers. But the main difference is that the correlation is performed between the received signal and its delayed version instead of a predefined pulse waveform. Therefore, each reference pulse is a template for its corresponding data pulse. So, the spacing, δ_{TRM}, has an important role in the receiver performance. "One of the benefits of this receiver is that it can capture the entire signal energy for a slowly varying channel without requiring channel estimation" [6]. However, it may have

a bad performance if the received reference signal is too noisy resulting in poor demodulation. Fig. 2.12 shows the structure of the TR receiver. It is obvious that shifting the received signal by δ_{TRM} units in time is necessary to align the reference pulse with the data pulse in each symbol.
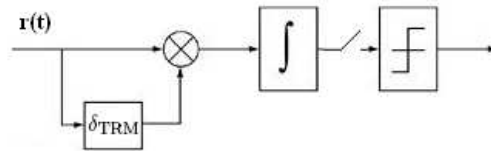
Figure 2.12: Block diagram of a TR receiver [2].

Note that the transmitter using TRM transmits the same pulse twice through an unknown channel. Therefore, both of the pulses are distorted by almost the same channel. Now, the receiver correlates the similarly distorted data and reference pulses which are highly correlated rather than correlating the distorted received pulse with a clean template. And hence, detection with a TR receiver becomes easier. Moreover, a TR receiver is self-synchronized. That means each reference pulse is like a preamble for the data pulse, providing rapid synchronization. Another interesting phenomenon about the TR receiver is that it exploits the propagated signals to improve its performance. In fact, multipath channel produces a longer duration signal and because the TR receiver correlates the reference and data pulses with each other, more signal energy can be captured at the output of the integrator.

The TRM is not all about advantages. One of the drawbacks of the TRM is that two pulses must be transmitted for one information bit. Therefore, more power is needed and also data rate decreases. Also, the fixed space between reference and data pulses can cause undesired spikes on the spectrum of the TR-modulated UWB signals [2, 4, 7].

2.8 Rake Receivers

"Wireless channel suffers from multipath, where reflections and other effects of the channel cause multiple copies of the transmitted pulse to appear at the receiver" [5]. But, the received signal energy can be improved in a multipath channel by utilizing a time diversity technique, such as employing a Rake receiver. The Rake receiver consists of multiple fingers. Each finger has a matched filter which is synchronized to one of the multipath components of the signal. Outputs of matched filters are com-

bined using some techniques such as absolute combining (AC), equal gain combining (EGC), and maximum ratio combining (MRC). Although combination of different signal components will increase the SNR in the Rake receiver, the complexity and cost also increase. Here, we discuss three popular types of Rake receivers. Also, various diversity combining techniques are briefly studied [1, 4–6].

2.8.1 Ideal Rake Receivers

If we assume that a multipath channel has L different paths, the received signal $r_{\mathrm{multipath}}(t)$ can be written as

$$r_{\mathrm{multipath}}(t) = \sum_{n=1}^{L} \gamma_n p(t - \lambda_n) + n(t) \tag{2.16}$$

where γ_n and λ_n are the gain and the delay of the nth path, respectively. The ideal Rake (I-Rake) receiver, also known as the all Rake receiver, captures all the power of the received signal by having a number of fingers equal to L. In practice, the problem is that the I-Rake receiver needs too many fingers and as a result too many matched filers. Nonetheless, if the MRC is used as the diversity combining technique, a performance close to the performance of the AWGN channel will be achieved. But for using the MRC scheme, some channel estimation methods must be employed to obtain the amplitude of each path [1, 4–7].

2.8.2 Selective Rake Receivers

In practice, it is impossible to have an infinite number of fingers in a receiver. Therefore, a more practical implementation of Rake receivers would be the selective Rake (S-Rake) receiver which only employs the S paths of the multipath channel with the highest power. The complexity of the S-Rake receiver is relatively lower than the I-Rake receiver. However, the receiver must use channel estimation methods in order to detect the strongest paths. Similar to the I-Rake receiver, in the S-Rake receiver, the SNR is maximized and performance is improved in comparison with a matched filter receiver [1, 7].

2.8.3 Partial Rake Receivers

A simplified version of the I-Rake receiver is the partial Rake (P-Rake) receiver which selects the first P paths of the multipath channel. The idea behind this selection is that usually the first propagation paths are the strongest paths in the

multipath channels. On the other hand, this is the disadvantage of the P-Rake receiver, because the first paths do not necessarily contain the most power of the signal [1, 7].

2.8.4 Diversity Combining Techniques for the Rake Receivers

Several diversity combining techniques can be used in the Rake receivers [1, 4]. These methods are divided into coherent and noncoherent groups. If the phases of the channel paths are used, the method is called coherent, otherwise it is noncoherent. The best scheme which is coherent and is proved as the optimal combiner for independent AWGN channels is the MRC scheme. Considering the received signal $r_{\text{multipath}}(t)$ defined in Section 2.8.1 the MRC decision statistic can be written as

$$Z_{\text{MRC}} = \sum_{L=1}^{n} \gamma_n^* \int_0^{T_p} r_{\text{multipath}}(t - \lambda_n)p(t)dt. \tag{2.17}$$

Another coherent scheme is EGC which adds all the received signals coherently. The EGC decision statistic can be written as

$$Z_{\text{EGC}} = \sum_{L=1}^{n} e^{-j\angle \gamma_n} \int_0^{T_p} r_{\text{multipath}}(t - \lambda_n)p(t)dt. \tag{2.18}$$

AC is one of the non-coherent schemes which adds the absolute values of the outputs of all the matched filters to get the decision statistic.

$$Z_{\text{AC}} = \sum_{L=1}^{n} \left| \int_0^{T_p} r_{\text{multipath}}(t - \lambda_n)p(t)dt \right|. \tag{2.19}$$

An advanced implementation of AC uses the amplitude of each path to improve the performance of the system. This method is very similar to MRC, but it does not need to know the phase information. The decision statistic of this method can be mathematically described as

$$Z = \sum_{L=1}^{n} \left| |\gamma_n| \int_0^{T_p} r_{\text{multipath}}(t - \lambda_n)p(t)dt \right|. \tag{2.20}$$

Chapter 3

MAI in TH-BPSK UWB Systems

The correlation receiver or conventional matched filter (CMF) maximizes the SNR at the output of receiver and therefore minimizes the probability of error in the presence of Gaussian noise. These receivers are widely employed for detecting IR-UWB signals [10,14–16] and they may perform well in MAI environments when the MAI is, to some degree of precision, approximated by a Gaussian random variable due to the well known central limit theorem (CLT). However, the MAI in UWB systems is known to be non-Gaussian and modeling the PDF of the MAI in an UWB system by a Gaussian process underestimates the BER performance of the system [17,18].

Several works have proposed more appropriate non-Gaussian statistical models for the MAI and derived nonlinear receivers that outperform the linear CMF receiver. In [19], a nonlinear soft-limiting receiver and its enhanced successor, namely, the adaptive threshold soft-limiting receiver are implemented based on a Laplacian model for the PDF of MAI. The Laplacian model is proposed due to the fact that the distribution of the MAI in IR-UWB systems has impulsive attributes. Both of these receivers outperform the CMF receiver in the presence of MAI and absence of Gaussian noise. However, in the presence of both MAI and Gaussian noise, only the performance of the adaptive version of the soft-limiting receiver is always equal to or better than that of the CMF receiver. Another receiver dubbed the "zonal" receiver has been discussed in [20]. This receiver is designed based of the following observation. It is possible to find lower and higher thresholds, t_l and t_h, such that if the correlator output falls outside $(-t_h, -t_l)$ and (t_l, t_h), it is unreliable to decide the information bit as $+1$ or -1. This is because the probabilities of the

correlator output being outside the mentioned intervals given information bit $+1$ or -1 is transmitted, are small and almost the same. For each value of SNR and signal-to-interference ratio (SIR), effective thresholds, t_l and t_h, can be determined in the receiver design phase; this receiver always performs equal to or better than the CMF receiver. The MAI can also be characterized by a Gaussian mixture model (GMM). In this model, the assumption is that total interference is a stochastic process with PDF which is given by a weighted sum of zero-mean Gaussian PDFs with assigned variances [21, 22]. Also, three different methods based on nonparametric estimation, the generalized Gaussian distribution and the α-stable distribution have been introduced in [23] to estimate the distribution of the MAI.

In [24], a receiver named the "p-order metric" receiver and its more advanced version, the p-order metric adaptive threshold limiting receiver, are designed based on the assumption that the PDF of the MAI can be well approximated by a generalized Gaussian distribution. A myriad filter detector was recently proposed in [25]. This new receiver is based on a symmetric α-stable model for the MAI. Some other methods for approximation of the PDF of the MAI can be found in [26–29].

While several improved TH-UWB receiver designs have been found, it is desirable to know how much further the performance can be improved. To avoid wasted efforts, it is crucial to obtain the optimal benchmark against which the performances of other receivers can be measured. The performance of the optimal, minimum BER, receiver for TH-UWB systems achieved using the MAP rule is the best attainable benchmark. However, knowledge of the PDF of the MAI is necessary to use the MAP rule. In this chapter, we construct a model which fully uncovers the salient features of the PDF of the MAI in TH-UWB systems. These features, which can be precisely anticipated by the proposed model include impulses, singularities, and the tail behaviour in the distribution of the MAI. The model reveals in quantitative terms why a Gaussian approximation for the MAI in TH-UWB systems is highly imprecise even in an environment with a large number of independent interferers. Applying the model to a realistic UWB system and employing the MAP rule, the optimal error rate performance can be determined using numerical results and simulation. Also, the proposed model will help us to understand why some UWB receivers such as the p-order metric receiver [24] and myriad filter detector [25] track the optimal receiver closely.

3.1 CMF Receiver Decision Statistics

Recall the system model introduced in Section 2.6. A correlator is used to detect a single desired user at the receiver. Consider that the mth user is the desired user to be detected. Without loss of generality, we can assume that $\tau^{(m)} = 0$ and $c_k^{(m)} = 0$ for all values of k [15]. The decision statistic of a correlation receiver which detects the 0th transmitted symbol of the mth user can be written as

$$R = \sum_{k=0}^{N_s-1} \int_{kT_f}^{(k+1)T_f} r(t)p(t - kT_f)dt = \sum_{k=0}^{N_s-1} R_k$$

$$= \sum_{k=0}^{N_s-1} S_k + I_k + N_k = \sum_{k=0}^{N_s-1} S_k + Y_k \tag{3.1}$$

where the signal component, S_k, in (3.1) is given by $A^{(m)}d_0^{(m)}\sqrt{E_b/N_s}$, and $Y_k = I_k + N_k$. N_k denotes the filtered Gaussian noise with variance $(N_0/2)$. I_k is the total MAI experienced by the kth pulse of the mth user resulting from the $N_u - 1$ other users. The time shift between the desired user and the other users can be represented by [29]

$$\tau^{(n)} - \tau^{(m)} = m_n T_f + \beta_n \tag{3.2}$$

in which m_n is an integer value, and β_n is the fractional part which is modeled by a random variable uniformly distributed on $[-T_f/2, T_f/2]$. Then, I_k can be expressed as

$$I_k = \sqrt{E_b/N_s} \sum_{\substack{n=1 \\ n \neq m}}^{N_u} \int_{kT_f}^{(k+1)T_f} A^{(n)} d_{\lfloor \frac{k-m_n}{N_s} \rfloor}^{(n)} p(t - kT_f) \times$$

$$p(t - \tau^{(n)} - (k - m_n)T_f - c_{(k-m_n)}^{(n)}T_c)dt. \tag{3.3}$$

Recall the ACF defined in (2.13). Considering the fact that $p(t)$ has non-zero values in the range $[-T_p/2, T_p/2]$ and assuming $T_p \ll T_f$, which means that the duration of UWB pulses is effectively limited to one frame, the limits of integration in (2.13) can be modified from $(-\infty, \infty)$ to $(-T_f/2, T_f/2)$ and ACF can be given by

$$R_p(x) = \int_{-T_f/2}^{T_f/2} p(t)p(t - x)dt. \tag{3.4}$$

Hence, when N_u asynchronous transmitters are active in a system, the interference corrupting each individual pulse can be concisely modeled by

$$I_k = \sum_{n=1}^{N_u-1} A^{(n)} b^{(n)} R_p(\alpha_n) = \sum_{n=1}^{N_u-1} I^{(n)} \tag{3.5}$$

26

where b_n is a binary random variable which takes values $\{-1, +1\}$ with equal probabilities and α_n is a random variable uniformly distributed on $[-T_f/2, T_f/2]$. Here, without loss of generality E_b is assumed to be equal N_s. The partial interference components are assumed to be statistically independent. This model is applied with some simple pulses in the next section to show some specific and significant characteristics of the PDF of MAI in TH-UWB systems.

3.2 The PDF of the MAI for Simple Pulses

In order to disclose significant features of the distribution of the MAI, two simple low-duty cycle pulses, rectangular and triangular, are employed. These two pulses are not suitable for practical UWB systems because they do not meet the FCC spectral emission restrictions. However, in our study here, we are able to derive the precise mathematical PDF of the MAI for these pulses, enabling prediction of features of the PDF of the MAI and explaining the failure of the Gaussian distribution to approximate the MAI.

3.2.1 Rectangular Pulse

Assume that the rectangular pulse shape is defined as

$$p(t) = u(-|t| + T_p/2) \text{ where } u(t) = \begin{cases} 0, & t < 0 \\ 1, & t \geq 0 \end{cases} \tag{3.6}$$

and the ACF can be obtained as

$$R_p(x) = \begin{cases} x + T_p, & -T_p < x < 0 \\ -x + T_p, & 0 \leq x < T_p \\ 0, & T_p \leq |x|. \end{cases} \tag{3.7}$$

The rectangular pulse shape and its ACF are shown in Fig. 3.1.
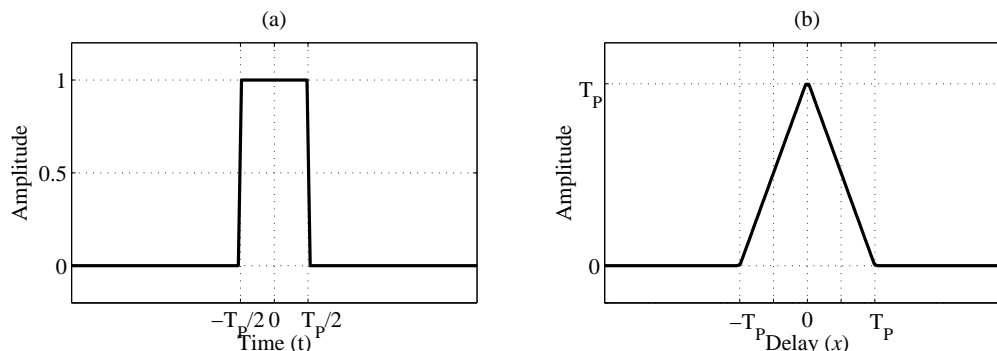
Figure 3.1: The (a) rectangular pulse shape and (b) its ACF.

Considering the uniform distribution of α_n and for constant $A^{(n)}$, we can accurately derive the PDF of $I^{(n)}$ by using the fundamental theorem for transformation of a random variable [30]. It can be written as

$$f_{I^{(n)}}(i) = \frac{1}{A^{(n)}T_f} u\left(-\left|\frac{i}{A^{(n)}}\right| + T_p\right) + \frac{(T_f - 2T_p)}{T_f}\delta(i) \qquad (3.8)$$

in which $\delta(i)$ is the impulse function. The PDF of $I^{(n)}$ for the rectangular pulse shape is depicted in Fig. 3.2.
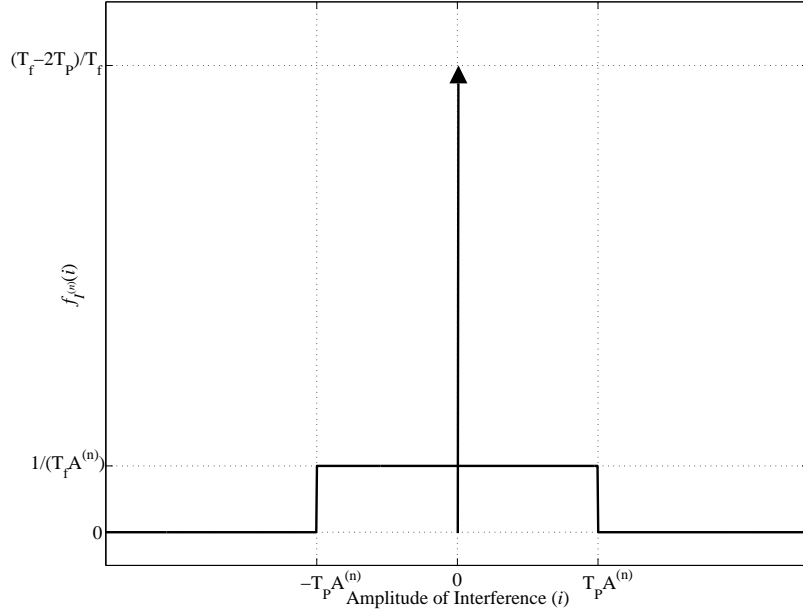
Figure 3.2: The PDF of the MAI for rectangular pulse shape (1 interferer).

Having the PDF of $I^{(n)}$, the characteristic function can be easily expressed as

$$\Phi_{I^{(n)}}(\omega) = E[e^{jI^{(n)}\omega}] = \left(\frac{2T_p}{T_f}\frac{sin(\omega A^{(n)}T_p)}{(\omega A^{(n)}T_p)} + \frac{T_f - 2T_p}{T_f}\right). \qquad (3.9)$$

The characteristic function of a sum of statistically independent random variables is equal to the product of the characteristic functions of the summands. Therefore, the characteristic function of I_k is

$$\Phi_{I_k}(\omega) = E[e^{jI_k\omega}] = E[e^{j\omega \sum_{n=1}^{N_u-1} I^{(n)}}] = \prod_{n=1}^{N_u-1} \left(\frac{2T_p}{T_f}\frac{sin(\omega A^{(n)}T_p)}{(\omega A^{(n)}T_p)} + \frac{T_f - 2T_p}{T_f}\right)$$

$$= \left(\frac{T_f - 2T_p}{T_f}\right)^{N_u-1} + \Phi_{\text{Tail}}(\omega) \qquad (3.10)$$

where $\Phi_{\text{Tail}}(\omega)$ contains all of the terms resulting from the expansion of $\Phi_{I_k}(\omega)$ except the term $\left((T_f - 2T_p)/T_f\right)^{N_u-1}$. According to the relationship between the

28

characteristic function and the PDF of a random variable, one should note that a constant value in the characteristic function corresponds to an impulse at the origin in the PDF of the random variable. Therefore, the constant $\left((T_f - 2T_p)/T_f\right)^{N_u-1}$ in (3.10) implies an impulse at the origin in the PDF of I_k. Considering the low-duty cycle of UWB pulses, i.e., $(T_f - 2T_p)/T_f \approx 1$, it is observed in (3.10) that almost all the mass of the PDF of I_k is captured in the impulse located at amplitude value zero. It is for this reason that the PDF does not converge to a Gaussian distribution in practical systems with a small or even moderately large number of users. The second term shows that the interference can take values from the finite range $(-T_p \sum_{n=1}^{N_u-1} A^{(n)}, +T_p \sum_{n=1}^{N_u-1} A^{(n)})$ clarifying the tail behaviour of the MAI.

Fig. 3.3 shows the PDF of the MAI for rectangular pulse shape for 3 and 15 interferers. In this example, it is assumed that the transmission powers of all the interferes are equal and D is chosen to equal 1 percent. As seen, by increasing the number of interferers, the amplitude of the impulse at the origin decreases. Also, the tails of the PDF of the MAI get heavier. This suggest that by having a very large number of users the PDF of the MAI might converge to a Gaussian shape. However, the operational area of an UWB system is a circle whose radius is on the order of 10 meters. For this range of coverage, the likely maximum number of users that can be served by the system is, say, between 10 to 20.
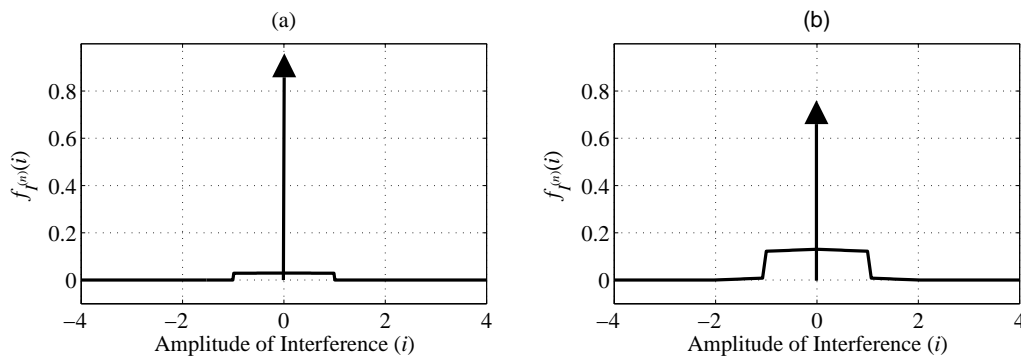
Figure 3.3: The PDF of the MAI for rectangular pulse shape ((a) 3 interferers, and (b) 15 interferers).

3.2.2 Triangular Pulse

In this section, a triangular pulse is considered as the UWB pulse shape. Then, $p(t)$ is written as

$$p(t) = \begin{cases} +\frac{2t}{T_p} + 1, & -\frac{T_p}{2} \le t < 0 \\ -\frac{2t}{T_p} + 1, & 0 < t < \frac{T_p}{2} \end{cases} \tag{3.11}$$

and the ACF is

$$
y = R_p(x) = \begin{cases}
\frac{2(x+T_p)^3}{3T_p^2}, & -T_p < x < -\frac{T_p}{2} \\
\frac{-(6x^3+6T_px^2-T_p^3)}{3T_p^2}, & -\frac{T_p}{2} \leq x < 0 \\
\frac{6x^3-6T_px^2+T_p^3}{3T_p^2}, & 0 \leq x \leq \frac{T_p}{2} \\
\frac{2(-x+T_p)^3}{3T_p^2}, & \frac{T_p}{2} < x < T_p \\
0, & |x| \geq T_p.
\end{cases} \tag{3.12}
$$

The triangular pulse shape and its ACF are shown in Fig. 3.4. Also, the points at which the ACF has derivative zero are marked.
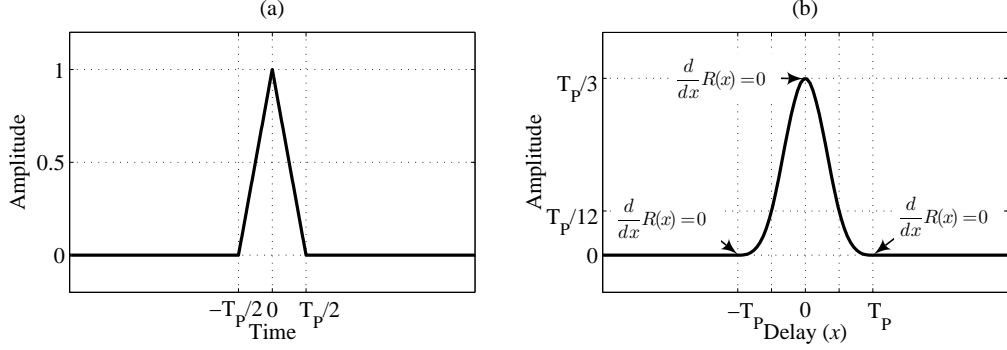
Figure 3.4: The (a) triangular pulse shape and (b) its ACF.

Now, in order to apply the fundamental theorem [30] to derive the PDF of $I^{(n)}$, it is required to find the inverse of $R_p(x)$ which can be defined in two regions as $R_{p1}^{-1}(\cdot)$ and $R_{p2}^{-1}(\cdot)$

$$
R_p^{-1}(y) = \begin{cases}
R_{p1}^{-1}(y) = \pm\left(0.5\sqrt[3]{12yT_p^2} - T_p\right), & 0 < y \leq \frac{T_p}{12} \\
R_{p2}^{-1}(y) = \frac{\pm 1}{3}\left(\frac{Z}{4} + \frac{T_p^2}{Z} + T_p + j\sqrt{3}\left(\frac{Z}{4} - \frac{T_p^2}{Z}\right)\right), & \frac{T_p}{12} < y \leq \frac{T_p}{3}
\end{cases} \tag{3.13a}
$$

where

$$
Z = \sqrt[3]{10T_p^3 - 54yT_p^2 + 6\sqrt{T_p^6 - 30yT_p^5 + 81y^2T_p^4}}. \tag{3.13b}
$$

Therefore, given $A^{(n)}$ and considering the uniform distribution of α_n, the PDF of $I^{(n)}$ is expressed as

$$
f_{I^{(n)}}(i) = \frac{T_p^2}{T_fA^{(n)}} \underbrace{\frac{u\left(-\left|\frac{i}{A^{(n)}}\right| + \frac{T_p}{3}\right) - u\left(-\left|\frac{i}{A^{(n)}}\right| + \frac{T_p}{12}\right)}{6\left(R_{p2}^{-1}\left(\left|\frac{i}{A^{(n)}}\right|\right)\right)^2 - 4\left|R_{p2}^{-1}\left(\left|\frac{i}{A^{(n)}}\right|\right)\right|T_p}}_{h(i)}
$$

$$
+ \frac{T_p^2}{T_fA^{(n)}} \frac{u\left(-\left|\frac{i}{A^{(n)}}\right| + \frac{T_p}{12}\right)}{\sqrt[3]{18\left(\frac{i}{A^{(n)}}T_p^2\right)^2}} + \frac{(T_f - 2T_p)}{T_f}\delta(i). \tag{3.14}
$$

30

The PDF of $I^{(n)}$ for the triangular pulse shape is depicted in Fig. 3.5. It is observed that the PDF of $I^{(n)}$ not only has an impulse located at amplitude value zero, but also contains three singularities at amplitude values, 0, $-T_p A^{(n)}/3$ and $T_p A^{(n)}/3$. The impulse at the origin originates for the same reason explained for the rectangular pulse. The singularities are located at points where the derivative of the ACF is zero and the locations can be obtained by equating the term $h(i)$ to zero. The origin of the singularities is the following. In the fundamental theorem for transformation of a random variable $(Y = g(X))$, one has [30]

$$f_y(y) = \frac{f_x(x_1)}{|g'(x_1)|} + \frac{f_x(x_2)}{|g'(x_2)|} + \cdots + \frac{f_x(x_n)}{|g'(x_n)|} \tag{3.15}$$

where $y = g(x_1) = g(x_2) = \cdots = g(x_n)$ and $g'(\cdot)$ is the derivative of $g(\cdot)$. Then, a zero of $g'(\cdot)$ will cause a singularity in the PDF of Y. These singularities are seen for the case of the triangular pulse. Note that these singularities are not seen for the rectangular pulse because its ACF does not have any point whose derivative is zero. The PDF of the sum of the interferers is obtained by convolving the PDFs of the individual interferers. The PDF of the total MAI which is the sum of $N_u - 1$ interferences inherits some singularities from the PDF's of each of the interferences.
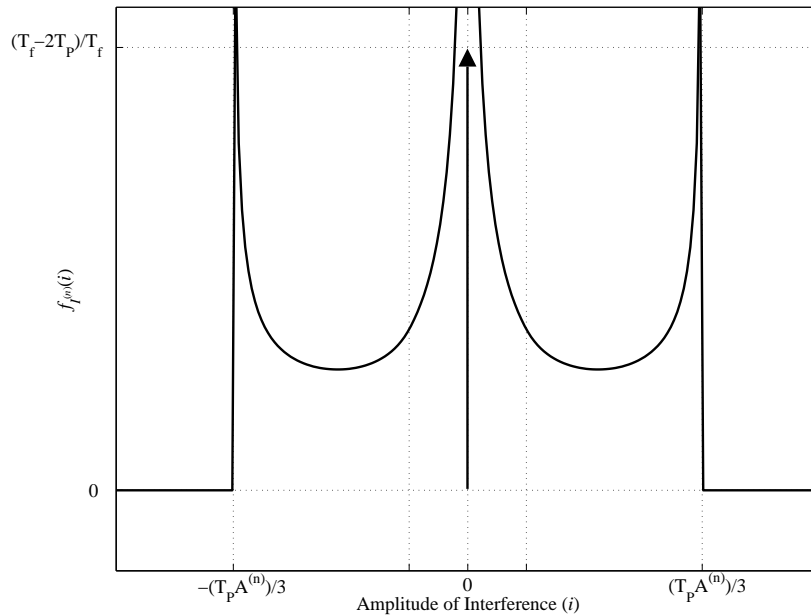
Figure 3.5: The PDF of the MAI for triangular pulse shape (1 interferer).

3.3   The PDF of the MAI for Practical UWB Pulses

One of the even pulses of [13] defined in (2.7) is employed to obtain the results using our model for practical UWB systems. According to [13], we choose $f_c = 6.85$ GHz, $\tau = 1/f_c = 0.146$ ns and $n = 3$. Since these pulses are even, the ACF can be easily obtained as

$$R_p(x) = p_n^e(t) * p_n^e(t) = \mathcal{F}^{-1}\left\{(P_n^e(f))^2\right\} \tag{3.16}$$

where convolution is represented by $*$, the inverse Fourier transform is denoted by $\mathcal{F}^{-1}\{\cdot\}$, and $P_n^e(f)$ is the Fourier transform of $p_n^e(t)$ obtained in [13]. The PDF of $I^{(n)}$ can be computed numerically based on the inverse of $R_p(x)$. Then, using convolution, the PDF of I_k can be computed from $I^{(n)}$. One should note that τf_c has to be an integer value in order to generate a pulse with zero DC component. The pulse $p_3^e(t)$ and its ACF are depicted in Fig. 3.6. Also, the points at which the ACF has derivative zero are marked.
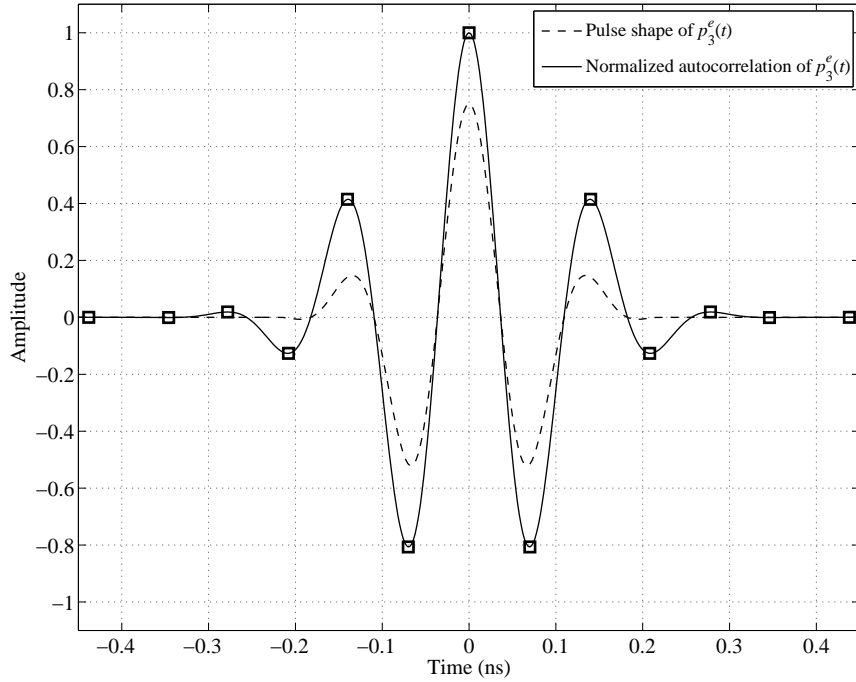
Figure 3.6: The pulse shape and the ACF of $p_3^e(t)$. The squares highlight the points at which the derivative of $R_p(x)$ is zero.

We are interested in the specific shape of the PDF of the MAI. Hence, by means of simulation, the PDF of the I_k for 15 interferers has been found and is shown in Fig. 3.7. Here, we have assumed that the transmission powers of all the users are equal, i.e., $A^{(n)} = 1$ for all values of n, and D is chosen to equal 1 percent.

32

An impulse at the origin, singularities and bounded tails are observed in Fig. 3.7. One should note that the values of total interference at which the sum interference has derivative zero result in the singularities in the PDF of the MAI. For comparison, the Gaussian, the Laplacian, the generalized Gaussian and the symmetric α-stable distribution are also plotted in Fig. 3.7. It is observed that a normal PDF is not a good approximation even when there is a moderately large number of interferers in the TH-UWB system. The existence of the impulse at the origin is the most important reason for the failure of the Gaussian approximation; because of this, the PDF of the MAI does not converge to the normal distribution for even tens of interferers. Although the Laplacian model approximates the PDF of the MAI better than the Gaussian model, both the generalized Gaussian and symmetric α-stable distribution better approximate the PDF of the MAI.
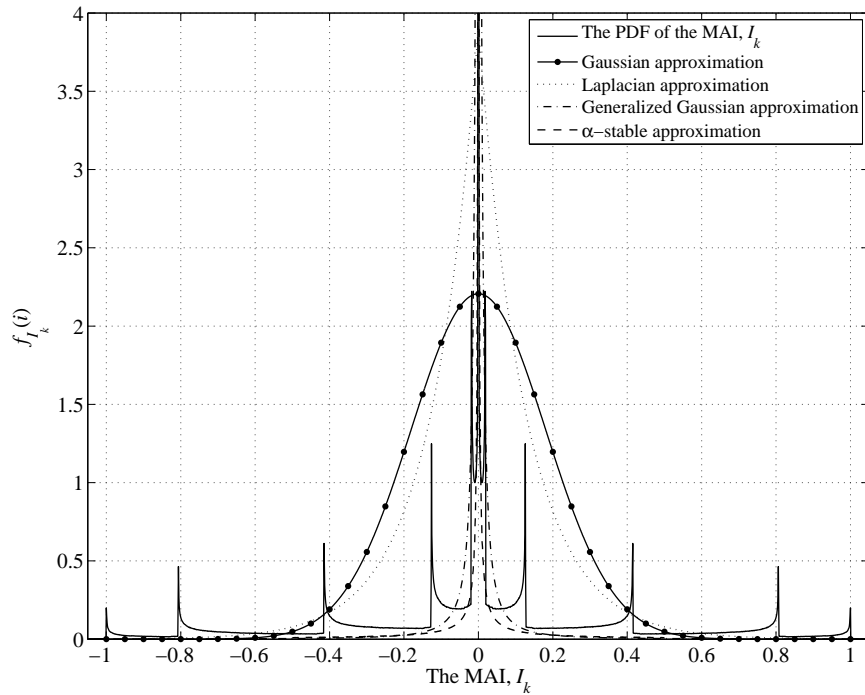
Figure 3.7: The PDF of the MAI for the practical TH-UWB pulse, $p_3^e(t)$, for 15 interferers. The Gaussian, the Laplacian, the generalized Gaussian and the symmetric α-stable approximation are shown for comparison.

3.4 The Optimal UWB Receiver Performance

The MAP receiver rule is used for the optimum detector in a TH-BPSK UWB system. Suppose that $r_0, ..., r_{N_s-1}$ are the partial correlator outputs for N_s pulses

transmitted to convey the 0th information bit. Considering our model in Section 2.6, the receiver decides $d_0^{(m)} = 1$ if

$$f\left(d_0^{(m)} = 1 | r_0, ..., r_{N_s-1}\right) > f\left(d_0^{(m)} = -1 | r_0, ..., r_{N_s-1}\right) \qquad (3.17)$$

where $f(\cdot | r_0, ..., r_{N_s-1})$ represents the conditional PDF of each of the transmitted information bits given the correlator outputs; otherwise, it decides $d_0^{(m)} = -1$. Assuming that $d_0^{(m)}$ takes values $\{-1, +1\}$ with the same probability, (3.17) can be simplified as

$$\sum_{k=0}^{N_s-1} \log\left(\frac{f_{R_k|D}\left(r_k | d_0^{(m)} = 1\right)}{f_{R_k|D}\left(r_k | d_0^{(m)} = -1\right)}\right) > 0 \qquad (3.18)$$

where $f_{R_k|D}(r_k | \cdot)$ denotes the conditional PDF of the correlator output when each of the information bits is transmitted. Now, using the knowledge of the PDF of the noise and MAI, (3.18) can be written as

$$\sum_{k=0}^{N_s-1} \log\left(\frac{f_{Y_k}(r_k - S_k)}{f_{Y_k}(r_k + S_k)}\right) > 0 \qquad (3.19)$$

where $f_{Y_k}(\cdot)$ denotes the PDF of the sum of noise and MAI. If we consider the case when the noise term is negligible, it is possible to employ $f_{I_k}(\cdot)$ instead of $f_{Y_k}(\cdot)$.

The performance of the optimum receiver for a TH-BPSK UWB system is obtained using numerical methods and simulation, and is compared with the performances of the CMF receiver, hard-limiting receiver [19], soft-limiting receiver [19], zonal receiver [20], p-order metric receiver [24] and myriad filter detector [25]. The pulse shape $p_3^e(t)$ is employed and all the pulse shape parameters are the same as in Section 3.3 except that D is equal to 2.92 percent. Using a larger value of D enables a very long but feasible simulation time. The number of interferers is either 7 or 15. Two types of simulations are considered. In the first case, we consider a TH-UWB system in the absence of AWGN and the BER as a function of SIR is plotted. Then, we compare the performances of different receivers in the presence of both AWGN and MAI with the optimum performance. All users transmit with equal power and all the simulations have been done with 10^6 bits.

3.4.1 The BER versus SIR

Assume that AWGN noise is ignored. The optimum attainable performance as well as the BER curves for the different receivers for $N_u = 8$ and 16 are depicted in Figs. 3.8 and 3.9, respectively. Dashed and solid lines indicate $N_s = 3$ and 5, respectively.

It can be seen that by increasing N_s all the receivers perform better except the CMF receiver which performs worse for smaller values of SIR. It is observed that the myriad filter detector and p-order metric receiver outperform all the other receivers. In fact, they track the optimal receiver closely, although there still is a small gap between the performances of these two receivers and the optimal performance. The important reason for the superiority of these receivers is that the PDF of the MAI is well approximated by the generalized Gaussian and α-stable distribution. As observed in Fig. 3.9, to achieve BER $= 10^{-3}$, for $N_s = 5$ the optimal receiver requires about 1.1 dB less SIR compared to the p-order metric receiver for $N_u = 16$.

In order to obtain the optimum performance, first the PDF of the MAI is computed and then signal detection is implemented using (3.19). For the myriad filter detector, the characteristic function of the α-stable distribution is fitted to the empirical characteristic function of the MAI and then the parameters of the α-stable distribution are found. To implement the decision rule of the myriad filter detector, the value of K^2 is calculated according to [25, Eq. (12)]

$$K^2 = \zeta^{\frac{2}{\alpha}} \left(\frac{\alpha}{2 - \alpha} \right) + C_e \sigma^2 \tag{3.20}$$

where ζ and α denote the scaling and the shaping parameters of the α-stable dis-
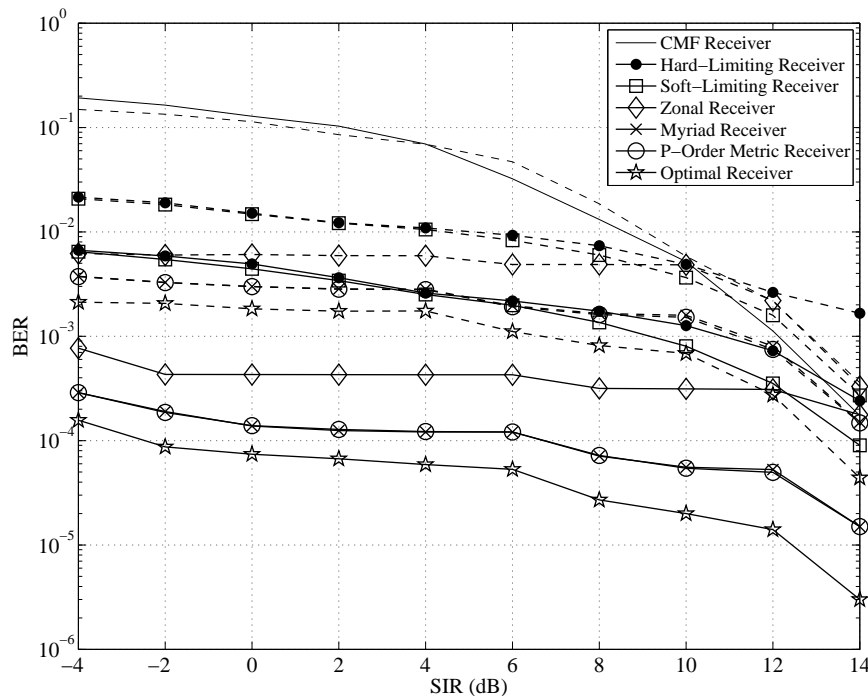
Figure 3.8: The BER versus SIR for 7 asynchronous interferers for the CMF, hard-limiting, soft-limiting, zonal, p-order metric, myriad filter detector and optimal receivers.

35
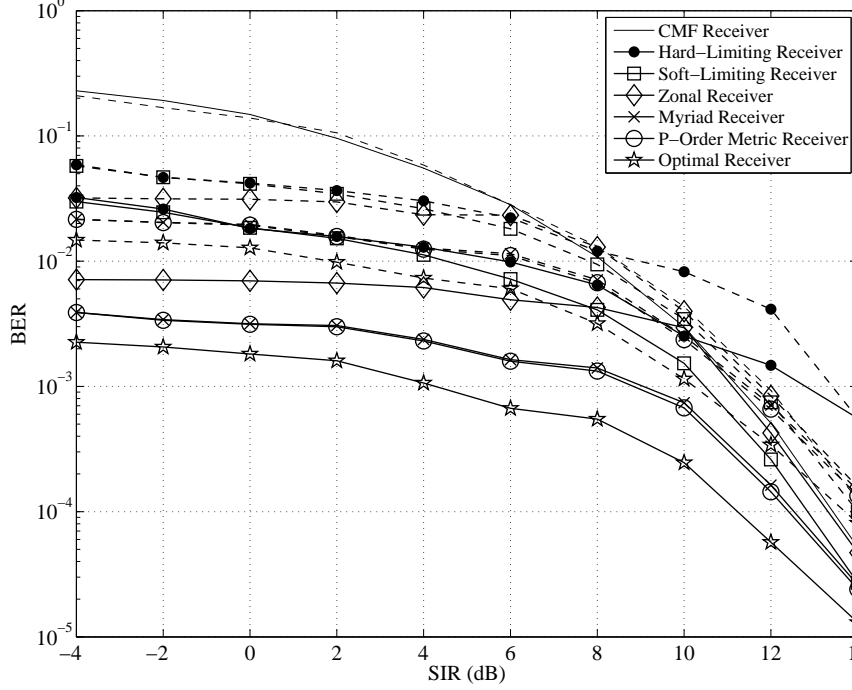
Figure 3.9: The BER versus SIR for 15 asynchronous interferers for the CMF, hard-limiting, soft-limiting, zonal, p-order metric, myriad filter detector and optimal receivers.

tribution model and $C_e\sigma^2$ accounts for the AWGN noise. For $N_u = 8$ and 16, the parameters of the myriad filter detector are shown in Table 3.1. For the zonal re-

Table 3.1: Parameters of the myriad filter detector

	ζ	α	C_e(Noiseless Channel)	C_e(AWGN Channel)
$N_u = 8$	0.2070	0.0964	0	10^{-17}
$N_u = 16$	0.4436	0.0964	0	10^{-10}

ceiver, near-optimal thresholds are computed and shown in Table 3.2 for each value of SIR and the transmitted symbols are detected using lower and higher thresholds. The value of p for the p-order metric receiver is chosen to equal 0.1 based on the results in [24].

3.4.2 The BER versus SNR

Now, we consider that both AWGN and MAI are present. In this simulation, we set $N_s = 5$ and $N_u = 8$. For each value of SIR, the PDF of the MAI is obtained. Also, for each value of SNR the variance of the noise is calculated and the PDF of the normal distribution is computed. Then, $f_{Y_k}(\cdot)$ is computed by convolving the PDF

Table 3.2: Near-optimal thresholds of the zonal receiver for different values of SIR

	SIR(dB)	−4	−2	0	2	4
Thresholds (t_l/t_h)	$N_u = 8, N_s = 3$	0.050/0.096	0.051/0.116	0.071/0.141	0.038/0.167	0.064/0.194
	$N_u = 8, N_s = 5$	0.040/0.063	0.052/0.080	0.066/0.098	0.059/0.126	0.060/0.155
	$N_u = 16, N_s = 3$	0.014/0.135	0.029/0.164	0.036/0.198	0.104/0.247	0.156/0.305
	$N_u = 16, N_s = 5$	0.041/0.109	0.053/0.132	0.028/0.144	0.044/0.193	0.277/2.077
	SIR(dB)	6	8	10	12	14
Thresholds (t_l/t_h)	$N_u = 8, N_s = 3$	0.146/0.265	0.023/0.349	0.034/0.404	0.235/3.084	0.386/3.209
	$N_u = 8, N_s = 5$	0.154/0.189	0.166/0.258	0.209/0.325	0.244/0.379	0.000/2.836
	$N_u = 16, N_s = 3$	0.059/0.377	0.000/2.687	0.229/2.634	0.120/2.736	0.267/2.955
	$N_u = 16, N_s = 5$	0.202/0.297	0.208/0.368	0.000/1.747	0.330/1.650	0.277/2.077

of the noise and the MAI, and signal detection is implemented using (3.19) to obtain the optimal performance. The value of p for each value of SNR is a near-optimal value selected from Table I in [24]. The values of the zonal receiver thresholds are shown in Table 3.3 for different SNR and SIR values. Also, Table 3.1 shows the parameters of the myriad filter detector.

The BER versus SNR curves for SIR = 5 and 10 dB are shown in Figs. 3.10 and 3.11. One may note that for large values of SNR, the BER curves reach an error floor which is due to the MAI which is present. It is seen that both the myriad filter detector and the p-order metric receiver achieve performances which are close to the optimum performance, and the myriad filter detector outperforms slightly the p-order metric receiver. It is observed in Fig. 3.11 that the error floor of an optimal receiver is lowered to $\frac{1}{3}$ of the error floor of the myriad filter detector.

Some discussion of the practicality and specification of the simulations is warranted. All the simulations have been performed under the Linux operating system on a network of 5 IBM computers interconnected with total processing power of 10.9 GHz and memory of 10 GBytes. In order to be accurate in finding the optimum performance, the PDF of the MAI has to be obtained precisely, i.e., the locations of singularities have to be specified with a high resolution. On the other hand, increasing the resolution results in greater statistical variation in the empirical PDF of the MAI for a given simulation time. Therefore, to achieve a smooth distribution, more trials are required. In our simulation, the resolution is 10^{-4} and the PDF of the MAI is obtained using 10^{10} trials. When all 5 computers are employed, this type
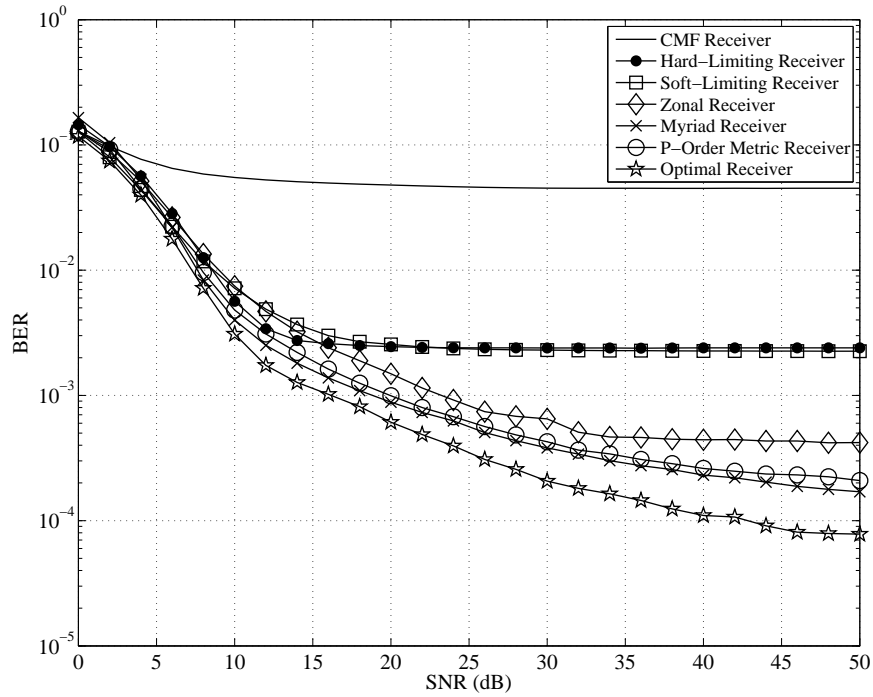
Figure 3.10: The BER versus SNR of the nonlinear single-user and optimal receivers for SIR = 5 dB and 7 asynchronous interferers.
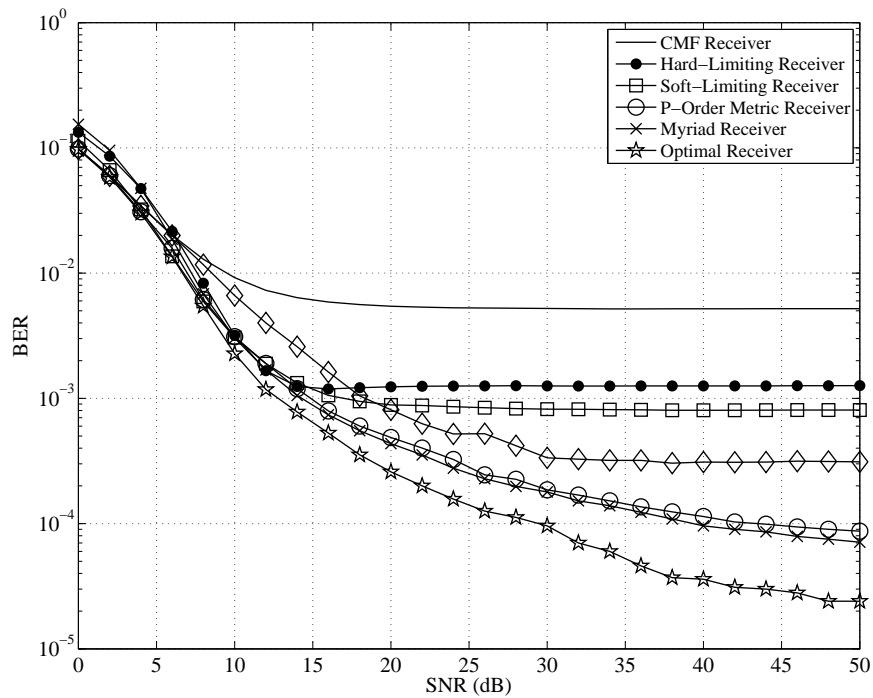
Figure 3.11: The BER versus SNR of the nonlinear single-user and optimal receivers for SIR = 10 dB and 7 asynchronous interferers.

Table 3.3: Near-optimal thresholds of the zonal receiver for different values of SNR

	SNR(dB)	0	2	4	6	8
t_l/t_h	SIR = 5 dB	0.000/1.845	0.006/0.671	0.017/0.503	0.011/0.403	0.006/0.369
	SIR = 10 dB	0.000/3.281	0.015/3.281	0.015/3.281	0.000/1.789	0.015/0.656
	SNR(dB)	10	12	14	16	18
t_l/t_h	SIR = 5 dB	0.000/0.319	0.006/0.302	0.000/0.268	0.000/0.252	0.017/0.235
	SIR = 10 dB	0.015/0.570	0.015/0.492	0.045/0.453	0.045/0.453	0.104/0.415
	SNR(dB)	20	22	24	26	28
t_l/t_h	SIR = 5 dB	0.000/0.218	0.000/0.218	0.000/0.201	0.011/0.201	0.000/0.201
	SIR = 10 dB	0.134/0.415	0.134/0.376	0.134/0.376	0.149/0.376	0.149/0.337
	SNR(dB)	30	32	34	36	38
t_l/t_h	SIR = 5 dB	0.022/0.185	0.011/0.185	0.034/0.185	0.034/0.183	0.034/0.180
	SIR = 10 dB	0.164/0.337	0.179/0.328	0.149/0.343	0.164/0.337	0.149/0.337
	SNR(dB)	40	42	44	46	48
t_l/t_h	SIR = 5 dB	0.034/0.177	0.034/0.176	0.034/0.176	0.034/0.176	0.034/0.176
	SIR = 10 dB	0.134/0.337	0.164/0.337	0.164/0.337	0.164/0.337	0.164/0.337

of simulation for finding the PDF of the MAI for 15 interferers takes approximately 13 days to be completed.

In order to obtain the optimum performance in UWB multipath channels, the optimum performance of a TH-UWB system must be obtained over approximately 100 different channel realizations and then the average performance is computed [31]. Considering just one channel realization, the optimum rake receiver structure has to be designed with a number of fingers, namely, L. Then, the L-dimensional PDF must be obtained through computer simulation to find the optimum achievable performance. Therefore, for each channel realization, definitely more than 13 days is required to complete the simulation and simulating the system for 100 channel realizations would take more than 1300 days. Consequently, finding the optimum performance in multipath channels is currently not feasible.

3.5 Conclusion

In this chapter, an accurate mathematical model explaining important features of the PDF of the MAI in TH-UWB systems namely impulses, singularities and the behaviour of tails, was derived. Using the model and the MAP receiver design rule,

the performance of an optimal receiver for single user detection in TH-UWB systems was obtained. The performances of several nonlinear UWB receivers were compared to each other and to the optimal benchmark. It was found that the p-order metric receiver and the myriad filter detector outperform all the other receivers and their performances are near the optimal performance.

Chapter 4

Novel Partial-Multiuser TH-UWB Receiver Structures

The MAI in TH-UWB systems has been studied in many works [15–18,28] and it has been shown that MAI cannot be accurately modeled by a Gaussian process. This fact suggests that Gaussian approximation for the PDF of the MAI in TH-UWB underestimates the BER performance of the system. Instead, several appropriate statistical models such as the Laplacian distribution [19], generalized Gaussian distribution [32,33], and α-stable distribution [25] have been introduced for approximating the PDF of the MAI. Based on these models, different single-user nonlinear TH-UWB receivers have been proposed, achieving better performances compared to the performance of the CMF receiver [19,20,24,25,32–37]. Therefore, the CMF receiver is not necessarily the optimal structure in multiuser TH-UWB systems.

One should note that similar to the CMF receiver, chip correlator outputs are employed as the decision statistics for all of aforementioned single-user nonlinear receivers. However, for each receiver, a nonlinear transformation is applied to the chip decision statistics in order to better detect which bit was transmitted. In this chapter, we claim and prove that the output of the matched filter in the conventional TH-UWB receiver cannot provide a sufficient decision statistic for detecting the information bits transmitted by the desired user in multiuser interference. Further, we study sufficient decision statistics which are required for multiuser detection (MUD) algorithms in TH-UWB systems [38]. Exploiting concepts from the theory and algorithms of MUD, two novel partial-multiuser receivers are introduced that employ only one matched filter. However, the complexity of these receivers is significantly less than that of corresponding MUD algorithms. All the TH-UWB single-user receivers are outperformed by these two receivers in both ideal free-space propagation

channels and real UWB multipath channels. Simulation results show that one of the partial-multiuser receivers performs close to the performance of the CMF receiver operating in a single-user system in ideal free-space propagation channels.

4.1 Sufficiency of the Decision Statistic of the CMF Receiver

Considering the system model discussed in Section 2.6, it is understood that there exist N_u users transmitting asynchronously on the UWB channel. In this section, without loss of generality, we first simplify the system model as well as the mathematical expression for the decision statistic of a correlation receiver. Then, the insufficiency of the decision statistics of the CMF receiver is proved.

4.1.1 System Model Simplification

Assume that the 0th user is the desired user. Without loss of generality, it is assumed that $\tau^{(0)} = 0$ and $c_k^{(0)} T_c = T_f/2$ for all values of k [15]. For sake of simplicity, two new random variables are defined. Let N_{uk} denote the number of collisions experienced by the desired user's pulse in the kth frame which can take values in the range $[0, N_u - 1]$. Note that T_c is at least twice larger than T_p. So, if a pulse of a user collides with the desired users pulse, the previous and the next pulses of the same user cannot interfere with the desired pulse. Therefore, in each frame, because of the asynchronous transmission, the interference on the desired user's pulse can result from at most $(N_u - 1)$ different full or partial pulses from other users.

Also, the new random variable $\theta_k^{(j)}$ is defined as the delay of the jth interfering pulse relative to the desired user's pulse in the kth frame where $j = 0, 1, \cdots, N_{uk}$. The random variable $\theta_k^{(0)}$ denotes the delay of the desired users pulse with itself, which is obviously equal to 0. Moreover, all the variables $\theta_k^{(j)}$ for $j = 1, \cdots, N_{uk}$ satisfy $|\theta_k^{(j)}| \leq T_p$ and are assumed to be uniformly distributed on $[-T_p, T_p]$. Recalling that $p(t)$ only takes non-zero values in the range $[-T_p/2, T_p/2]$, the observation time in the kth frame can be limited to $[\alpha_k = kT_f + (T_f - T_p)/2, \beta_k = kT_f + (T_f + T_p)/2]$ and the received signal in this interval can be expressed as

$$r_k(t) = \sqrt{\frac{E_b}{N_s}} \sum_{j=0}^{N_{uk}} A_k^{(j)} b_k^{(j)} p(t - kT_f - T_f/2 - \theta_k^{(j)}) + n_k(t) \qquad (4.1)$$

where the amplitude and the information bits of the jth interfering pulse in the kth frame are represented by $A_k^{(j)}$ and $b_k^{(j)}$. Also, the noise signal in this interval

is denoted by $n_k(t)$. In order to further simplify the notation, $p(t - kT_f - T_f/2)$ is denoted by $p_k(t)$. Then, (4.1) can be rewritten as

$$r_k(t) = \sqrt{\frac{E_b}{N_s}} A_k^{(0)} b_k^{(0)} p_k(t) + i_k(t) + n_k(t) \tag{4.2a}$$

where

$$i_k(t) = \sqrt{\frac{E_b}{N_s}} \sum_{j=1}^{N_{uk}} A_k^{(j)} b_k^{(j)} p_k(t - \theta_k^{(j)}). \tag{4.2b}$$

Using a correlator to detect a single desired user at the receiver, the decision statistic in the kth frame is given by

$$R_k = \int_{\alpha_k}^{\beta_k} r_k(t) p_k(t) dt = S_k + I_k + N_k \tag{4.3}$$

in which the signal component, S_k, is $A_k^{(0)} b_k^{(0)} \sqrt{E_b/N_s}$. The noise component, N_k, and the interference component, I_k, represent the filtered Gaussian noise and the total MAI experienced by the desired user's pulse from the N_{uk} pulses of other users in the kth frame, respectively. Recalling the definition of the ACF from Section 2.6, I_k can be simplified as

$$I_k = \sqrt{\frac{E_b}{N_s}} \int_{\alpha_k}^{\beta_k} \sum_{j=1}^{N_{uk}} A_k^{(j)} b_k^{(j)} p_k(t - \theta_k^{(j)}) p_k(t) dt = \sqrt{\frac{E_b}{N_s}} \sum_{j=1}^{N_{uk}} A_k^{(j)} b_k^{(j)} R_p(\theta_k^{(j)}). \tag{4.4}$$

The decision statistic, R_k, given by the correlator can be considered as the projection of the received signal in each frame, $r_k(t)$, on the time shifted UWB pulse shape, $p_k(t)$. Therefore, the signal $r_k(t)$ in (4.2a) can be written as

$$\begin{aligned} r_k(t) &= S_k p_k(t) + i_k(t) + n_k(t) \\ &= S_k p_k(t) + I_k p_k(t) + i_k'(t) + N_k p_k(t) + n_k'(t) \\ &= R_k p_k(t) + i_k'(t) + n_k'(t) \end{aligned} \tag{4.5}$$

where $i_k'(t) = i_k(t) - I_k p_k(t)$ and $n_k'(t) = n_k(t) - N_k p_k(t)$ denote the interference and noise terms orthogonal to $p_k(t)$, respectively. In order for R_k to be a sufficient decision statistic, it must be independent of $n_k'(t) + i_k'(t)$ [39]. In the following subsections, it is shown that the noise term falling outside of the signal space, $n_k'(t)$, is independent of R_k; however, this is not true for the interference term, $i_k'(t)$, which proves the insufficiency of the CMF receiver.

4.1.2 Correlation Between the Decision Statistic and the Noise Term

We first investigate the correlation between R_k and $n'_k(t)$, which is given by

$$\mathbb{E}[n'_k(t)R_k] = \mathbb{E}[n'_k(t)(S_k + N_k + I_k)]$$
$$= \mathbb{E}[n'_k(t)]S_k + \mathbb{E}[n'_k(t)N_k] + \mathbb{E}[n'_k(t)]\mathbb{E}[I_k] \qquad (4.6)$$

in which $\mathbb{E}[\cdot]$ represents expectation. The terms $n'_k(t)$ and I_k are independent due to their physically independent origins. Also, the signal component S_k is deterministic due to the determinism of $p_k(t)$. So, it can be taken out of the expectation operator. The noise component N_k is Gaussian with mean and covariance obtained by

$$\mathbb{E}[N_k] = \int_{\alpha_k}^{\beta_k} \mathbb{E}[n_k(t)]p_k(t)dt = 0 \qquad (4.7)$$

$$\mathbb{E}[N_k^2] = \int_{\alpha_k}^{\beta_k} \int_{\alpha_k}^{\beta_k} \mathbb{E}[n_k(t)n_k(\tau)]p_k(t)p_k(\tau)dtd\tau$$
$$= \frac{1}{2}N_0 \int_{\alpha_k}^{\beta_k} \int_{\alpha_k}^{\beta_k} \delta(t-\tau)p_k(t)p_k(\tau)dtd\tau$$
$$= \frac{1}{2}N_0 \int_{\alpha_k}^{\beta_k} p_k(t)p_k(t)dt = \frac{1}{2}N_0. \qquad (4.8)$$

In (4.7) and (4.8), $\delta(\cdot)$ denotes the Dirac delta function. Recall from the last subsection that $n_k(t)$ is a zero-mean AWGN process. Therefore, $n'_k(t)$ representing the difference between $n_k(t)$ and the component resulting from the projection of $n_k(t)$ on $p_k(t)$ is also a zero-mean Gaussian process, i.e., $\mathbb{E}[n'_k(t)] = 0$. Therefore, (4.6) can be given by

$$\mathbb{E}[n'_k(t)R_k] = \mathbb{E}[n'_k(t)N_k] = \mathbb{E}[(n_k(t) - N_kp_k(t))N_k]$$
$$= \int_{\alpha_k}^{\beta_k} \mathbb{E}[n_k(t)n_k(\tau)]p_k(\tau)d\tau - \mathbb{E}[N_k^2]p_k(t)$$
$$= \frac{1}{2}N_0 p_k(t) - \frac{1}{2}N_0 p_k(t) = 0. \qquad (4.9)$$

Since $n'_k(t)$ and N_k are uncorrelated and jointly Gaussian, they are statistically independent. Moreover, R_k is the sum of the constant S_k and two random variables, N_k and I_k, both independent of $n'_k(t)$. Therefore, $n'_k(t)$ is independent of R_k and consequently does not have any information relevant to the decision statistic and can be ignored by an optimal receiver.

4.1.3 Correlation Between the Decision Statistic and the Interference Term

Now, we examine the correlation between R_k and $i'_k(t)$, which can be written as

$$\mathbb{E}[i'_k(t)R_k] = \mathbb{E}[i'_k(t)(S_k + N_k + I_k)]$$

$$= \mathbb{E}[i'_k(t)]S_k + \mathbb{E}[i'_k(t)]\mathbb{E}[N_k] + \mathbb{E}[i'_k(t)I_k]. \qquad (4.10)$$

In order to find $\mathbb{E}[i'_k(t)]$, both $i_k(t)$ and I_k have to be studied.

$$\mathbb{E}[I_k] = \sqrt{\frac{E_b}{N_s}} \sum_{j=1}^{N_{uk}} \mathbb{E}[b_k^{(j)}]\mathbb{E}[A_k^{(j)}R_p(\theta_k^{(j)})] = 0 \qquad (4.11)$$

$$\mathbb{E}[i_k(t)] = \sqrt{\frac{E_b}{N_s}} \sum_{j=1}^{N_{uk}} \mathbb{E}[b_k^{(j)}]\mathbb{E}[A_k^{(j)}p_k(t - \theta_k^{(j)})] = 0. \qquad (4.12)$$

Note that in (4.11) and (4.12), $b_k^{(j)}$ is independent of $A_k^{(j)}$ and $\theta_k^{(j)}$. In addition, $\mathbb{E}[b_k^{(j)}] = 0$ because each random variable $b_k^{(j)}$ takes values -1 and $+1$ with the same probability. Considering (4.11) and (4.12), the interface term $i'_k(t)$ is also a zero-mean random variable. So, (4.10) can be simply written as

$$\mathbb{E}[i'_k(t)R_k] = \mathbb{E}[i'_k(t)I_k] = \mathbb{E}[(i_k(t) - I_k p_k(t))I_k]$$

$$= \mathbb{E}[i_k(t)I_k] - \mathbb{E}[I_k^2]p_k(t). \qquad (4.13)$$

Considering that $\mathbb{E}[b_k^{(l)}b_k^{(m)}] = 0$ for $l \neq m$, $\mathbb{E}[i_k(t)I_k]$ in (4.13) can be written as

$$\mathbb{E}[i_k(t)I_k] = \mathbb{E}[i_k(t) \int_{\alpha_k}^{\beta_k} i_k(v)p_k(v)dv]$$

$$= \mathbb{E}[\int_{\alpha_k}^{\beta_k} \left(\sqrt{\frac{E_b}{N_s}} \sum_{j_1=1}^{N_{uk}} A_k^{(j_1)}b_k^{(j_1)}p_k(v - \theta_k^{(j_1)}) \right) \times$$

$$\left(\sqrt{\frac{E_b}{N_s}} \sum_{j_2=1}^{N_{uk}} A_k^{(j_2)}b_k^{(j_2)}p_k(t - \theta_k^{(j_2)}) \right) p_k(v)dv]$$

$$= \frac{E_b}{N_s} \int_{\alpha_k}^{\beta_k} \sum_{j=1}^{N_{uk}} \mathbb{E}[(A_k^{(j)})^2]\mathbb{E}[(b_k^{(j)})^2] \times$$

$$\mathbb{E}[p_k(v - \theta_k^{(j)})p_k(t - \theta_k^{(j)})]p_k(v)dv \qquad (4.14a)$$

where $\mathbb{E}[p_k(v - \theta_k^{(j)})p_k(t - \theta_k^{(j)})]$ is given by

$$\mathbb{E}[p_k(v - \theta_k^{(j)})p_k(t - \theta_k^{(j)})] = \frac{1}{2T_p} \int_{-T_p}^{T_p} p_k(v - \theta_k^{(j)})p_k(t - \theta_k^{(j)})d\theta_k^{(j)} = \frac{R_p(v - t)}{2T_p}. \qquad (4.14b)$$

Therefore, $\mathbb{E}[i_k(t)I_k]$ in (4.14a) can be simplified as

$$\mathbb{E}[i_k(t)I_k] = \frac{E_b}{2N_sT_p}\sum_{j=1}^{N_{uk}}\mathbb{E}[(A_k^{(j)})^2]\int_{\alpha_k}^{\beta_k}R_p(v-t)p_k(v)dv. \tag{4.15}$$

The other term in (4.13), $\mathbb{E}[I_k^2]$, can be expressed as

$$\mathbb{E}[I_k^2] = \mathbb{E}\Big[\Big(\sqrt{\frac{E_b}{N_s}}\sum_{j_1=1}^{N_{uk}}A_k^{(j_1)}b_k^{(j_1)}R_p(\theta_k^{(j_1)})\Big)\times$$

$$\Big(\sqrt{\frac{E_b}{N_s}}\sum_{j_2=1}^{N_{uk}}A_k^{(j_2)}b_k^{(j_2)}R_p(\theta_k^{(j_2)})\Big)\Big]$$

$$= \frac{E_b}{N_s}\sum_{j=1}^{N_{uk}}\mathbb{E}[(A_k^{(j)})^2]\mathbb{E}[(b_k^{(j)})^2]\mathbb{E}[(R_p(\theta_k^{(j)}))^2] \tag{4.16}$$

where $\mathbb{E}[(R_p(\theta_k^{(j)}))^2]$ is given by

$$\mathbb{E}[(R_p(\theta_k^{(j)}))^2] = \frac{1}{2T_p}\int_{-T_p}^{T_p}(R_p(\theta_k^{(j)}))^2 d\theta_k^{(j)}$$

$$= \frac{1}{2T_p}\int_{-T_p}^{T_p}\Big(\int_{\alpha_k}^{\beta_k}p_k(s)p_k(s-\theta_k^{(j)})ds\Big)\times$$

$$\Big(\int_{\alpha_k}^{\beta_k}p_k(u)p_k(u-\theta_k^{(j)})du\Big)d\theta_k^{(j)}$$

$$= \frac{1}{2T_p}\int_{\alpha_k}^{\beta_k}p_k(s)\int_{\alpha_k}^{\beta_k}p_k(u)\int_{-T_p}^{T_p}p_k(u-\theta_k^{(j)})p_k(s-\theta_k^{(j)})d\theta_k^{(j)}duds$$

$$= \frac{1}{2T_p}\underbrace{\int_{\alpha_k}^{\beta_k}p_k(s)\int_{\alpha_k}^{\beta_k}p_k(u)R_p(u-s)duds}_{C_I} = \frac{C_I}{2T_p} \tag{4.17}$$

where C_I is a constant. Substituting (4.17) in (4.16), $\mathbb{E}[I_k^2]$ can be rewritten as

$$\mathbb{E}[I_k^2] = \frac{E_b}{2N_sT_p}\sum_{j=1}^{N_{uk}}\mathbb{E}[(A_k^{(j)})^2]C_I. \tag{4.18}$$

Consequently, considering (4.13), (4.15) and (4.18), $\mathbb{E}[i_k'(t)R_k]$ is given by

$$\mathbb{E}[i_k'(t)R_k] = \frac{E_b}{2N_sT_p}\sum_{j=1}^{N_{uk}}\mathbb{E}[(A_k^{(j)})^2]\times$$

$$\underbrace{\Big(\int_{\alpha_k}^{\beta_k}R_p(v-t)p_k(v)dv - C_Ip_k(t)\Big)}_{\eta(t)}. \tag{4.19}$$

In order to study the behaviour of $\eta(t)$, several practical TH-UWB pulses are employed. The first pulse is one of the even pulses proposed in [13] whose parameters

for our simulation are $f_c = 6.85$ GHz, $\tau = 1/f_c = 0.146$ ns and $n = 3$ (defined in (2.7)). The second pulse is the 2nd-order Gaussian monocycle introduced in [10] with $\tau = 0.1533$ (defined in (2.4)). The third pulse is the Rayleigh monocycle [11], $p_r(t)$, with σ equal to 0.0626 (defined in (2.5)). Finally, the modified Hermite pulse in [12] with $n = 3$ and $\tau = 0.034$ is used as the fourth pulse (defined in (2.6)). Fig. 2.3 shows all of these pulses as well as their ACFs in the interval $[-T_p, T_p]$.

The function $\eta(t)$ for the four pulses is depicted in Fig. 4.1 in the range $[\alpha_k, \beta_k]$ where $p_k(t)$ takes non-zero values. It can be seen that for practical UWB pulses, $\eta(t)$ is not equal to zero, meaning that $i'_k(t)$ is correlated with R_k, which in turn implies dependency between $i'_k(t)$ and the decision statistic. Therefore, the decision statistic, R_k, and $i'_k(t) + n'_k(t)$ are also dependent. So, R_k cannot be considered as a sufficient decision statistic for detecting the transmitted information bit of the desired user in the kth frame. Note that a sufficient decision statistic would be provided by the TH-UWB CMF receiver if the interference component, I_k, could be modeled by a Gaussian distribution. However, the PDF of I_k is non-Gaussian resulting in non-sufficiency of the decision statistic of the CMF receiver.
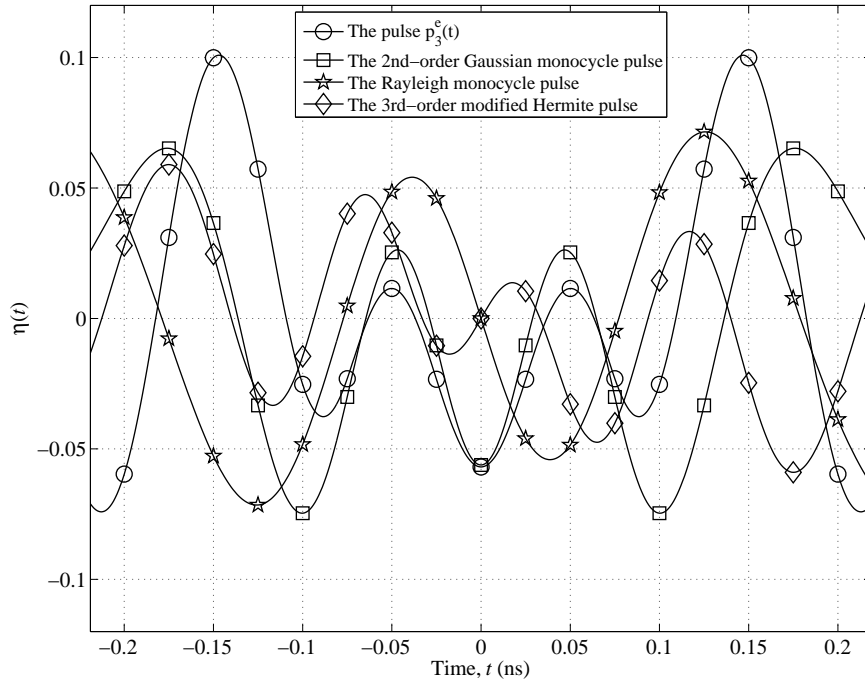
Figure 4.1: The function $\eta(t)$ for four practical UWB pulses.

4.2 New Receiver Structures

In a multiuser detection system, in order to detect the information bits of all the users, a bank of matched filters with each filter synchronized with the delayed pulse waveform of one distinct user is employed to obtain the receiver decision statistics. It has been shown in [38], that the outputs of the matched filters constitute sufficient decision statistics for optimally detecting the transmitted symbols of all the users. Having obtained the vector of decision statistics, we must use the MUD algorithms to decide on the received signals. Although MUD algorithms offer superior BER performances, they are too complex to be implemented in simple and low-cost TH-UWB receivers. Therefore, a novel scheme is introduced, based on which, two novel partial-multiuser TH-UWB receivers which use similar methodologies to the MUD algorithms are proposed. In these receivers, only one matched filter is employed, which in turn results in lowering the complexity required to implement the proposed algorithms compared to MUD methods. However, simulations results show that they outperform all the single-user TH-UWB receivers. Hereafter, we assume that the amplitudes and delays of the interfering users are known to the receiver. Efficient amplitude and delay estimators for UWB applications are discussed in [40].

Considering the decision statistic obtained in (4.3) and the interference component derived in (4.4), the vector model governing the relationship between the decision statistic and the transmitted bits from different users in the kth frame can be expressed by

$$R_k = \sqrt{\frac{E_b}{N_s}} \mathbf{h}_k^T \mathbf{b}_k + N_k \tag{4.20}$$

where $\mathbf{b}_k = [b_k^{(0)}, b_k^{(1)}, \ldots, b_k^{(N_{uk})}]^T$ and $\mathbf{h}_k$ is a $(N_{uk}+1)$-ary vector whose jth element is

$$[\mathbf{h}_k]_j = A_k^{(j)} R_p(\theta_k^{(j)}). \tag{4.21}$$

The first receiver is based on a minimum mean square error (MMSE) detector and is dubbed the MMSE partial-multiuser receiver. The idea is to estimate the vector $\mathbf{b}_k$ given the decision statistic R_k, i.e., $\hat{\mathbf{b}}_{k,\text{ MMSE}} = \mathbf{\Psi} R_k$ is chosen such that

$$\hat{\mathbf{b}}_{k,\text{ MMSE}} = \underset{\mathbf{\Psi}}{\operatorname{argmin}} \ \mathbb{E}[(\mathbf{b}_k - \hat{\mathbf{b}}_{k,\text{ MMSE}})^2]. \tag{4.22}$$

The goal is to find the vector $\mathbf{\Psi}$. We take the derivative of $\mathbb{E}[(\mathbf{b}_k - \hat{\mathbf{b}}_{k,\text{ MMSE}})^2]$ and equate it to zero,

$$\frac{\partial}{\partial \mathbf{\Psi}} \mathbb{E}[(\mathbf{b}_k - \hat{\mathbf{b}}_{k,\text{ MMSE}})^2] = \frac{\partial}{\partial \mathbf{\Psi}} \mathbb{E}[(\mathbf{b}_k - \mathbf{\Psi} R_k)^2] = 2\mathbb{E}[(\mathbf{b}_k - \mathbf{\Psi} R_k) R_k^T] = 0. \tag{4.23}$$

Then $\mathbb{E}[(\mathbf{b}_k - \boldsymbol{\Psi} R_k)R_k^T]$ can be rewritten as

$$\begin{aligned}
\mathbb{E}[(\mathbf{b}_k - \boldsymbol{\Psi} R_k)R_k^T] &= \mathbb{E}[\mathbf{b}_k R_k^T] - \boldsymbol{\Psi}\mathbb{E}[R_k R_k^T] \\
&= \mathbb{E}[\mathbf{b}_k(\sqrt{\frac{E_b}{N_s}}\mathbf{b}_k^T\mathbf{h}_k + N_k)] \\
&\quad - \boldsymbol{\Psi}\mathbb{E}[(\sqrt{\frac{E_b}{N_s}}\mathbf{h}_k^T\mathbf{b}_k + N_k)(\sqrt{\frac{E_b}{N_s}}\mathbf{b}_k^T\mathbf{h}_k + N_k)] = 0.
\end{aligned} \quad (4.24)$$

One should note that $\mathbb{E}[\mathbf{b}_k N_k] = 0$ because $\mathbf{b}_k$ and N_k are independent. Also, $\mathbb{E}[\mathbf{b}_k\mathbf{b}_k^T] = I$ where I is the identity matrix. So, (4.24) can be be simplified as

$$\mathbb{E}[(\mathbf{b}_k - \boldsymbol{\Psi} R_k)R_k^T] = \sqrt{\frac{E_b}{N_s}}\mathbf{h}_k - \boldsymbol{\Psi}(\frac{E_b}{N_s}\mathbf{h}_k^T\mathbf{h}_k + \frac{N_0}{2}) = 0. \quad (4.25)$$

Therefore, $\boldsymbol{\Psi}$ can be obtained as

$$\boldsymbol{\Psi} = \frac{\sqrt{\frac{E_b}{N_s}}\mathbf{h}_k}{(\frac{E_b}{N_s}\mathbf{h}_k^T\mathbf{h}_k + \frac{N_0}{2})}. \quad (4.26)$$

For detection, the statistic $\hat{b}_{k,\,\text{MMSE}}^{(0)}$ for each frame is computed and then the transmitted bit is detected based on the sign of the sum of the $\hat{b}_{k,\,\text{MMSE}}^{(0)}$ values from N_s frames representing that bit. That is,

$$\hat{d}_{m,\,\text{MMSE}}^{(0)} = \begin{cases} +1, & \text{if } \sum_{k=p_m}^{q_m} \hat{b}_{k,\,\text{MMSE}}^{(0)} \geq 0 \\ -1, & \text{if } \sum_{k=p_m}^{q_m} \hat{b}_{k,\,\text{MMSE}}^{(0)} < 0 \end{cases} \quad (4.27)$$

where $p_m = mN_s$ and $q_m = (m+1)N_s - 1$.

For the second receiver, dubbed the optimal partial-multiuser detector, the goal is to optimally decide $\hat{b}_{k,\,\text{OPT}}^{(0)}$, which is achieved by minimizing the probability of error $\Pr(b_k^{(0)} \neq \hat{b}_{k,\,\text{OPT}}^{(0)})$. Therefore, $\hat{b}_{k,\,\text{OPT}}^{(0)}$ is chosen such that

$$\hat{b}_{k,\,\text{OPT}}^{(0)} = \underset{b \in \{-1,+1\}}{\text{argmax}} \Pr(b_k^{(0)} = b|R_k). \quad (4.28)$$

When binary quantities are concerned, it is easiest to work with the logarithmic likelihood ratio (LLR). The conditional LLR of a binary random variable b given $\mathbf{r}$ is defined as

$$L(b|\mathbf{r}) = \ln\frac{\Pr(b = +1|\mathbf{r})}{\Pr(b = -1|\mathbf{r})}. \quad (4.29)$$

Therefore, the conditional LLR of $b_k^{(0)}$ given R_k is defined by

$$
\begin{aligned}
L(b_k^{(0)}|R_k) &= \ln \frac{\Pr(b_k^{(0)} = +1|R_k)}{\Pr(b_k^{(0)} = -1|R_k)} \\
&= \ln \frac{\sum_{\forall \mathbf{b}_k : b_k^{(0)} = +1} \Pr(\mathbf{b}_k|R_k)}{\sum_{\forall \mathbf{b}_k : b_k^{(0)} = -1} \Pr(\mathbf{b}_k|R_k)} \\
&= \ln \frac{\sum_{\forall \mathbf{b}_k : b_k^{(0)} = +1} f(R_k|\mathbf{b}_k)}{\sum_{\forall \mathbf{b}_k : b_k^{(0)} = -1} f(R_k|\mathbf{b}_k)}
\end{aligned}
\tag{4.30a}
$$

where

$$
f(R_k|\mathbf{b}_k) = \frac{1}{\sigma\sqrt{2\pi}} \exp\left(-\frac{(R_k - \sqrt{E_b/N_s}\,\mathbf{h}_k^T \mathbf{b}_k)^2}{2\sigma^2} \right).
\tag{4.30b}
$$

Finally, the decision rule in (4.28) for the information symbol transmitted in the kth frame is given by

$$
\hat{b}_{k,\,\text{OPT}}^{(0)} = \begin{cases} +1, & \text{if } L(b_k^{(0)}|R_k) \geq 0 \\ -1, & \text{if } L(b_k^{(0)}|R_k) < 0. \end{cases}
\tag{4.31}
$$

In order to implement soft detection for the mth information bit transmitted by the desired user, $d_{m,\,\text{SD}}^{(0)}$, the LLR values of the N_s corresponding frames are summed and the sign of the summation determines the transmitted bit. That is,

$$
\hat{d}_{m,\,\text{SD}}^{(0)} = \begin{cases} +1, & \text{if } \sum_{k=p_m}^{q_m} L(b_k^{(0)}|R_k) \geq 0 \\ -1, & \text{if } \sum_{k=p_m}^{q_m} L(b_k^{(0)}|R_k) < 0. \end{cases}
\tag{4.32}
$$

In hard detection, the majority logic rule decides which bit was transmitted based on the signs of the LLRs of N_s corresponding frames. That is,

$$
\hat{d}_{m,\,\text{HD}}^{(0)} = \begin{cases} +1, & \text{if } \sum_{k=p_m}^{q_m} \hat{b}_{k,\,\text{OPT}}^{(0)} \geq 0 \\ -1, & \text{if } \sum_{k=p_m}^{q_m} \hat{b}_{k,\,\text{OPT}}^{(0)} < 0. \end{cases}
\tag{4.33}
$$

Note that in the optimal partial-multiuser receiver, the expression $f(R_k|\mathbf{b}_k)$ must be computed $2^{N_{uk}+1}$ times for each frame, which is much less complex than the optimal MUD algorithm. This is because N_{uk} is less than N_u resulting from the low duty cycle of TH-UWB systems. Also, the noise term N_k is just a scalar and the inverse computation of the covariance matrix is equivalent to a division. However, in the MMSE partial-multiuser receiver, the vector $\boldsymbol{\Psi}$ can be computed once and it can be used while the channel is constant for all the users. This makes the MMSE partial-multiuser receiver more practical and less complex compared to the optimal partial-multiuser receiver. Also, for both of the receivers, only one matched filter is required instead of a bank of matched filters, reducing the cost of the TH-UWB receiver.

4.3 Performance Comparisons

In this section, we determine the BER performances of the proposed receivers in a TH-BPSK UWB system by simulation. In the simulations, the pulse shape $p_3^e(t)$ is employed and all the pulse shape parameters are the same as in Section 4.1. The duty cycle, D, is equal to 2 percent (This value is chosen to reduce the time required for simulation.). The number of users, N_u, is 8, and the number of pulses representing one information bit, N_s, is 5. Two types of simulation results are presented. In the first case, the ideal free-space propagation with AWGN and MAI is considered. In the second case, the BER performances of the proposed receivers in multipath fading UWB channels are obtained. We assume that all the users are transmitting with equal powers. All the simulations have been done with 10^6 bits.

4.3.1 Ideal Free-Space Propagation with AWGN and MAI

The BER performances of the new partial-multiuser receivers are evaluated and compared to those of the CMF UWB receiver, the soft-limiting UWB receiver [19], the p-order metric UWB receiver [24,32,33], and the myriad filter UWB detector [25]. All the simulations have been performed for a free-space propagation channel in the presence of AWGN and MAI. For the sake of comparison, the performance of the theoretically optimal single-user detector which knows the exact PDF of the MAI, which is obtained in Chapter 3, is shown as well as the performance of the CMF receiver operating in a single-user system.

The BER versus SNR curves for SIR = 5 and 10 dB are depicted in Figs. 4.2 and 4.3, respectively. As seen, due to the presence of MAI, all the single-user TH-UWB receivers reach error floors for moderate and large values of SNR. Also, comparing the results in Fig. 4.2 to the results in Fig. 4.3, it is observed that the CMF UWB receiver performs approximately an order of magnitude better, when the SIR value increases from 5 to 10 dB. However, this much improvement in the performance does not occur for the other single-user UWB receivers. This is because they already have been designed to combat the MAI which is not true for the case of the CMF UWB receiver. It is observed in Figs. 4.2 and 4.3 that both the p-order metric UWB receiver and the myriad filter UWB detector track closely the performance of a theoretically optimal single-user UWB receiver. This fact expresses that putting more effort into proposing more accurate statistical models for the
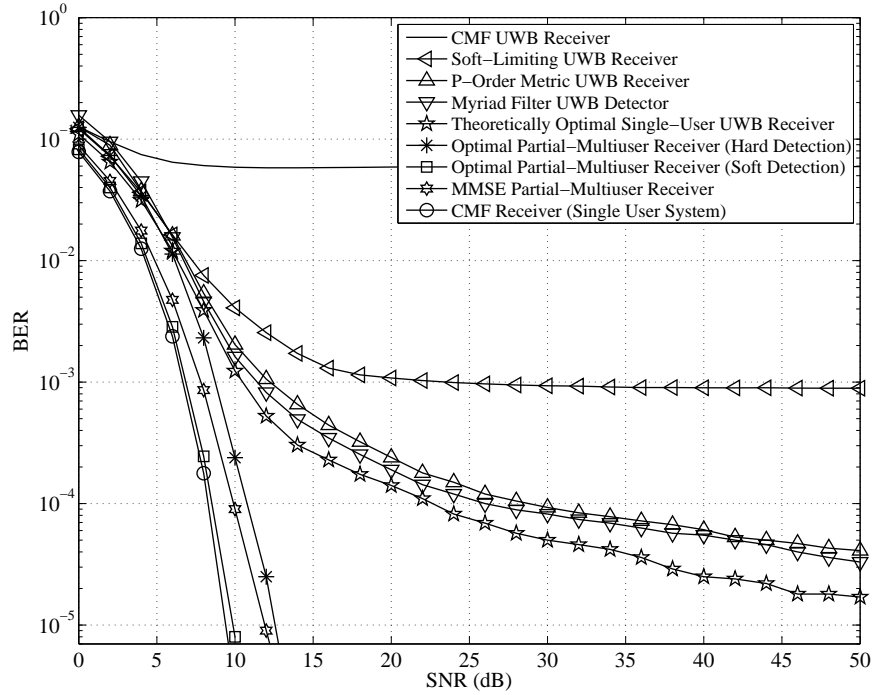
Figure 4.2: The BER versus SNR of the single-user and partial-multiuser receivers operating in a free-space propagation channel for SIR $= 5$ dB and $N_u = 8$.
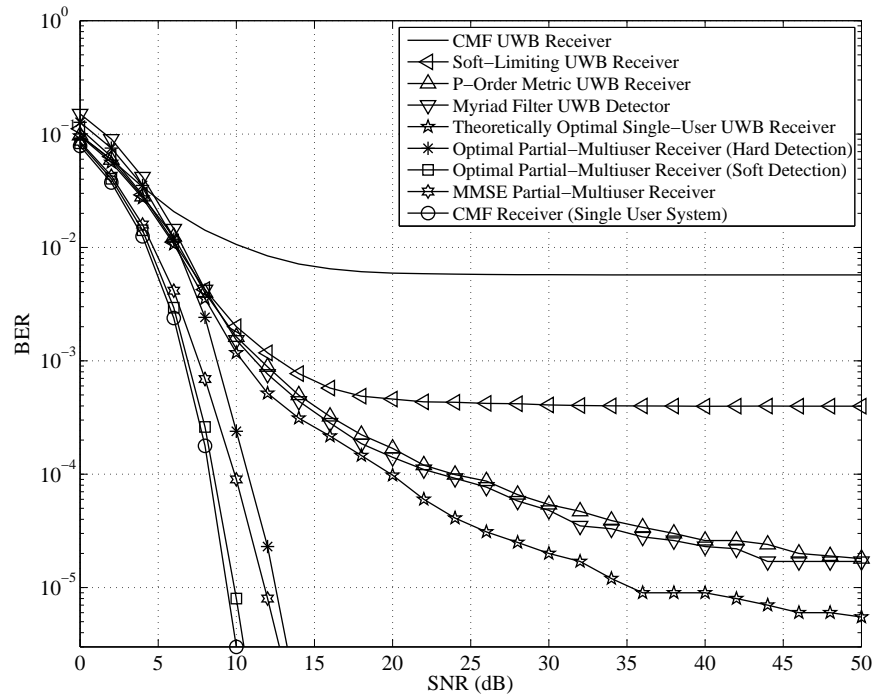
Figure 4.3: The BER versus SNR of the single-user and partial-multiuser receivers operating in a free-space propagation channel for SIR $= 10$ dB and $N_u = 8$.

PDF of the MAI may be ill conceived, because performances close to the optimal attainable performance have already been achieved. Therefore, further substantial improvements in UWB receiver performance must be achieved by changing the way that the MAI is dealt with.

The new receiver structures use a new way to combat the MAI. It is observed that both of the partial-multiuser receivers not only outperform all the other receivers but also remove the error floor resulting from the MAI. Moreover, it is seen by comparing curves in Fig. 4.2 with curves in Fig. 4.3 that independent of the value of SIR, the performances of the new receivers remain the same. One may note that the performance of the optimal partial-multiuser receiver using soft detection nearly achieves the performance of the CMF receiver operating in a single-user system. More importantly, although the MMSE partial-multiuser detector is much less complex than the optimal partial-multiuser detector with soft detection, we note that there is only approximately 1 dB gap in SNR between the performances of these two receivers.

4.3.2 Multipath Fading UWB Channel with AWGN

For obtaining the BER performances of the purposed receivers in multipath fading UWB channels, the realizations of the CM1, CM2, CM3, and CM4 channel models introduced in [31] are used. In the simulations, an S-Rake receiver is used which collects the 5 strongest paths. The S-Rake receiver employs the CMF UWB receiver, the soft-limiting UWB receiver, the p-order metric UWB receiver, the MMSE partial-multiuser receiver, or the optimal partial-multiuser receiver as its receiving fingers. Then, the outputs of the fingers are combined to make the decision statistics. Here, two diversity combining methods are used, EGC and MRC. In order to obtain the performances of the receivers, the simulations must be done in approximately 100 different channel realizations and then the average performances are computed for each of the UWB multipath channels [31]. In the simulations, the SIR is equal to 10 dB.

Figs. 4.4, 4.5, 4.6, and 4.7 show the BER curves of several nonlinear single-user receivers and the partial-multiuser detectors in practical UWB environments where both MAI and AWGN are present. Observe that both the MMSE and optimal partial-multiuser receivers outperform the single-user receivers. Especially, the optimal partial-multiuser receiver (for both EGC and MRC Rake combining)

53

Figure 4.4: The BER versus SNR of the single-user and partial-multiuser receivers operating in the CM1 UWB multipath channel for SIR = 10 dB and $N_u = 8$.
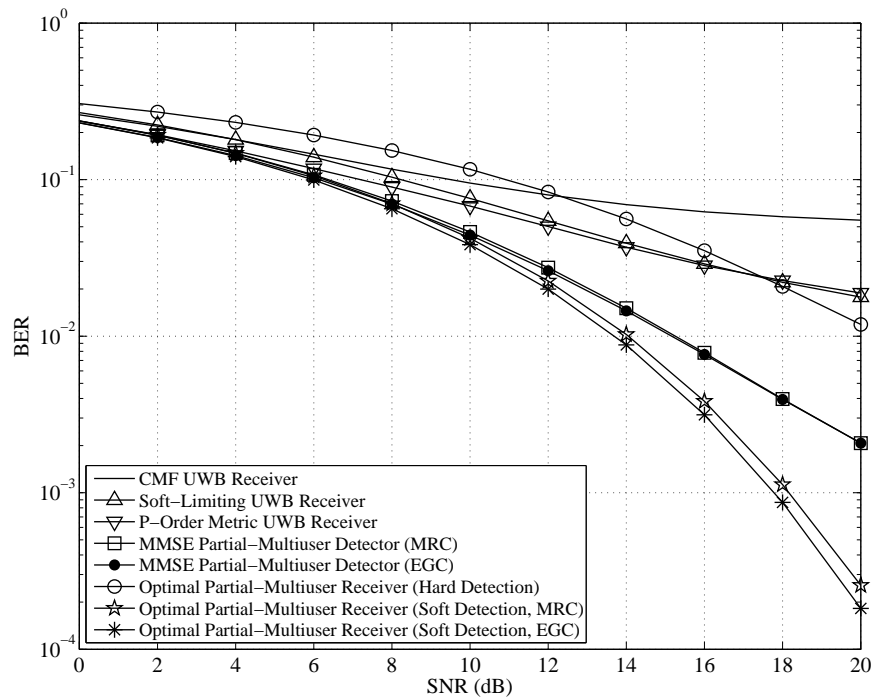
Figure 4.5: The BER versus SNR of the single-user and partial-multiuser receivers operating in the CM2 UWB multipath channel for SIR = 10 dB and $N_u = 8$.
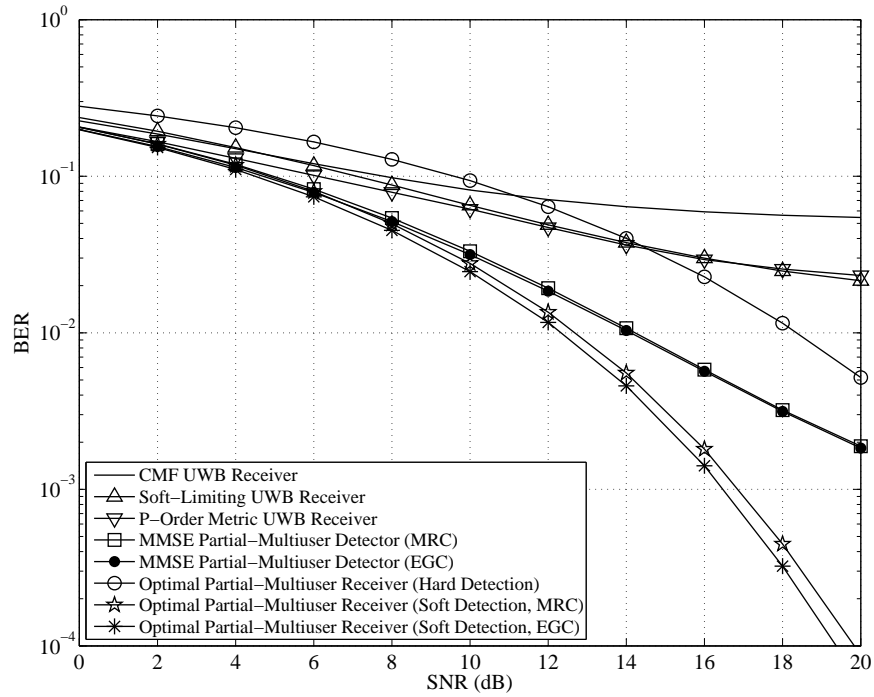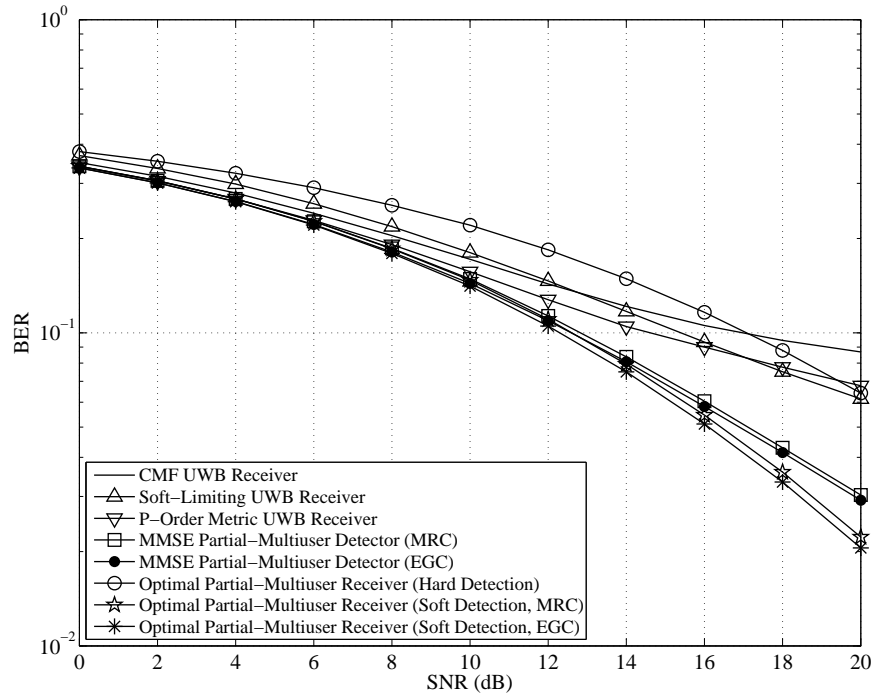
Figure 4.6: The BER versus SNR of the single-user and partial-multiuser receivers operating in the CM3 UWB multipath channel for SIR = 10 dB and $N_u = 8$.
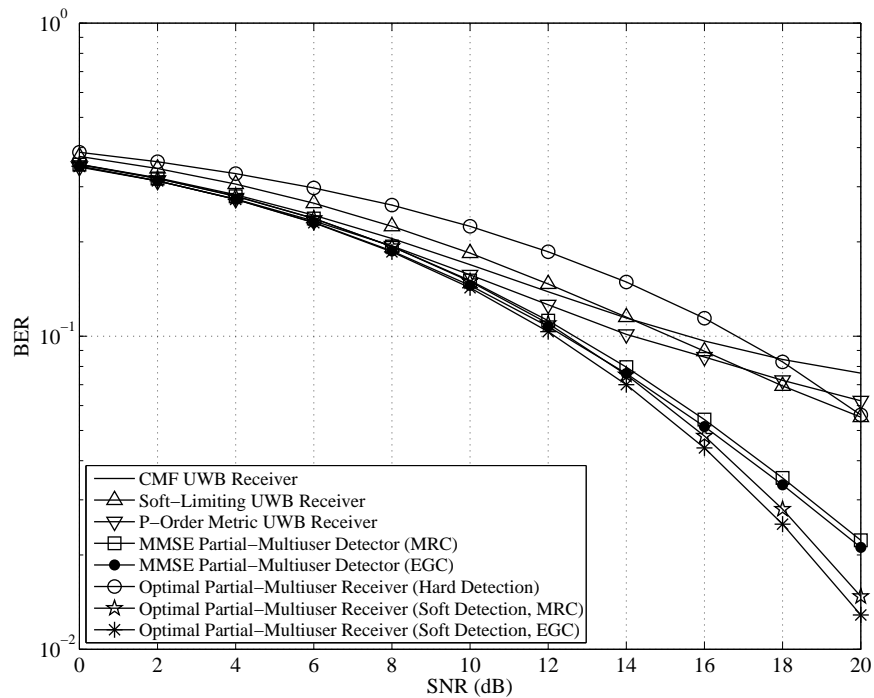
Figure 4.7: The BER versus SNR of the single-user and partial-multiuser receivers operating in the CM4 UWB multipath channel for SIR = 10 dB and $N_u = 8$.

functions significantly better than all single-user nonlinear receivers, e.g., as seen in Fig. 4.4, it performs more than two orders of magnitude better than the p-order metric receiver. Also, the error floors are removed by the optimal partial-multiuser receivers. Considering the optimal partial-multiuser receiver with soft detection, the performance of EGC Rake combining is slightly better than that of MRC Rake combining.

4.4 Conclusion

It was proved that the outputs of the chip correlators in a CMF UWB receiver cannot provide sufficient decision statistics for detecting the information bits transmitted by the desired user. Two new receivers, the MMSE and optimal partial-multiuser detectors, were proposed that exploit concepts from MUD algorithms in TH-UWB systems. These new receivers employ only one matched filter rather than a bank of matched filters as used in conventional MUD methods. Also, the complexity of computation in both of these receivers is much less than the optimal MUD algorithm. Therefore, these new receiver structures are much more efficient than the optimal MUD algorithms in terms of both computation and implementation cost. Finally, it was shown that the new receivers outperform the nonlinear single-user UWB receivers in ideal free-space propagation channels as well as in real UWB multipath channels.

Chapter 5

Low-Complexity Multisampling Multiuser Detector for TH-UWB Systems

The performance degradation resulting from the MAI and the fact that all the nonlinear single-user receivers reach an error floor are good motivations to exploit MUD in TH-UWB systems. MUD has some distinguishing properties. First, it is an effective means of detection for achieving superior performances; however, its complexity is challenging and grows exponentially with the number of existing users, N_u [38]. Secondly, it has sensitivity to phase/frequency offsets of the transmitting users' signals. This is because of the imperfections of carrier phase recovery which result in undesired cross-correlation between the hypothesized signals which in turn implies degradation of the receiver's performance [41]. However, one may note that TH-UWB systems are carrier-less meaning that MUD for TH-UWB does not suffer from frequency/phase offset. Also, TH-UWB systems have a small number of effective interfering users due to their low duty cycle, e.g., in a system with 16 active users, it is quite unlikely to have more than 5 interferers collide on a specific user. So, the complexity of the MUD algorithm is dramatically reduced. Consequently, MUD can be considered for simple and low-cost TH-UWB receivers.

Recently, some research has focused on applying MUD in TH-UWB Systems. In [42], an optimal multiuser detector for TH-UWB systems employing PPM modulation is derived and it is demonstrated that the complexity of the detector is $\mathcal{O}(2^{N_u})$ which is very high and is not practical for TH-UWB systems. In [43], for the special case of synchronized users, three multiuser detectors, the blinking receiver, the quasidecorrelator and the quasi-MMSE multiuser detectors, are described. In addi-

tion, an iterative ("turbo" like) receiver based on the symbol and pulse detectors is discussed, also for the case of synchronized users. Some other MUD receivers can be found in [44–46].

In this chapter, we discuss the sparsity of TH-UWB signals due to the low duty cycle of TH-UWB systems and clarify the concept of effective interfering users. After introducing UWB partial-multiuser receivers in Chapter 4, optimal MUD algorithms with frame-duration and pulse-duration observation times are studied and their pros and cons are discussed. Further, a new low-complexity multisampling MUD algorithm is proposed and its advantages are described.

5.1 Time Sparsity of the TH-UWB Signals

Fig. 5.1 shows a frame snapshot of a TH-UWB signal when there are 15 interferers and $D = 2\%$ where an excessively large value (factor of 4) of D has been chosen for the purpose of illustration and ease of simulation. Observe that due to the low duty cycle of TH-UWB systems, the total received TH-UWB signal is a sparse signal in time even when the TH-UWB system has a moderately large number of interferers. Hence, unlike full duty wireless CDMA systems, the number of collisions corrupting a specific user's signal is much less than the number of active users in the system.
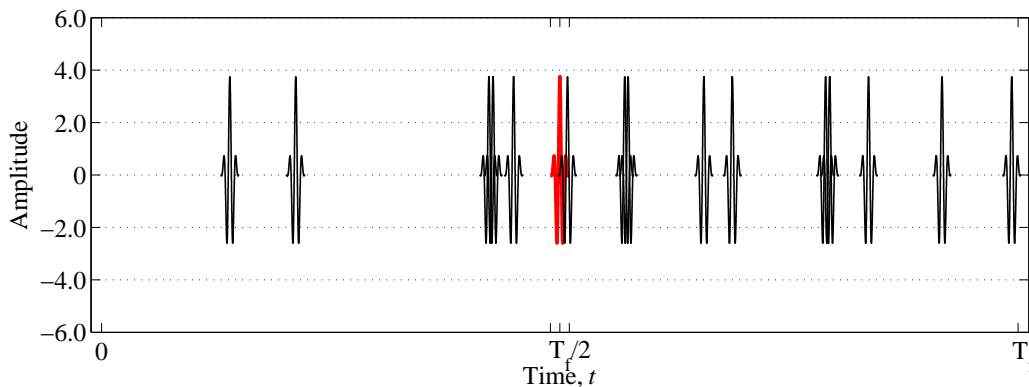
Figure 5.1: A frame snapshot of a received TH-UWB signal for 16 asynchronous users with $D = 2\%$. The pulse of the desired user is drawn in red.

A histogram of the number of collisions from 15 active asynchronous interferers that corrupt the pulse of the desired user is depicted in Fig. 5.2. It is observed that it is quite unlikely to have more than 5 interferers collide; the probability of this event is on the order of 10^{-5}. So, heuristically, one might say that the number of effective interfering users in a TH-UWB system with 15 interferers and $D = 2\%$ is

5. This is the underlying rationale for the low-complexity MUD algorithm which will be developed in the next section.
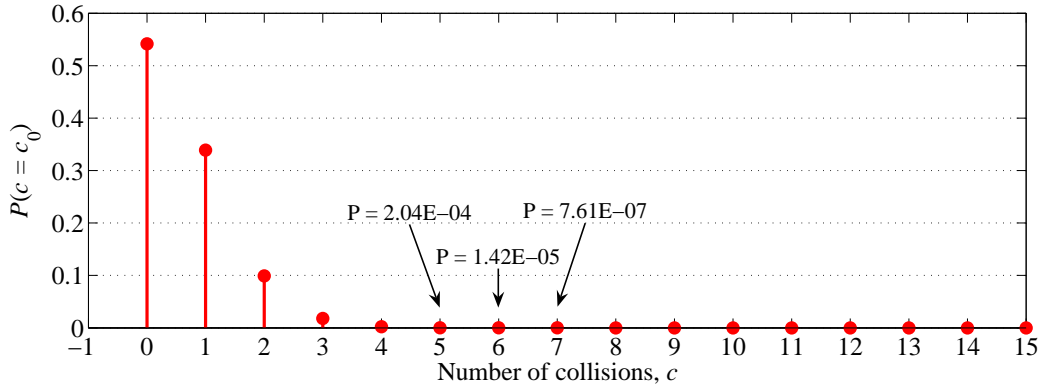
Figure 5.2: A histogram of the number of collisions from 15 asynchronous interferers corrupting the pulse of the desired user for $D = 2\%$.

5.2 MUD Algorithms

Considering the system model discussed in Section 2.6, it is understood that N_s pulses in N_s frames are transmitted to convey one symbol. In this section, we first obtain the individually optimum multiuser detector for the case when the observation time for each pulse of the desired user's signal is limited to the duration of the frame in which it appears. According to the previous discussion, almost no information is lost if the observation time for each pulse is shortened to its duration because of the sparsity of the TH-UWB signals. Later, this hypothesis will be verified by simulation results. However, if we limit the observation time to the pulse duration, we will face some practical difficulties in real implementations of the MUD algorithm. Therefore, we introduce a novel low-complexity multisampling multiuser detector which takes advantage of the short duration observation time and the small value of the number of effective interfering users in TH-UWB systems, but has a feasible implementation.

5.2.1 Optimal MUD Algorithm with Frame-Duration Observation Time (FDOT)

The 0th user is considered as the user of interest. Without loss of generality, we can assume that $\tau^{(0)} = 0$ and $c_k^{(0)}T_c = T_f/2$ for all values of k [15]. Hereafter, we focus on detecting the mth transmitted symbol of the desired user. Because of the

asynchronous channel, each transmitted frame of the desired user can experience at most $2(N_u - 1)$ different full or partial pulses from $(N_u - 1)$ other users in its duration. Denote the number of interfering pulses in the jth frame by N_{uj}^F, which can take an integer value in the range $0 \leq N_{uj}^F \leq 2(N_u - 1)$. In order to avoid obtaining lengthy equations, we define a new random variable, $\delta_{j(i)}^F$, denoting the time difference between the ith interfering pulse and the desired user's pulse in the jth frame where $i = 0, 1, \ldots, N_{uj}^F$. The random variable $\delta_{j(0)}^F$ denotes the delay of the desired user's pulse with itself which is always equal to 0.

A bank of matched filters, each matched to the pulse shape, $p(t)$, and synchronized with the delay of each interfering pulse, is used to convert the received signal into the discrete-time receiver decision statistics. Let $r_{j(i)}^F$ denote the output of the ith matched filter at the jth frame

$$r_{j(i)}^F = \int_{\alpha_j^F}^{\beta_j^F} r(t)p(t - jT_f - T_f/2 - \delta_{j(i)}^F)dt$$
$$= \int_{\alpha_j^F}^{\beta_j^F} r(t)p_j(t - \delta_{j(i)}^F)dt \tag{5.1}$$

where $\alpha_j^F = jT_f$, $\beta_j^F = (j+1)T_f$, $p_j(t) = p(t - jT_f - T_f/2)$, and $j = 0, 1, \ldots, N_s - 1$. The following model governs the relationship between the outputs of the matched filters and the transmitted bits from different users for the jth frame,

$$\mathbf{r}_j^F = \sqrt{\frac{E_b}{N_s}}\mathbf{S}_j^F \mathbf{A}_j^F \mathbf{b}_j^F + \mathbf{n}_j^F \tag{5.2}$$

where $\mathbf{r}_j^F = [r_{j(0)}^F, r_{j(1)}^F, \ldots, r_{j(N_{uj}^F)}^F]^T$. It can be easily proved that vector $\mathbf{r}_j^F$ is a sufficient statistic for detecting the information bit transmitted by the desired user at the jth frame. Matrix $\mathbf{A}_j^F = \text{diag}[A_{j(0)}^F, A_{j(1)}^F, \ldots, A_{j(N_{uj}^F)}^F]$ is a diagonal matrix whose diagonal elements are the amplitudes of the interfering pulses, and $\mathbf{b}_j^F = [b_{j(0)}^F, b_{j(1)}^F, \ldots, b_{j(N_{uj}^F)}^F]^T$ is a vector containing the information bits conveyed by each pulse. The matrix $\mathbf{S}_j^F$ is a symmetric matrix whose elements, $(\mathbf{S}_j^F)_{mn}$, are defined by

$$(\mathbf{S}_j^F)_{mn} = \int_{\alpha_j^F}^{\beta_j^F} p_j(t - \delta_{j(m)}^F)p_j(t - \delta_{j(n)}^F)dt. \tag{5.3}$$

Since $n(t)$ is AWGN, $\mathbf{n}_j^F$ is a zero-mean Gaussian random vector with covariance matrix $\boldsymbol{\Sigma}_j^F$, where $\boldsymbol{\Sigma}_j^F = (N_0/2)\mathbf{S}_j^F$.

It is well known that the optimal detection minimizing the probability of error

$\Pr(b_{j(0)}^F \neq \hat{b}_{j(0)}^F)$ is achieved by setting $\hat{b}_{j(0)}^F$ such that

$$\hat{b}_{j(0)}^F = \underset{b \in \{-1,+1\}}{\operatorname{argmax}} \Pr(b_{j(0)}^F = b | \mathbf{r}_j^F). \tag{5.4}$$

When binary quantities are concerned, it is easiest to work with the LLR. The conditional LLR of a binary random variable b given $\mathbf{r}$ is defined in (4.29). Therefore, the conditional LLR of $b_{j(0)}^F$ given $\mathbf{r}_j^F$ is given by

$$\begin{aligned}
L(b_{j(0)}^F | \mathbf{r}_j^F) &= \ln \frac{\Pr(b_{j(0)}^F = +1 | \mathbf{r}_j^F)}{\Pr(b_{j(0)}^F = -1 | \mathbf{r}_j^F)} \\
&= \ln \frac{\sum_{\forall \mathbf{b}_j^F : b_{j(0)}^F = +1} \Pr(\mathbf{b}_j^F | \mathbf{r}_j^F)}{\sum_{\forall \mathbf{b}_j^F : b_{j(0)}^F = -1} \Pr(\mathbf{b}_j^F | \mathbf{r}_j^F)} \\
&= \ln \frac{\sum_{\forall \mathbf{b}_j^F : b_{j(0)}^F = +1} f(\mathbf{r}_j^F | \mathbf{b}_j^F)}{\sum_{\forall \mathbf{b}_j^F : b_{j(0)}^F = -1} f(\mathbf{r}_j^F | \mathbf{b}_j^F)}
\end{aligned} \tag{5.5}$$

where

$$f(\mathbf{r}_j^F | \mathbf{b}_j^F) = f_g(\mathbf{r}_j^F, \sqrt{\frac{E_b}{N_s}} \mathbf{S}_j^F \mathbf{A}_j^F \mathbf{b}_j^F, \frac{N_0}{2} \mathbf{S}_j^F, N_{uj}^F) \tag{5.6}$$

and $f_g(\mathbf{x}, \overline{\mathbf{x}}, \mathbf{\Gamma}, N)$ represents the multivariate Gaussian PDF

$$f_g(\mathbf{x}) = \frac{\exp\left(-\frac{1}{2}(\mathbf{x} - \overline{\mathbf{x}})^T (\mathbf{\Gamma})^{-1}(\mathbf{x} - \overline{\mathbf{x}})\right)}{\sqrt{(2\pi)^N |\mathbf{\Gamma}|^{\frac{1}{2}}}} \tag{5.7}$$

in which, $\overline{\mathbf{x}}$, $\mathbf{\Gamma}$, and N denote the mean vector, the covariance matrix and the dimension of the multivariate Gaussian random vector $\mathbf{x}$, respectively. Now, the decision rule (5.4) can be written as

$$\hat{b}_{j(0)}^F = \begin{cases} +1, & L(b_{j(0)}^F | \mathbf{r}_j^F) \geq 0 \\ -1, & L(b_{j(0)}^F | \mathbf{r}_j^F) < 0. \end{cases} \tag{5.8}$$

Finally, the decision rule for the mth information bit of the desired user based on the LLRs of all N_s frames is given by

$$\hat{d}_m^{(0)} = \begin{cases} +1, & \sum_{j=p_m}^{q_m} L(b_{j(0)}^F | \mathbf{r}_j^F) \geq 0 \\ -1, & \sum_{j=p_m}^{q_m} L(b_{j(0)}^F | \mathbf{r}_j^F) < 0. \end{cases} \tag{5.9}$$

where $p_m = mN_s$ and $q_m = (m+1)N_s - 1$.

In this method, for each frame, the expression $f(\mathbf{r}_j^F | \mathbf{b}_j^F)$ has to be computed for all possible values of $\mathbf{b}_j^F$, so the complexity is $\mathcal{O}(2^{N_{uj}^F + 1})$. Also, the covariance matrix $\mathbf{\Sigma}_j^F = (N_0/2)\mathbf{S}_j^F$ is changing in each frame. Therefore, the inverse of the covariance matrix has to be computed for each frame with complexity of $\mathcal{O}((N_{uj}^F + 1)^3)$. Both of these tasks are computationally demanding and cannot be implemented in TH-UWB receivers at low cost. Thus, in the next subsection, we introduce a low-complexity MUD algorithm whose observation time is limited to the pulse duration.

5.2.2 Optimal MUD Algorithm with Pulse-Duration Observation Time (PDOT)

The pulse $p(t)$ as well as two neighboring pulses with delays of $-T_p$ and $+T_p$ are depicted in Fig. 5.3. It can be seen that if the absolute value of the time difference between a pulse and the desired users's pulse is more than T_p, then that particular pulse will not interfere with the desired user's pulse. So, the number of interfering pulses corrupting the desired user's pulse denoted by N_{uj}^P, is certainly less than N_u. This is because if a pulse of a user collides with the desired user's pulse, the previous and the next pulses of the same user cannot interfere with the desired pulse due to the fact that the chip duration is at least twice larger than the pulse duration. Note that $N_{uj}^P \leq N_{uj}^F$ for all values of j. Moreover, based on the discussion in Section 5.1, N_{uj}^P is much less than N_u with a high probability. Therefore, we shorten the observation time from a frame duration to a pulse duration and obtain the optimal MUD with PDOT. To this end, for the jth frame each $\delta_{j(i)}^F$ satisfying $|\delta_{j(i)}^F| \leq T_p$ is chosen. These new variables are denoted by $\delta_{j(i)}^P$ where $i = 0, 1, \ldots, N_{uj}^P$.
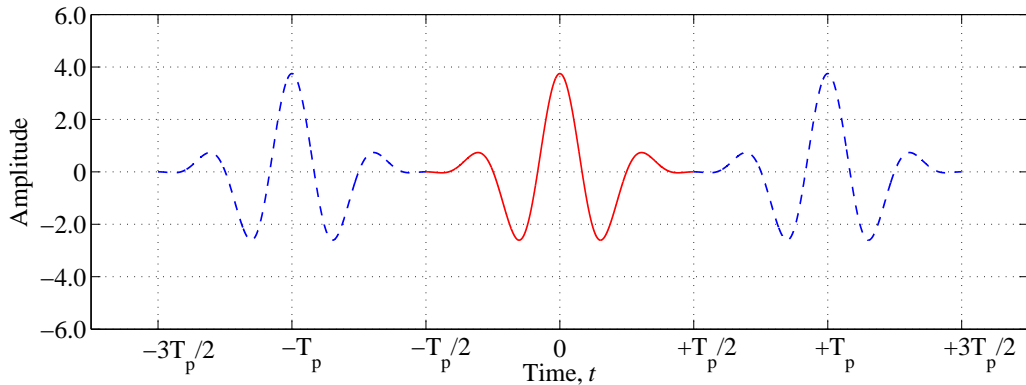
Figure 5.3: The pulse $p(t)$ and two neighboring pulses with delays of $-T_p$ and $+T_p$.

Here, the same notation as in the previous subsection is used; however, all the vectors and matrices must be redefined. Our general model is given by

$$\mathbf{r}_j^P = \sqrt{\frac{E_b}{N_s}} \mathbf{S}_j^P \mathbf{A}_j^P \mathbf{b}_j^P + \mathbf{n}_j^P \tag{5.10}$$

where $\mathbf{r}_j^P = [r_{j(0)}^P, r_{j(1)}^P, \ldots, r_{j(N_{uj}^P)}^P]^T$ and

$$r_{j(i)}^P = \int_{\alpha_j^P}^{\beta_j^P} r(t) p_j(t - \delta_{j(i)}^P) dt \tag{5.11}$$

where $\alpha_j^P = jT_f + (T_f - T_p)/2$, and $\beta_j^P = jT_f + (T_f + T_p)/2$. The amplitudes matrix, $\mathbf{A}_j^P = \text{diag}[A_{j(0)}^P, A_{j(1)}^P, \ldots, A_{j(N_{uj}^P)}^P]$, and the information bits vector, $\mathbf{b}_j^P =$

$[b_{j(0)}^P, b_{j(1)}^P, \ldots, b_{j(N_{uj}^P)}^P]^T$. The noise vector, $\mathbf{n}_j^P$, is a zero-mean Gaussian random vector with covariance matrix $\boldsymbol{\Sigma}_j^P$, where $\boldsymbol{\Sigma}_j^P = (N_0/2)\mathbf{S}_j^P$. The elements of the symmetric matrix $\mathbf{S}_j^P$ are defined by

$$(\mathbf{S}_j^P)_{mn} = \int_{\alpha_j^P}^{\beta_j^P} p_j(t - \delta_{j(m)}^P)p_j(t - \delta_{j(n)}^P)dt. \qquad (5.12)$$

To calculate the conditional LLRs, it is required to have the conditional PDF of $\mathbf{r}_j^P$ given $\mathbf{b}_j^P$ which is expressed by

$$f(\mathbf{r}_j^P|\mathbf{b}_j^P) = f_g(\mathbf{r}_j^P, \sqrt{\frac{E_b}{N_s}}\mathbf{S}_j^P\mathbf{A}_j^P\mathbf{b}_j^P, \frac{N_0}{2}\mathbf{S}_j^P, N_{uj}^P). \qquad (5.13)$$

Finally, using the LLRs of all N_s frames, the mth information bit of the desired user is decided according to

$$\hat{d}_m^{(0)} = \begin{cases} +1, & \sum_{j=p_m}^{q_m} L(b_{j(0)}^P|\mathbf{r}_j^P) \geq 0 \\ -1, & \sum_{j=p_m}^{q_m} L(b_{j(0)}^P|\mathbf{r}_j^P) < 0. \end{cases} \qquad (5.14)$$

For the MUD algorithm with PDOT, the expression $f(\mathbf{r}_j^P|\mathbf{b}_j^P)$ is computed $2^{N_{uj}^P+1}$ times for each frame, which is much less complex than the MUD algorithm with FDOT. In spite of the fact that $\boldsymbol{\Sigma}_j^P = (N_0/2)\mathbf{S}_j^P$ is a $(N_{uj}^P + 1) \times (N_{uj}^P + 1)$ covariance matrix and the complexity of computing its inverse is less than that of computing the inverse of the covariance matrix in the MUD algorithm with FDOT, it is still changing in each frame, making the PDOT MUD receiver computationally complex. Therefore, we seek an algorithm in which the covariance matrix of the noise vector is constant for all the frames.

Although the complexity of the MUD algorithm with PDOT is reduced compared to the MUD algorithm with FDOT, its implementation is not feasible. This is because the matched filters used in PDOT MUD algorithm are matched to either full or partial pulses. Thus, their frequency responses must change in each frame, which is not practical for a low-cost TH-UWB receiver. Note that in the MUD algorithm with FDOT, all the matched filters are matched to the full pulse shape, $p(t)$, and just the time of switching on/off for each of them is changing. So, the frequency responses of all the matched filters are constant. In the next subsection, we introduce a novel MUD algorithm which has matched filters with predetermined frequency responses as well as constant reduced-size covariance matrix for the noise vector.

5.2.3   Multisampling Suboptimal MUD Algorithm

Denote the number of effective interfering users in a TH-UWB system by the constant, N_u^E. Then, in each frame, $N_u^E + 1$ of $N_{uj}^F + 1$ delay variables $\delta_{j(i)}^F$ with smallest absolute values are selected and named $\delta_{j(i)}^E$. Also, the vector $\mathbf{\Lambda}^E$, called the matched filters' delay vector, is defined by $[\lambda_{(0)}^E, \lambda_{(1)}^E, \ldots, \lambda_{(N_u^E)}^E]$ where $\lambda_i^E = -\frac{T_p}{2} + i\Delta$, $\Delta = \frac{T_p}{N_u^E}$ and $i = 0, 1, \ldots, N_u^E$.

To obtain the receiver decision statistics, a bank of $N_u^E + 1$ matched filters, each matched to the pulse shape, $p(t)$, and synchronized with each element of the vector $\mathbf{\Lambda}^E$, is employed. The vector of decision statistics, $\mathbf{r}_j^E$, is defined by $[r_{j(0)}^E, r_{j(1)}^E, \ldots, r_{j(N_u^E)}^E]^T$ and

$$r_{j(i)}^E = \int_{\alpha_j^E + i\Delta}^{\beta_j^E + i\Delta} r(t) p_j(t - \lambda_{(i)}^E) dt \tag{5.15}$$

where $\alpha_j^E = jT_f + T_f/2 - T_p$, and $\beta_j^E = jT_f + T_f/2$. The vector, $\mathbf{r}_j^E$, obeys the condition

$$\mathbf{r}_j^E = \sqrt{\frac{E_b}{N_s}} \mathbf{S}_j^E \mathbf{A}_j^E \mathbf{b}_j^E + \mathbf{e}_j^E + \mathbf{n}_j^E \tag{5.16}$$

where $\mathbf{A}_j^E = \text{diag}[A_{j(0)}^E, A_{j(1)}^E, \ldots, A_{j(N_u^E)}^E]$, and $\mathbf{b}_j^E = [b_{j(0)}^E, b_{j(1)}^E, \ldots, b_{j(N_u^E)}^E]^T$. The elements of the non-symmetric square matrix $\mathbf{S}_j^E$ are defined by

$$(\mathbf{S}_j^E)_{mn} = \int_{\alpha_j^E + m\Delta}^{\beta_j^E + m\Delta} p_j(t - \lambda_{(m)}^E) p_j(t - \delta_{j(n)}^E) dt. \tag{5.17}$$

The noise vector, $\mathbf{n}_j^E$, is a zero-mean Gaussian random vector with covariance matrix $\mathbf{\Sigma}^E$, where $\mathbf{\Sigma}^E = (N_0/2)\mathbf{R}^E$ and the elements of the symmetric matrix $\mathbf{R}^E$ are given by

$$(\mathbf{R}^E)_{mn} = \int_{\alpha_j^E + m\Delta}^{\beta_j^E + m\Delta} p_j(t - \lambda_{(m)}^E) p_j(t - \lambda_{(n)}^E) dt. \tag{5.18}$$

In this algorithm, observe that the noise covariance matrix is related to the matrix $\mathbf{R}^E$ rather than the matrix $\mathbf{S}_j^E$. As mentioned before, it is very unlikely to have more than N_u^E interfering users hit the desired user's pulse. However, suppose that it happens and that the AWGN is not present. In this case, $\mathbf{r}_j^E \neq \sqrt{E_b/N_s} \mathbf{S}_j^E \mathbf{A}_j^E \mathbf{b}_j^E$ and there will be some residual error which is caused by the other interfering users and is modeled by the vector $\mathbf{e}_j^E$. In fact, because of the sparsity of TH-UWB signals, with a high probability the vector $\mathbf{e}_j^E$ is zero or has small values compared

to the vector $\mathbf{r}_j^E$. In our suboptimal model, the vector $\mathbf{e}_j^E$ is ignored. Therefore, we can easily write the conditional PDF $f(\mathbf{r}_j^E|\mathbf{b}_j^E)$ as

$$f(\mathbf{r}_j^E|\mathbf{b}_j^E) = f_g(\mathbf{r}_j^E, \sqrt{\frac{E_b}{N_s}}\mathbf{S}_j^E\mathbf{A}_j^E\mathbf{b}_j^E, \frac{N_0}{2}\mathbf{R}^E, N_u^E). \tag{5.19}$$

Finally, the decision rule for the mth information bit of the desired user based on the LLRs of all N_s frames is given by

$$\hat{d}_m^{(0)} = \begin{cases} +1, & \sum_{j=p_m}^{q_m} L(b_{j(0)}^E|\mathbf{r}_j^E) \geq 0 \\ -1, & \sum_{j=p_m}^{q_m} L(b_{j(0)}^E|\mathbf{r}_j^E) < 0. \end{cases} \tag{5.20}$$

Similar to the MUD algorithm with PDOT, the complexity of the multisampling suboptimal MUD algorithm for computing LLRs is much less than the MUD algorithm with FDOT. Based on the choice of N_u^E, this algorithm can be less or more complex than the MUD algorithm with PDOT. But, unlike the MUD algorithm with PDOT, the covariance matrix in this algorithm is fixed, so its inverse can be computed once in the stage of receiver design lowering the cost of the TH-UWB MUD receiver. In addition the frequency responses of the matched filters do not change with time, making the implementation feasible. This MUD algorithm is called the multisampling MUD algorithm, because one matched filter with sampling rate $1/\Delta$ can be used instead of a bank of matched filters with lower sampling rates. Thus, a higher sampling rate is the cost of reducing the number of filters, without any effect on the performance.

5.3   Simulation Results

In our simulation, one of the pulses from the family of even pulses of [13], $p_n^e(t)$, is used as the pulse shape with the parameters $f_c = 6.85$ GHz, $\tau = 1/f_c = 0.146$ ns and $n = 3$. The TH-UWB system has the following set of parameters, $D = 2\%$, $N_s = 5$, and $N_u = 8$. All the simulations have been done with 10^6 bits and the transmission powers of all the interfering users are equal. The BER performances are obtained in the ideal free-space propagation channels with AWGN and MAI as well as the multipath fading UWB channels.

5.3.1   Ideal Free-Space Propagation with AWGN and MAI

In Figs. 5.4 and 5.5, the performances of several different nonlinear single-user detectors, the hard-limiting UWB receiver [19], soft-limiting UWB receiver [19], p-order metric UWB receiver [24] and myriad filter UWB detector [25] are compared
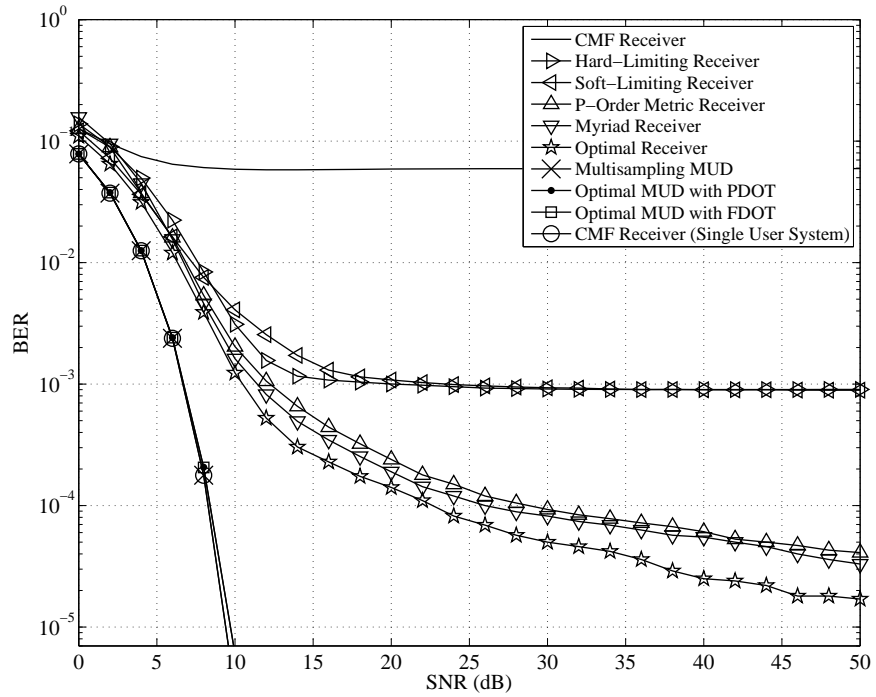
Figure 5.4: The BER versus SNR of single-user and MUD receivers for SIR $= 5$ dB and $N_u = 8$.
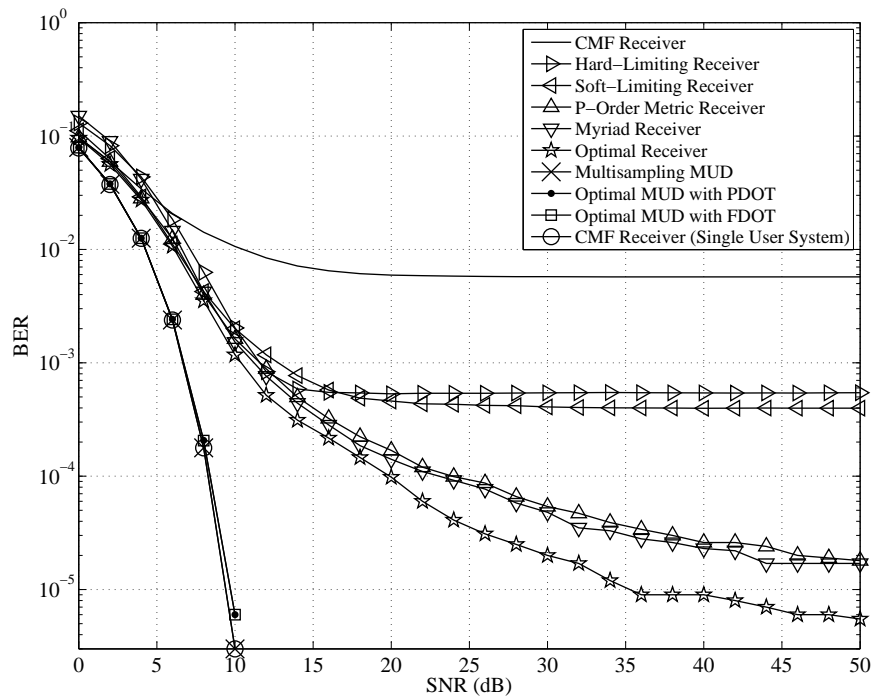
Figure 5.5: The BER versus SNR of single-user and MUD receivers for SIR $= 10$ dB and $N_u = 8$.

with those of the PDOT, FDOT and multisampling MUD receivers in an ideal free-space propagation channel with AWGN and MAI for SIR = 5 and 10 dB, respectively. Here, for the multisampling MUD algorithm, N_u^E is assumed to be 4. For the sake of comparison, the performance of the theoretically optimal single-user detector obtained in Chapter 3 is shown as well as the performance of the CMF receiver operating in a single-user system.

It can be seen that the BER curves of all the single-user receivers for large values of SNR reach error floors which are due to the MAI. However, the MUD receivers not only outperform all the other receivers but also remove the error floor resulting from the MAI. Furthermore, by comparing curves in Fig. 5.4 with curves in Fig. 5.5, it is observed that independent of the value of SIR, the performances of all the MUD receivers achieve the performance of the CMF receiver operating in a single-user system. An interesting result is that although the multisampling MUD receiver is suboptimal, its performance tracks closely the performances of the two optimal MUD receivers with PDOT and FDOT.

The performance of the multisampling MUD receiver for SIR = 5 dB, $N_u = 8$ and $N_u^E = 1, \ldots, 4$ is shown in Fig. 5.6 for two cases of soft and hard detection. For
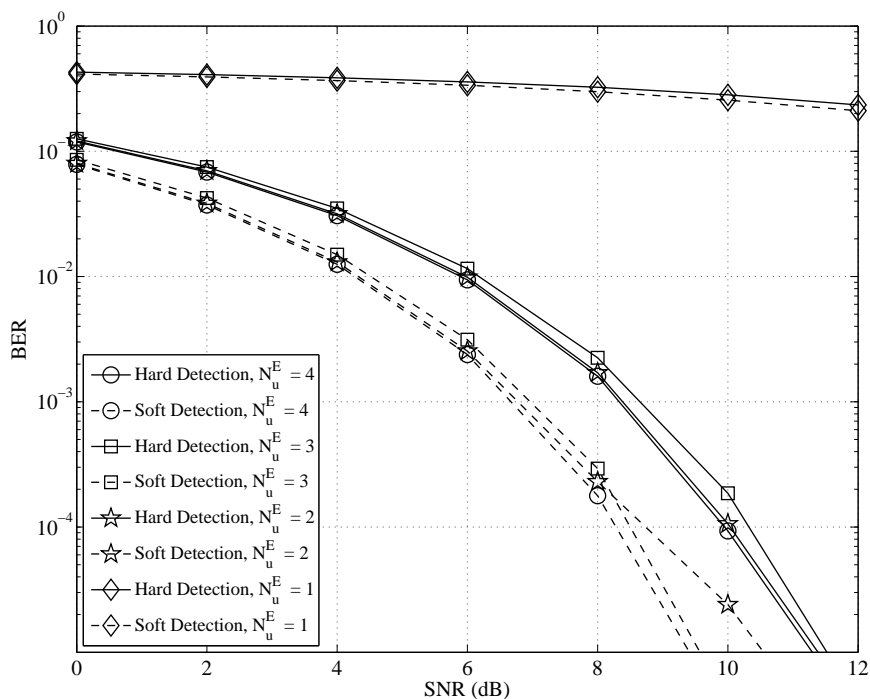
Figure 5.6: The BER versus SNR of the multisampling MUD receiver for SIR = 5 dB, $N_u = 8$ and $N_u^E = 1, \ldots, 4$.

soft detection, the LLR value for each frame is computed and then the transmitted bit is detected based on the sign of the sum of N_s LLRs of frames representing that bit. In hard detection, the majority logic rule decides which bit is transmitted based on the signs of the LLRs of N_s frames. It is observed that by decreasing N_u^E, generally the multisampling receiver performs worse. However, for $N_u^E = 2, 3, 4$, the degradation in performance is negligible and one should consider the performance-complexity tradeoffs for choosing the value of N_u^E. In the case of $N_u^E = 1$, it is seen that the multisampling MUD receiver cannot overcome the MAI because the number of effective interfering users has been underestimated. Also, observe that the receiver with $N_u^E = 2$ outperforms the receiver with $N_u^E = 3$. This is because when N_u^E has an even value, one of the matched filters exactly matches the pulse shape of the desired user and can capture more energy, which is true for $N_u^E = 2$, but not for $N_u^E = 3$.

5.3.2 Multipath Fading UWB Channel with AWGN

Figs. 5.7, 5.8, 5.9, and 5.10 show the BER curves of the UWB nonlinear single-user receivers, the partial-multiuser receivers and the multisampling MUD receiver in practical UWB environments where both MAI and AWGN are present.

For obtaining the BER performances of the purposed receivers in multipath fading UWB channels, the channel models introduced in [31] are employed which are known as CM1, CM2, CM3, and CM4 channels. In our simulations, the SIR is equal to 10 dB. An S-Rake receiver structure is used with 5 fingers. The S-Rake receiver employs the CMF UWB receiver, the soft-limiting UWB receiver, the p-order metric UWB receiver, the MMSE partial-multiuser receiver, the optimal partial-multiuser detector, or the multisampling MUD receiver as its receiving fingers. Then, the outputs of the fingers are combined to make the decision statistics. Here, EGC and MRC are used as the two diversity combining methods. In order to obtain the performances of the receivers, the simulations must be done in approximately 100 different channel realizations and then the average performances are computed for each of the UWB multipath channels [31]. Here, for the multisampling MUD algorithm, N_u^E is assumed to be 4.

As seen, the multisampling MUD receiver with EGC and MRC techniques outperforms all the nonlinear single-user receivers as well as the partial-multiuser receivers proposed in Chapter 4. Note that although the multisampling MUD receivers
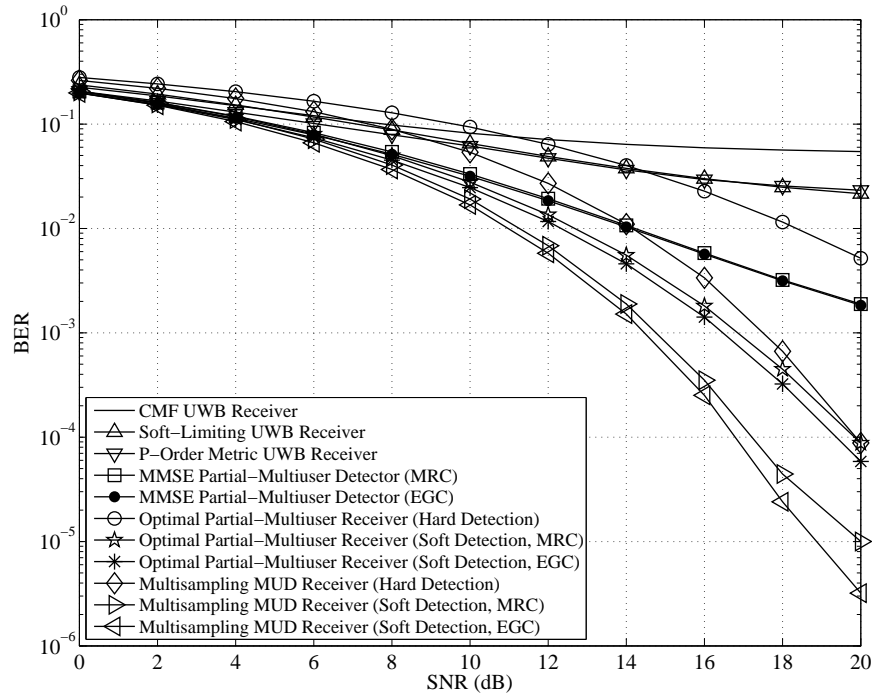
Figure 5.7: The BER versus SNR of the single-user, partial-multiuser, and multisampling MUD receivers operating in the CM1 UWB multipath channel for SIR $= 10$ dB and $N_u = 8$.
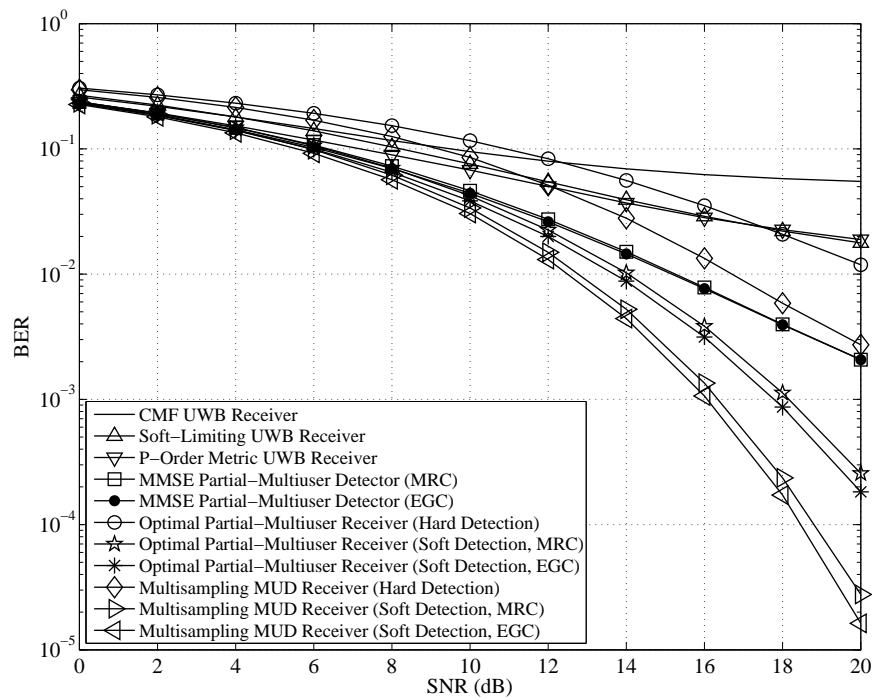
Figure 5.8: The BER versus SNR of the single-user, partial-multiuser, and multisampling MUD receivers operating in the CM2 UWB multipath channel for SIR $= 10$ dB and $N_u = 8$.
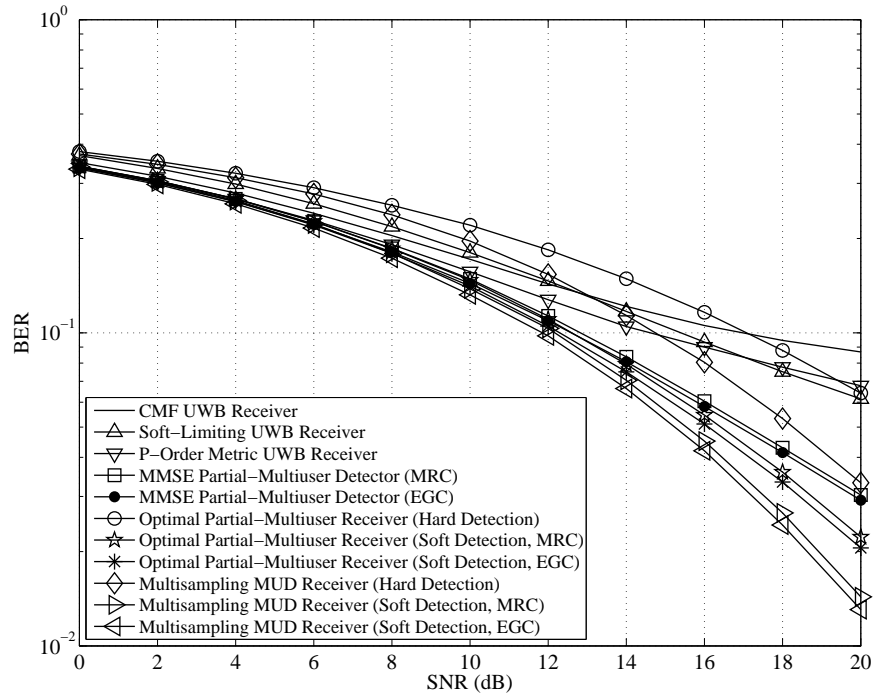
Figure 5.9: The BER versus SNR of the single-user, partial-multiuser, and multisampling MUD receivers operating in the CM3 UWB multipath channel for SIR $= 10$ dB and $N_u = 8$.

Figure 5.10: The BER versus SNR of the single-user, partial-multiuser, and multisampling MUD receivers operating in the CM4 UWB multipath channel for SIR $= 10$ dB and $N_u = 8$.

with hard detection, soft detection and the EGC Rake combining, and soft detection and the MRC Rake combining work better than their corresponding optimal partial-multiuser receivers, the multisampling MUD receivers are more complex. Therefore, one should always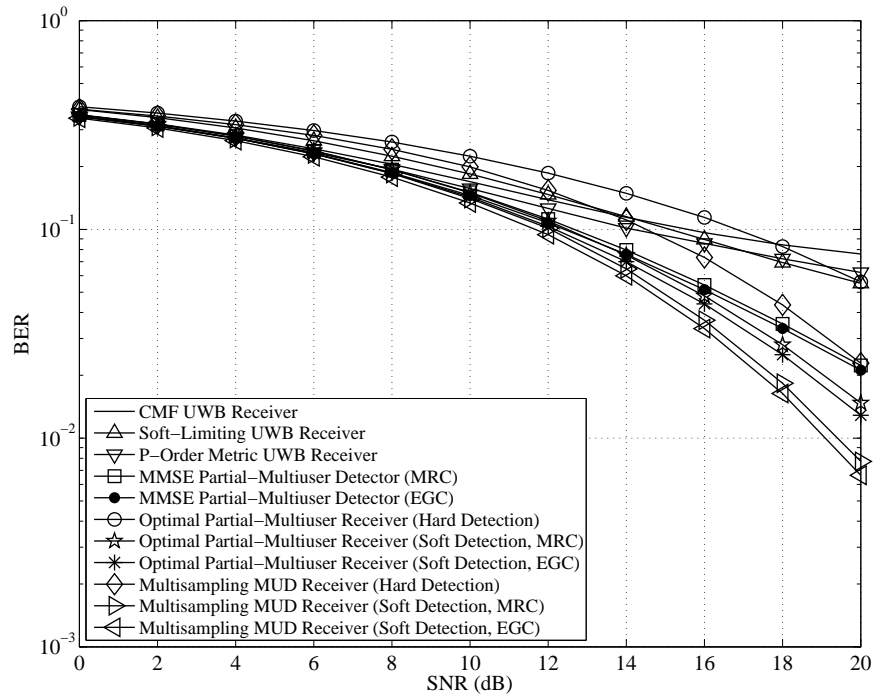 consider performance-complexity tradeoffs for designing UWB receivers. Also, for moderate and large values of SNR, the multisampling MUD receiver with hard detection outperforms all the single-user receivers in CM1 to CM4 UWB channels. Moreover, observe that the multisampling MUD receiver with the EGC Rake combining outperforms the multisampling MUD receiver with the MRC Rake combining in all the multipath UWB channels.

5.4   Conclusion

In this chapter, we discussed the time sparsity of TH-UWB signals which results from the low duty cycle of TH-UWB systems. Then, the optimal MUD algorithm whose observation time is limited to a frame duration was studied. This algorithm is too complex and cannot be implemented with low cost for a TH-UWB receiver. The optimal MUD algorithm with pulse-duration observation time was examined. Its complexity is significantly reduced, but it does not have a feasible implementation. Finally, a novel multisampling MUD algorithm was proposed which not only has a low complexity, but also outperforms all the nonlinear single-user receivers and partial-multiuser detectors.

Chapter 6

Conclusion

The single-user CMF receiver is widely used for detecting IR-UWB signals. This is known to be optimal for Gaussian noise, maximizing the SNR and minimizing the probability of detection error in the absence of non-Gaussian interference. Yet, the MAI in TH-UWB systems is known to be non-Gaussian and it is further known that the Gaussian model for the MAI underestimates the BER performance of the system. Therefore, more appropriate statistical models such as the Laplacian model, the GMM, and the α-stable distribution have been proposed for the MAI, and based on them various nonlinear single-user receivers have been designed that outperform the CMF receiver. It should be mentioned that all of the non-linear single receivers use the chip correlator outputs of the CMF receiver as their decision statistics, but apply a non-linear transformation to the output of each correlator to decide which bit was transmitted.

Since so much effort has been successfully put into the design of nonlinear single-user receivers for TH-UWB systems, it becomes crucial to know how much further the performance can be enhanced. In addition, one should always consider performance-complexity tradeoffs for designing UWB receivers which are supposed to have low cost. Therefore, it is essential to have the optimal benchmark against which the performances of other receivers can be measured. The best achievable benchmark is the performance of the optimal receiver for TH-UWB systems. The optimum performance can be obtained based on the MAP rule. However, the MAP rule requires knowledge of the PDF of the MAI. In our work, we introduced an accurate mathematical model explaining important features of the PDF of the MAI in TH-UWB systems namely impulses, singularities and the behaviour of tails. Then, based on that model for a practical UWB pulse and using the MAP rule, the optimal

error rate performance was obtained.

According to the simulation results, it was found that the p-order metric receiver and the myriad filter detector outperform all the other receivers and their performances are near the performance of the theoretically optimal single-user UWB receiver which knows the exact PDF of the MAI. This fact expresses that putting more effort into proposing more accurate statistical models for the PDF of the MAI may be ill conceived, because performances close to the optimal attainable performance have already been achieved. Therefore, the way that the MAI is dealt with must be changed. Considering the fact that the CMF receiver is not an optimal receiver in TH-UWB systems, we claimed and proved that the CMF receiver even does not provide a sufficient decision statistic for detecting the information bits of the desired user in TH-UWB systems. Further, what is required for having a sufficient decision statistic for multiuser TH-UWB systems was examined. Exploiting concepts from the optimal MUD algorithm, two novel receivers called the MMSE and optimal partial-multiuser detectors were introduced that employ only one matched filter and outperform all the non-linear single user receivers.

MUD has some distinguishing properties and it can be considered for simple and low-cost TH-UWB receivers. This is because TH-UWB systems are carrierless meaning that MUD for TH-UWB does not suffer from frequency/phase offset. Also, TH-UWB systems have a small number of effective interfering users, which reduce the complexity of MUD algorithms. In our work, we discussed the sparsity of TH-UWB signals due to the low duty cycle of TH-UWB systems and clarified the concept of effective interfering users. Then, optimal MUD algorithms with frame-duration and pulse-duration observation times were studied, and their pros and cons were described. A novel low-complexity multisampling multiuser detector inspired by the inferiority of single-user receivers and the small number of effective interfering users in TH-UWB systems was proposed. Simulation results show that this detector outperforms all single-user and partial-multiuser receivers both in ideal free-space propagations and real UWB multipath channels.

Bibliography

[1] I. Oppermann, M. Hämäläinen, and J. Iinatti, *UWB: Theory and Applications.* John Wiley & Sons, 2004.

[2] F. Nekoogar, *Ultra-Wideband Communications: Fundamentals and Applications.* Prentice Hall, 2005.

[3] Federal Communications Commission, "Revision of part 15 of the communication's rules regarding ultra-wideband transmission systems," *First Report and Order, ET Docket 98-153, FCC 02-48*, pp. 1–118, Feb. 2002.

[4] J. H. Reed, *An Introduction to Ultra Wideband Communication Systems.* Prentice Hall, 2005.

[5] M. Ghavami, L. B. Michael, and R. Kohno, *Ultra Wideband Signals and Systems in Communication Engineering*, 2nd ed. John Wiley & Sons, 2007.

[6] H. Arslan, Z. N. Chen, and M.-G. D. Benedetto, *Ultra Wideband Wireless Communication.* John Wiley & Sons, 2006.

[7] X. Shen, M. Guizani, R. C. Qiu, and T. Le-Ngoc, *Ultra-Wideband Wireless Communications and Networks.* John Wiley & Sons, 2006.

[8] IEEE 802.15 WPAN high rate alternative PHY task group 3a (TG3a). Available online at http://www.ieee802.org/15/pub/TG3a.html .

[9] IEEE 802.15 WPAN low rate alternative PHY task group 4a (TG4a). Available online at http://www.ieee802.org/15/pub/TG4a.html .

[10] M. Z. Win and R. A. Scholtz, "Ultra-wide bandwidth time-hopping spread-spectrum impulse radio for wireless multiple-access communications," *IEEE Trans. Commun.*, vol. 48, no. 4, pp. 679–689, Apr. 2000.

[11] J. T. Conroy, J. L. LoCicero, and D. R. Ucci, "Communication techniques using monopulse waveforms," in *Proc. IEEE Military Commun. Conf. (MILCOM)*, vol. 2, Atlantic City, NJ, Oct./Nov. 1999, pp. 1181–1185.

[12] M. Ghavami, L. B. Michael, S. Haruyama, and R. Kohno, "A novel UWB pulse shape modulation system," *Kluwer International Journal on Wireless Personal Communications*, vol. 23, no. 1, pp. 105–120, Oct. 2002.

[13] N. C. Beaulieu and B. Hu, "A pulse design paradigm for ultra-wideband communication systems," *IEEE Trans. Wireless Commun.*, vol. 5, no. 6, pp. 1274–1278, Jun. 2006.

[14] A. Taha and K. M. Chugg, "A theoretical study on the effects of interference UWB multiple access impulse radio," in *Proc. Asilomar Conf. Signals, Syst., Comput.*, vol. 1, Pacific Grove, CA, Nov. 2002, pp. 728–732.

[15] G. Durisi and S. Benedetto, "Performance evaluation of TH-PPM UWB systems in the presence of multiuser interference," *IEEE Commun. Lett.*, vol. 7, no. 5, pp. 224–226, May 2003.

[16] B. Hu and N. C. Beaulieu, "Accurate performance evaluation of time-hopping and direct-sequence UWB systems in multi-user interference," *IEEE Trans. Commun.*, vol. 53, no. 6, pp. 1053–1062, Jun. 2005.

[17] G. Durisi and G. Romano, "On the validity of Gaussian approximation to characterize the multiuser capacity of UWB TH PPM," in *Proc. IEEE Conf. Ultra Wideband Syst. Technol.*, Baltimore, MD, May 2002, pp. 157–161.

[18] A. R. Forouzan, M. Nasiri-Kenari, and J. A. Salehi, "Performance analysis of time-hopping spread-spectrum multiple-access systems: uncoded and coded schemes," *IEEE Trans. Wireless Commun.*, vol. 1, no. 4, pp. 671–681, Oct. 2002.

[19] N. C. Beaulieu and B. Hu, "Soft-limiting receiver structures for time-hopping UWB in multiple-access interference," *IEEE Trans. Veh. Technol.*, vol. 57, no. 2, pp. 810–818, Mar. 2008.

[20] H. Shao and N. C. Beaulieu, "A novel zonal UWB receiver with superior performance," *IEEE Trans. Commun.*, vol. 57, no. 4, pp. 1197–1206, Apr. 2009.

[21] V. Cellini and G. Dona, "A novel joint channel and multi-user interference statistics estimator for UWB-IR based on Gaussian mixture model," in *Proc. IEEE Int. Conf. Ultra Wideband (ICU)*, Sep. 2005, pp. 655–660.

[22] B. Hu and N. C. Beaulieu, "On characterizing multiple access interference in TH-UWB systems with impulsive noise models," in *Proc. IEEE Radio Wireless Symp.*, Jan. 2008, pp. 879–882.

[23] H. El Ghannudi, L. Clavier, and P. A. Rolland, "Modeling multiple access interference in ad hoc networks based on IR-UWB signals up-converted to 60 GHz," in *Proc. European Conf. on Wireless Technol.*, Oct. 2007, pp. 106–109.

[24] N. C. Beaulieu, H. Shao, and J. Fiorina, "P-order metric UWB receiver structures with superior performance," *IEEE Trans. Commun.*, vol. 56, no. 10, pp. 1666–1676, Oct. 2008.

[25] S. Niranjayan and N. C. Beaulieu, "A myriad filter detector for UWB multiuser communication," in *Proc. IEEE Int. Conf. Commun. (ICC)*, Beijing, China, May 2008, pp. 3918–3922.

[26] K. A. Handi and X. Gu, "Bit error rate analysis for TH-CDMA/PPM impulse radio networks," in *Proc. IEEE Wireless Commun. Netw. Conf. (WCNC)*, vol. 1, Mar. 2003, pp. 167–172.

[27] M. Sabattini, E. Masry, and L. B. Milstein, "A non-Gaussian approach to the performance analysis of UWB TH-BPPM systems," in *Proc. IEEE Conf. Ultra Wideband Syst. Technol.*, Nov. 2003, pp. 52–55.

[28] B. Hu and N. C. Beaulieu, "Exact bit error rate analysis of TH-PPM UWB systems in the presence of multiple-access interference," *IEEE Commun. Lett.*, vol. 7, no. 12, pp. 572–574, Dec. 2003.

[29] B. Hu and N. C. Beaulieu, "Accurate evaluation of multiple-access performance in TH-PPM and TH-BPSK UWB systems," *IEEE Trans. Commun.*, vol. 52, no. 10, pp. 1758–1766, Oct. 2004.

[30] A. Papoulis and U. S. Pillai, *Probability, Random Variables, and Stochastic Processes*, 4th ed.   McGraw Hill Higher Education, 2002, pp. 130–131.

[31] J. E. Foerster, "Channel modeling sub-committee report final," IEEE, Document IEEE P802.15-02/490r1-SG3a, Feb 2003.

[32] J. Fiorina, "On the benefit of a one-bit sampling receiver and hard decoding in impulse radio ultra wide band communications with multi-user interferences," in *Proc. IEEE Int. Symp. on Personal, Indoor and Mobile Radio Commun. (PIMRC)*, Helsinki, Finland, Sep. 2006, pp. 1–4.

[33] J. Fiorina, "A simple IR-UWB receiver adapted to multi-user interferences," in *Proc. IEEE Global Telecommun. Conf. (GLOBECOM)*, Nov./Dec. 2006, pp. 1–4.

[34] M. Flury and J. Y. Le Boudec, "Interference mitigation by statistical interference modeling in an impulse radio UWB receiver," in *Proc. IEEE Int. Conf. Ultra Wideband (ICUWB)*, Waltham, MA, Sep. 2006, pp. 393–398.

[35] T. Erseghe, "A low-complexity impulse radio receiver based upon Gaussian mixtures," in *Proc. IEEE Int. Conf. Commun. (ICC)*, San Francisco, CA, Jun. 2007, pp. 4311–4316.

[36] J. Mitra and L. Lampe, "Robust detectors for TH IR-UWB systems with multiuser interference," in *Proc. IEEE Int. Conf. Ultra Wideband (ICUWB)*, Singapore, Sep. 2007, pp. 745–750.

[37] N. C. Beaulieu and S. Niranjayan, "New UWB receiver designs based on a Gaussian-Laplacian noise-plus-MAI model," in *Proc. IEEE Int. Conf. Commun. (ICC)*, Glasgow, Scotland, Jun. 2007, pp. 4128–4133.

[38] S. Verdú, *Multiuser Detection*. Cambridge University Press, 1998.

[39] J. Proakis, *Digital Communications*, 4th ed. McGraw-Hill Science/Engineering/Math, 2000, pp. 232–236.

[40] Y. Chen and N. C. Beaulieu, "Superior NDA ML delay and gain estimators for UWB channels," in *Proc. IEEE Int. Conf. Commun. (ICC)*, Dresden, Germany, Jun. 2009.

[41] A. M. Rabiei and N. C. Beaulieu, "Exact error probability of a bandlimited single-interferer maximum-likelihood BPSK receiver in AWGN," *IEEE Trans. Wireless Commun.*, vol. 6, no. 1, pp. 30–34, Jan. 2007.

[42] Y. C. Yoon and R. Kohno, "Optimum multi-user detection in ultra-wideband (UWB) multiple-access communication systems," in *Proc. IEEE Int. Conf. Commun. (ICC)*, vol. 2, 2002, pp. 812–816.

[43] E. Fishler and H. V. Poor, "Low-complexity multiuser detectors for time-hopping impulse-radio systems," *IEEE Trans. Signal Process.*, vol. 52, no. 9, pp. 2561–2571, Sep. 2004.

[44] N. Boubaker and K. B. Letaief, "Combined multiuser successive interference cancellation and partial RAKE reception for ultra-wideband wireless communications," in *Proc. IEEE Veh. Technol. Conf. (VTC)*, vol. 2, Sep. 2004, pp. 1209–1212.

[45] N. Guney, H. Delif, and M. Koca, "Robust multiuser detection for impulse radio in non-Gaussian UWB channels," in *Proc. IEEE Int. Conf. Acoust., Speech, Signal Process. (ICASSP)*, vol. 4, May 2006, pp. 493–496.

[46] C.-C. Hu, H.-Y. Lin, T.-H. Liu, and Y.-S. Cheng, "Time-hopping UWB multiuser detection using adaptive multistage matrix Wiener filtering schemes," in *Proc. IEEE Int. Conf. Commun. (ICC)*, Jun. 2007, pp. 2540–2544.